

Copyright  
by  
Sang Putra Pasca Rante Patta  
2014

The Dissertation Committee for Sang Putra Pasca Rante Patta certifies that this is the approved version of the following dissertation:

**Analysis of Soil-Structure System Response with  
Adjustments to Soil Properties by Perturbation Method**

Committee:

---

John L. Tassoulas, Supervisor

---

Michael D. Engelhardt

---

Todd Helwig

---

Mark E. Mear

---

Krishnaswamy Ravi-Chandar

**Analysis of Soil-Structure System Response with  
Adjustments to Soil Properties by Perturbation Method**

by

**Sang Putra Pasca Rante Patta, B.Eng.**

**DISSERTATION**

Presented to the Faculty of the Graduate School of  
The University of Texas at Austin  
in Partial Fulfillment  
of the Requirements  
for the Degree of

**DOCTOR OF PHILOSOPHY**

THE UNIVERSITY OF TEXAS AT AUSTIN

May 2014

Dedicated to my family.

## Acknowledgments

First and foremost, I would like to gratefully thank my advisor Professor John L. Tassoulas for his heartfelt support. It has been truly an honor to be his Ph.D. student. Without his guidance and encouragement, this dissertation would not have been possible.

My gratitude also goes toward my dissertation committee members, Professor Michael D. Engelhardt, Professor Todd A. Helwig, Professor Mark E. Mear, and Professor Krishnaswamy Ravi-Chandar for their insights, valuable discussions and accessibility. Additionally, I would like to express my appreciation to Professor José M. Roesset for his suggestions regarding the Mexico City case study.

I thank Professor Amit Bhasin for his suggestions and advice throughout my graduate study. I would also like to thank Pam Dahl, M.Ed. for her assistance and guidance, and for providing me with the opportunity to gain valuable teaching experiences during my time here.

To my supportive colleagues and friends, thank you for all your help. My life as a graduate student would have not been meaningful without you.

Most importantly, I would like to thank my family. Their continued support, encouragement, patience and love have been the motivation to finish this dissertation.

# **Analysis of Soil-Structure System Response with Adjustments to Soil Properties by Perturbation Method**

Publication No. \_\_\_\_\_

Sang Putra Pasca Rante Patta, Ph.D.  
The University of Texas at Austin, 2014

Supervisor: John L. Tassoulas

The research described in this dissertation undertakes a computational study of wave motion due to ground excitation in layered soil media. Adjustments of soil properties consistent with the level of deformation is applied using an equivalent linear approach. The finite element method provides the basis of the numerical procedure for soil-structure system response calculation in conjunction with a first-order perturbation scheme. Available experimental data are employed for shear-modulus and damping adjustments. The findings of the research are expected to lead to efficient calculation of structural response to earthquake ground motion.

# Table of Contents

<b>Acknowledgments</b>	<b>v</b>
<b>Abstract</b>	<b>vi</b>
<b>List of Figures</b>	<b>ix</b>
<b>Chapter 1. Introduction</b>	<b>1</b>
1.1 Problem Description . . . . .	2
1.2 Analysis Methods . . . . .	5
1.3 Organization of Dissertation . . . . .	8
<b>Chapter 2. Problem Formulation and Modeling</b>	<b>11</b>
2.1 Analysis of Regular Layered Media . . . . .	12
2.2 Inclusions in Layered Media . . . . .	18
2.3 Finite Element Analysis and Formulation . . . . .	25
2.3.1 Quadrilateral Elements . . . . .	26
2.3.2 Rigid-Foundation Elements . . . . .	30
2.3.3 Hyperelements . . . . .	34
2.4 Soil-Structure System Model . . . . .	38
<b>Chapter 3. Soil Properties Consistent with Deformation</b>	<b>45</b>
3.1 Theoretical Site Characterization . . . . .	48
3.2 Mexico City Site Characterization . . . . .	49
3.2.1 General Site Conditions . . . . .	50
3.2.2 Site Conditions at Recording Stations . . . . .	53
3.3 Adjustments of Soil Properties . . . . .	60
3.3.1 Reduction Curves . . . . .	60
3.3.2 Hyperbolic Model . . . . .	62
3.3.3 Darendeli Model . . . . .	64
3.3.4 Site-Specific Reduction Curves . . . . .	70

<b>Chapter 4. Equivalent Linear Analysis with Perturbation Method</b>	<b>78</b>
4.1 Process of Equivalent Linear Analysis . . . . .	78
4.2 Equation of Motion . . . . .	85
4.3 Boundary Conditions . . . . .	88
4.4 Consistent Nodal Forces . . . . .	92
4.5 Solution Process for System of Equations . . . . .	96
4.6 Application of LU Decomposition . . . . .	99
4.7 Soil-Property Adjustments using Perturbation Method . . . . .	102
<b>Chapter 5. Case Studies</b>	<b>113</b>
5.1 Theoretical Case Study . . . . .	114
5.2 Mexico City Case Study . . . . .	124
5.2.1 Analysis Parameters . . . . .	125
5.2.2 Analysis of Surface and Embedded Foundations . . . . .	127
5.2.3 Analysis of Structures of Various Heights . . . . .	133
5.2.4 System Response for Various Foundation Depths . . . . .	142
5.2.5 System Response for Various Foundation Sidewall Heights	147
<b>Chapter 6. Conclusion</b>	<b>154</b>
<b>Bibliography</b>	<b>156</b>
<b>Vita</b>	<b>161</b>



## List of Figures

1.1	Soil-Structure System . . . . .	3
1.2	Discretization of the Soil Medium . . . . .	4
1.3	Process of Equivalent Linear Analysis . . . . .	6
2.1	Inclusion in Layered Medium . . . . .	19
2.2	Near-Field Discretization with Quadrilateral Elements . . . . .	26
2.3	Rigid Foundation . . . . .	30
2.4	Representation of Foundation using Rigid Links . . . . .	31
2.5	Rigid Connection . . . . .	31
2.6	Structure Embedded in a Soil Layer . . . . .	39
2.7	Simple Structure Representation . . . . .	39
2.8	Equivalent Horizontal Stiffness of the Structure . . . . .	40
2.9	Displacement of Structural Mass and Foundation . . . . .	42
3.1	El Centro Recorded Ground Motion . . . . .	49
3.2	Recording Stations and Lakebeds of Mexico City (from Seed et al., 1988) . . . . .	51
3.3	Basin of Valley of Mexico (from Zeevaert, 1971) . . . . .	52
3.4	East-West Profile of Mexico City (from Celebi et al., 1987) . . . . .	53
3.5	SCT Suspension Logging Test (from Ovando-Shelley et al., 2007) . . . . .	55
3.6	Representative Soil Profile (from Seed et al., 1988) . . . . .	56
3.7	UNAM and SCT Recorded Motion . . . . .	57
3.8	Frequency Domain Representations . . . . .	58
3.9	Spectral Ratio for UNAM-SCT . . . . .	59
3.10	Effect of Plasticity Index on Site Response (from Vucetic and Dobry, 1991) . . . . .	61
3.11	Modulus Reduction and Damping of Clays of Various Plasticity Index Values (from Vucetic and Dobry, 1991) . . . . .	61
3.12	Stress-Strain Curve based on the Hyperbolic Model . . . . .	63

3.13	Hyperbolic Model (from Darendeli, 2001) . . . . .	64
3.14	Masing Behavior Hysteresis Loop . . . . .	66
3.15	Reduction Curves for Theoretical Case Study based on Darendeli Model . . . . .	69
3.16	Mexico City Empirical Reduction Curves (from Leon et al., 1974; Romo and Jaime, 1986) . . . . .	70
3.17	Depth to Hard Formation (from Jaime, 1987) . . . . .	72
3.18	Texcoco Lakebed Stratigraphic Profile (from Romo et al., 1988) . . . . .	73
3.19	Stress-Strain Relationship for Preloaded Texcoco Lakebed (from Romo et al., 1988) . . . . .	74
3.20	Shear Modulus Reduction Curves for SCT Site (from Romo et al., 1988) . . . . .	75
3.21	Damping Curves for SCT Site (from Romo et al., 1988) . . . . .	76
3.22	Measured Damping Level of Normally Consolidated Clay (from Dobry and Vucetic, 1987) . . . . .	76
4.1	Process for a One-Dimensional Equivalent Linear Analysis . . . . .	80
4.2	Process for a Two-Dimensional Equivalent Linear Analysis . . . . .	82
4.3	Element Contributions to the Global Dynamic Stiffness Matrix . . . . .	88
4.4	Determination of Base Motion . . . . .	90
4.5	Equivalent Nodal Forces . . . . .	93
4.6	Cross-Section of Regular Layered Medium . . . . .	93
4.7	Consistent Nodal Forces . . . . .	95
4.8	Banded Stiffness Matrix . . . . .	97
4.9	Reorganized Stiffness Matrix . . . . .	97
4.10	Row Indices for Global Matrix Elements and Corresponding Sparse Matrix Indices . . . . .	98
4.11	Iterative Process of First Order Perturbation Method . . . . .	106
5.1	Embedded Foundation Supporting Massive Structure . . . . .	115
5.2	Structural Response from One-Dimensional and Two-Dimensional Analyses . . . . .	116
5.3	Converged Soil Properties in the Free Field and Near Field . . . . .	117
5.4	Near-Field Adjustments for Various Clearances . . . . .	118
5.5	Converged Strain-Consistent Free-Field Properties . . . . .	119

5.6	Converged Shear Strain Level from Near-Field Analysis . . . . .	120
5.7	Converged Strain-Consistent Near-Field Properties . . . . .	121
5.8	Kinematic and Inertial Interaction Effects on Structural Response	122
5.9	Foundation Rotation . . . . .	123
5.10	Structural Acceleration . . . . .	123
5.11	Modeling of Mexico City Structure Supported by Embedded Foundation . . . . .	124
5.12	Acceleration Response Spectra from Free-Field and Near-Field Iterations . . . . .	128
5.13	Comparison of Embedded Foundation Response using Free-Field and Near-Field Iterated Properties . . . . .	129
5.14	Comparison of Surface Foundation Response using Free-Field and Near-Field Iterated Properties . . . . .	130
5.15	Surface vs Embedded Foundation - Free-Field Properties . . .	132
5.16	Surface vs Embedded Foundation - Near-Field Properties . . .	132
5.17	Horizontal Response of Foundation for Structures of Varying Heights . . . . .	134
5.18	Rotational Response of Foundation for Structures of Varying Heights . . . . .	135
5.19	Acceleration Response for Structures of Varying Heights . . .	136
5.20	Displacement Response for Structures of Varying Heights . . .	137
5.21	Converged Strain Levels for Structures of Varying Heights . .	139
5.22	Converged Shear Modulus Levels for Structures of Varying Heights	140
5.23	Converged Damping Levels for Structures of Varying Heights .	141
5.24	Acceleration Response Spectra for Various Foundation Depths obtained using Free-Field and Near-Field Converged Properties	142
5.25	Comparison of Acceleration Response Spectra for Various Foun- dation Depths . . . . .	143
5.26	Converged Soil Properties for Various Foundation Depths . . .	145
5.27	Acceleration Response Spectra for Various Foundation Wall Heights obtained using Free-Field and Near-Field Converged Properties	148
5.28	Comparison of Acceleration Response Spectra for Various Foun- dation Wall Heights . . . . .	149
5.29	Converged Soil Properties for Various Foundation Wall Heights	150
5.30	Horizontal Response Equivalent Linear Analysis vs Recorded SCT Motion . . . . .	151

5.31 Converged Deformation Level for Various Configurations . . . 153

# Chapter 1

## Introduction

The analysis of soil-structure systems due to earthquake motion is a significant part of structural design in earthquake-prone regions. Design criteria for critical and high-occupancy structures are determined based on the expected structural response during earthquake events. Numerous factors affect the response of a soil-structure system and must be accounted for in the design process. The effects of these factors on the overall response of the system can be studied by comparing the system responses for different soil and structural configurations.

It is of great interest to develop an accurate and efficient method to predict the dynamic response of soil-structure systems under earthquake loading. Determination of the soil-structure system response can be achieved through different approaches. An ideal analysis would accurately model every detail of the soil-structure system, but a comprehensive analysis can be computationally demanding, even impractical. Conventional site-response analyses use efficient procedures based on simplifying assumptions but the results obtained can be overly conservative.

This dissertation seeks to introduce improvements to the conventional analysis of soil-structure systems that provide more accurate results with minimal addition to the computational effort. Soil-structure system response in relevant case studies will be computed using both conventional and improved methods. Results obtained will be compared to determine the extent of response calculation improvement using the modified procedure. Different configurations of the soil-structure system will be analyzed to determine conditions where the improvements are most significant.

## **1.1 Problem Description**

The behavior of an actual structure on deformable soil can be analyzed by an idealized soil-structure system representation. The system is composed of a layered soil medium, a representation of the structural mass and stiffness, and a representation of the interface between the soil and structure which is the foundation. An illustration of the soil-structure system is shown in Figure 1.1.

The layered soil medium is divided into two parts. Regions far away from the embedded foundation and structure are identified as the far field. Regions close to the foundation and structure are referred to as the near-field regions. Calculation of the far-field response can be achieved by assuming absence of the foundation and structure.

Analysis of a layered soil medium without inclusion constitutes a free-field analysis. The response obtained from the free-field analysis is equivalent

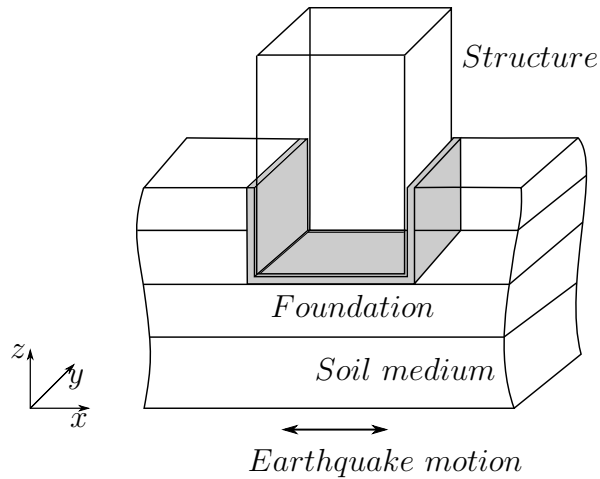
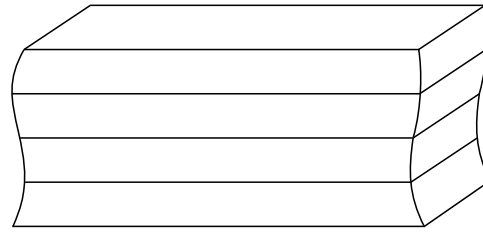


Figure 1.1: Soil-Structure System

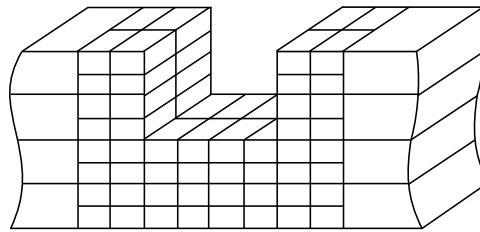
to the response of the far-field region. Analysis of the soil domain with considerations of the foundation and structure constitutes a near-field analysis.

Free-field analysis of a soil domain consists of one-dimensional linear elastic propagation of horizontal shear waves through the layered soil medium. Discretization of the domain in the vertical direction does not account for localized deviations in the horizontal direction due to the presence of foundation and structure. Near-field analysis allows for greater detail in the region near the structure, and accounts for the loading the structure and foundation exert on the soil. Illustration of the free-field and near-field discretizations are shown in Figure 1.2.

Several previous works provide the basis of the formulation for these analyses. Formulations of the regular layered media have been presented by Ikeda (2008) based on the works of Kausel (1981). Derivation of the effects



(a) Free Field



(b) Near Field

Figure 1.2: Discretization of the Soil Medium

of inclusions extend from the concepts used to derive the solutions of the regular layered media. Analysis of the near-field region can be done using a finite element approach. The transmitting boundary of the near-field region is represented by hyperelements which are derived on the basis of the work by Waas (1972).

Analysis of the soil media incorporates soil properties appropriate for the level of deformation experienced by the soil layers. Nonlinear behavior of the soil is primarily characterized by modulus and damping adjustments as functions of shear strain. Nonlinear analysis of the free-field and near-field regions can be done using these adjustments. Representative modulus reduction and damping curves based on empirical studies have been constructed in



the works of Seed and Idriss (1970) and Vucetic and Dobry (1991). Several models were developed to describe the reduction curves including the hyperbolic model (Hardin and Drnevich, 1972) and the Darendeli model (Darendeli, 2001).

## **1.2 Analysis Methods**

A complete analysis of a soil-structure system ideally consists of a fully nonlinear analysis using a hysteretic soil model. Nonlinear analysis considers the soil layers as lumped masses connected by nonlinear shear springs, which are analyzed in the time domain. Nonlinear methods differ in terms of the complexity of the stress-strain relationships and the soil behavior under cyclic loading. Comprehensive discussion on available methods of nonlinear analysis has been reported by Stewart et al. (2008). A fully nonlinear analysis allows the use of any soil constitutive model but is computationally expensive for most practical purposes.

Simplification of the solution process can be achieved through the use of equivalent linear analysis. Such analysis assumes a linear soil behavior, and calculates the system response in the frequency domain for a given set of initial soil properties. An updated set of soil properties is determined based on the calculated level of deformation. The site-response analysis is repeated using the strain dependent properties, and further iterations are performed until the soil properties converge. Kramer (1996) provides a more detailed review of the theory and applications of the equivalent linear method. A sample equivalent

linear process is illustrated in the flowchart of Figure 1.3 below.

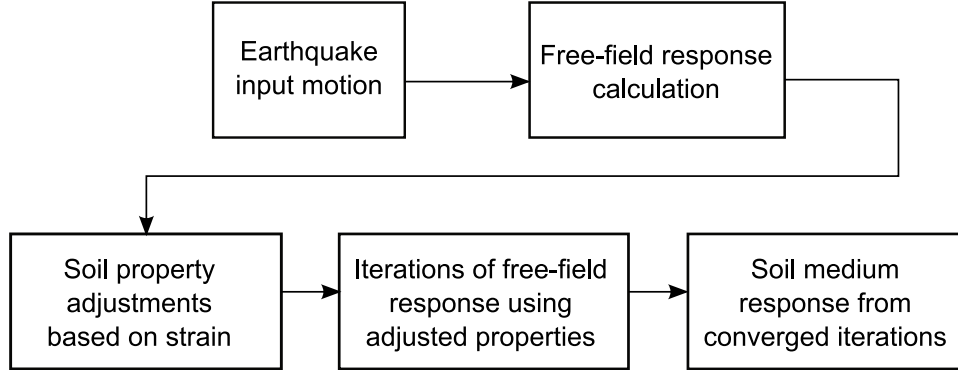


Figure 1.3: Process of Equivalent Linear Analysis

Several analysis tools have been developed and are readily available to analyze soil-structure systems. Application of equivalent linear analysis first appeared in the SHAKE computer program (Schnabel et al., 1972) and (Idriss and Sun, 1992), which was later developed into the commercial tool PROSHAKE. A more recent site-response analysis program STRATA developed at The University of Texas incorporates stochastic variation of site properties into the equivalent linear approach (Kottke and Rathje, 2008). The analyses performed by SHAKE and STRATA are based on one-dimensional vertical wave propagation to find the free-field response and strain dependent properties. More computationally intensive programs QUAD4M and SASSI allow for two and three-dimensional soil-structure analysis (Hudson et al., 1994; Lysmer et al., 1981).

The iteration process described in Figure 1.3 and used in the commonly available analysis tools determines the strain consistent properties in

the free-field region only. Many conventional analyses assume that the converged free-field soil properties represent the soil properties in the near-field region. Analysis of the soil-structure response is carried out by applying the converged free-field properties to the near-field, and without further iteration of the soil properties near the structure.

Calculation of soil-structure response using the free-field soil properties avoids the additional computational effort needed in iterating with adjusted near-field properties. However, soil properties in the near-field region are affected by the motion and loading of the structure and the foundation. Converged free-field properties do not accurately represent the nonlinear adjustments of soil properties in the near-field region.

Iterating with adjusted near-field properties requires extensive computational effort due to the significantly greater number of degrees of freedom involved in near-field analysis. Response calculation in the near-field region consists of a significantly larger system of equations which cannot be solved quickly by a conventional approach. Iteration of the near-field soil properties requires solving the equation of motion numerous times and quickly becomes impractical.

Adjustments to the conventional method are needed to reduce the computational effort and make near-field analysis feasible. A perturbation method can be applied to calculate incremental addition to the system response due to incremental adjustment of near-field properties. Instead of solving the near-field equations numerous times, the system of equations can be solved only

once for the initial set of properties. Subsequent iterations of the near-field analysis can be solved based on the solution of the initial system of equations using a perturbation method.

Determining the effects of adjusting near-field properties during analysis of soil-structure systems is the goal of this research. Calculations of additional response due to near-field adjustments will be achieved through the use of a perturbation method in conjunction with the equivalent linear approach. System response obtained by including near-field adjustments will be compared with results obtained by conventional approaches. The extent to which near-field adjustments affect the overall response of soil-structure systems will be studied. It is believed that such examination will demonstrate the benefits of applying a perturbation method to incorporate near-field adjustments in soil-structure response calculation.

### **1.3 Organization of Dissertation**

This dissertation explores the application of equivalent linear analysis in conjunction with a perturbation method to determine the effects of near-field adjustments on the response of soil-structure systems. Formulations of response calculation for regular layered soil media will be adjusted to account for inclusions due to the presence of the foundation and structure. Numerical models will be developed to adequately represent the free-field and near-field cases to be analyzed using equivalent linear analysis. Procedures used to calculate strain-consistent soil properties in free-field analysis will be extended

to near-field analysis.

The analysis of a soil-structure system begins with the construction of numerical models that appropriately represent the system. Formulations and discussions of the numerical models for the different parts of the system will be described in Chapter 2. The soil medium is first modeled by assuming that it is composed of horizontal layers of homogeneous soil. Vertical wave propagation analysis through the regular layered medium provides the free-field response. The presence of an inclusion is then examined and the effects inclusions have on the system response are considered. Finite element models are developed to facilitate efficient calculation in the near-field region, including models for the foundation and the structure.

The nonlinear soil behavior that will be incorporated into the analysis will be discussed in Chapter 3. Soil properties of a theoretical and an actual site characterization will be defined, along with corresponding input ground motions. The site characterization which represents an actual earthquake event will be based on the 1985 Mexico City earthquake. Models describing the soil property adjustments for both site characterizations will be explored. Theoretical and empirical modulus reduction and damping curves will be presented. Reduction curves to be used in the analysis will then be defined based on the available curves.

Procedures of calculating soil-structure response based on the equivalent linear approach will be detailed in Chapter 4. The process will first be applied to the free field and then extended to the near field. Improvements

to the analysis procedure will be introduced to reduce the computational effort in accounting for near-field adjustments. The system of equations will be rewritten in terms of sparse matrices, which will be solved using LU decomposition and the implementation of the SuperLU routine. Improvement of the solution process will be developed using the perturbation method to efficiently calculate changes of equation solutions without reprocessing the entire system of equations. Incremental addition to the system response due to updating properties in the near-field can then be determined in terms of the incremental change in soil properties.

Equivalent linear analysis in conjunction with the perturbation method will be applied to the finite element models to perform case studies of theoretical and actual earthquake events. Case studies of interest are the theoretical case study using the El Centro earthquake motion, and the Mexico City 1985 earthquake motion. Response of the soil-structure systems in both case studies will be presented in Chapter 5 along with commentary and analytical discussion of the results. Site-response analysis will be carried out for varying properties and site configurations. Examination of results will provide insight into the effects different configurations have on the site-response analysis as well as the overall significance of updating soil properties in the near-field region.

Summary of the work carried out in this dissertation, along with concluding remarks and possible future research will be discussed in Chapter 6.

## Chapter 2

### Problem Formulation and Modeling

The analysis of soil-structure interaction requires an accurate way of modeling both the soil and the structure. Additional consideration must also be extended to the foundation, which represents the interface between the soil and the structure. Formulations and discussions of the numerical models for the different aspects of the analysis will be discussed in this chapter.

Two types of analysis of the soil are of interest. First, an analysis of the overall medium is needed to determine the level of deformation that occurs throughout the entire soil domain. This constitutes a free-field analysis with an underlying assumption that the entire domain is a regular layered medium. Such analysis can be carried out one-dimensionally as the soil response will be constant in the horizontal direction, assuming seismic waves are propagating vertically.

The second type of analysis deals with treatment of the near-field region. This region consists of parts of the soil medium where geometric or material properties deviate from properties of the regular layered medium. A near-field analysis provides a more accurate treatment of the region in the vicinity of the foundation. Results of near-field analyses provide more accurate

estimations to the soil-structure system response.

Appropriate models needed to carry out both the free-field and near-field analyses are described in the following sections.

## 2.1 Analysis of Regular Layered Media

The analysis of the soil medium starts with determination of the regular layered medium response. Free-field analysis will provide a first approximation of the soil response which is accurate for regions far away from localized inclusions.

A regular layered medium consists of soil layers that extend without bounds to infinity, with no variation in the  $x$  direction with regards to both geometric and material characteristics of the layers. Heights of the layers are constant everywhere, and material properties are constant throughout each layer.

Formulation of the free-field analysis begins with the differential equations of equilibrium. Plane-strain conditions are assumed. For a layered medium without variation in the  $x$  direction, the equilibrium equations are expressed as:

$$\frac{\partial \sigma_x}{\partial x} + \frac{\partial \tau_{zx}}{\partial z} = \rho \frac{\partial^2 u}{\partial t^2} \quad (2.1)$$

$$\frac{\partial \tau_{zx}}{\partial x} + \frac{\partial \sigma_z}{\partial z} = \rho \frac{\partial^2 w}{\partial t^2} \quad (2.2)$$



In Equations 2.1 and 2.2,  $u$  and  $w$  represent the soil displacements in the horizontal and vertical directions, respectively. The mass density is  $\rho$ , and  $\sigma_x$ ,  $\tau_{zx}$ ,  $\sigma_z$  represent the (in-plane) stress components for the plane-strain case.

In free-field analysis of regular layered media, all material properties and loads are constant in the  $x$  direction. Therefore stress components do not vary in the  $x$  direction, which leads to the following expressions:

$$\frac{\partial \tau_{zx}}{\partial z} = \rho_i \frac{\partial^2 u}{\partial t^2} \quad (2.3)$$

$$\frac{\partial \sigma_z}{\partial z} = \rho_i \frac{\partial^2 w}{\partial t^2} \quad (2.4)$$

The Principle of Virtual Work can be developed as in Ikeda (2008). Both sides of the differential equations are multiplied by an arbitrary function of  $z$  and integrated with respect to  $z$ . The Principle of Virtual Work is only applied to the  $z$ -direction.

$$\int_{z_{i+1}}^{z_i} \delta u \frac{\partial(\tau_{zx})}{\partial z} dz = \int_{z_{i+1}}^{z_i} \delta u \frac{\partial^2 u}{\partial t^2} \rho_i dz \quad (2.5)$$

$$\int_{z_{i+1}}^{z_i} \delta w \frac{\partial \sigma_z}{\partial z} dz = \int_{z_{i+1}}^{z_i} \delta w \frac{\partial^2 w}{\partial t^2} \rho_i dz \quad (2.6)$$

This can be expanded to:

$$\delta u \tau_{zx} \Big|_{z=z_{i+1}}^{z=z_i} - \int_{z_{i+1}}^{z_i} \frac{\partial(\delta u)}{\partial z} \tau_{zx} dz = \int_{z_{i+1}}^{z_i} \delta u \frac{\partial^2 u}{\partial t^2} \rho_i dz \quad (2.7)$$

$$\delta w \sigma_z \Big|_{z=z_{i+1}}^{z=z_i} - \int_{z_{i+1}}^{z_i} \frac{\partial(\delta w)}{\partial z} \sigma_z dz = \int_{z_{i+1}}^{z_i} \delta w \frac{\partial^2 w}{\partial t^2} \rho_i dz \quad (2.8)$$

The shear stress  $\tau_{zx}$  along layer interface  $i$  is constant, and because the layer interfaces are flat,  $\tau_{zx}$  is the only contributor to the  $x$ -traction at that interface,  $T_x|_{z=z_i}$ . Likewise,  $\sigma_z$  is the only contributor to  $T_z|_{z=z_i}$ .

For perfectly horizontal interfaces, as is the case with a regular layered medium, the following relationships between stresses and tractions of the layer interfaces apply.

$$\tau_{zx}|_{z=z_i} = T_x \Big|_{z=z_i} \quad (2.9)$$

$$\sigma_z|_{z=z_i} = T_z \Big|_{z=z_i} \quad (2.10)$$

$$\tau_{zx}|_{z=z_{i+1}} = -T_x \Big|_{z=z_{i+1}} \quad (2.11)$$

$$\sigma_z|_{z=z_{i+1}} = -T_z \Big|_{z=z_{i+1}} \quad (2.12)$$

Substituting the equivalence for the stresses and rearranging, we find:

$$\int_{z_{i+1}}^{z_i} \frac{\partial(\delta u)}{\partial z} \tau_{zx} dz + \int_{z_{i+1}}^{z_i} \delta u \frac{\partial^2 u}{\partial t^2} \rho_i dz = \delta u \left[ T_x \Big|_{z=z_i} + T_x \Big|_{z=z_{i+1}} \right] \quad (2.13)$$

$$\int_{z_{i+1}}^{z_i} \frac{\partial(\delta w)}{\partial z} \sigma_z dz + \int_{z_{i+1}}^{z_i} \delta w \frac{\partial^2 w}{\partial t^2} \rho_i dz = \delta w \left[ T_z \Big|_{z=z_i} + T_z \Big|_{z=z_{i+1}} \right] \quad (2.14)$$

We can add Equations 2.13 and 2.14 and express the sum as:

$$\int_{z_{i+1}}^{z_i} \frac{\partial}{\partial z} \left[ \delta u \ \delta w \right] \begin{bmatrix} \tau_{zx} \\ \sigma_z \end{bmatrix} + \int_{z_{i+1}}^{z_i} \left[ \delta u \ \delta w \right] \begin{bmatrix} \frac{\partial^2 u}{\partial t^2} \\ \frac{\partial^2 w}{\partial t^2} \end{bmatrix} \rho_i dz = \left[ \delta u \ \delta w \right] \begin{bmatrix} T_x|_{z=z_i} + T_x|_{z=z_{i+1}} \\ T_z|_{z=z_i} + T_z|_{z=z_{i+1}} \end{bmatrix} \quad (2.15)$$

The semidiscretization scheme discussed by Ikeda (2008) is used to transform the above relationship into a matrix equation of motion that describes the regular layered medium. In order to do so, it is assumed that the displacement field within a soil layer can be described by means of a linear interpolation of the displacements of the layer boundaries. All linear interpolation in the  $z$  direction can be represented by the following functions:

$$N_i(z) = \frac{z - z_{i+1}}{z_i - z_{i+1}} \quad (2.16)$$

$$N_{i+1}(z) = \frac{z_i - z}{z_i - z_{i+1}} \quad (2.17)$$

For a regular layered medium, both  $z_i$  and  $z_{i+1}$  are constant, and  $z_i - z_{i+1}$  represents the thickness of the layer,  $h_i$ . It is noted that the thickness of all layers must be sufficiently small to achieve adequate accuracy with the linear interpolation. Therefore, if necessary, physical layers should be subdivided for computational purposes.

A matrix that relates the nodal displacement of the layer boundaries to the displacement field within the soil layer represented by  $N_i$  for layer  $i$ , can be expressed in terms of the nodal interpolation functions above as:

$$\mathbf{N}_i = \begin{bmatrix} N_i(z) & 0 & N_{i+1}(z) & 0 \\ 0 & N_i(z) & 0 & N_{i+1}(z) \end{bmatrix} \quad (2.18)$$

The semidiscretization approximates the displacement field as the product of the matrix above and the nodal displacement vectors  $U_i$ . The displace-

ment field is written out as:

$$\begin{bmatrix} u \\ w \end{bmatrix} = \mathbf{N}_i \mathbf{U}_i \quad (2.19)$$

where  $U_i$  consists of the nodal displacement of the interfaces of layer  $i$ :

$$\mathbf{U}_i = \begin{bmatrix} U_i \\ W_i \\ U_{i+1} \\ W_{i+1} \end{bmatrix} \quad (2.20)$$

Using the semidiscretization above along with a Galerkin finite element approach, we obtain:

$$\int_{z_{i+1}}^{z_i} \frac{\partial \mathbf{N}_i^T}{\delta z} \begin{bmatrix} \tau_{zx} \\ \sigma_z \end{bmatrix} dz + \int_{z_{i+1}}^{z_i} \mathbf{N}_i^T \frac{\partial^2 \mathbf{N}_i}{\delta t^2} \rho_i dz = \begin{bmatrix} T_x|_{z=z_i} \\ T_z|_{z=z_i} \\ T_x|_{z=z_{i+1}} \\ T_z|_{z=z_{i+1}} \end{bmatrix} \quad (2.21)$$

For linear elastic homogeneous soil layers, we have a relationship between stress and strain as follows (in a horizontally layered medium, we have  $\frac{\partial u}{\partial x} = \frac{\partial w}{\partial x} = 0$ ):

$$\sigma_x = \lambda_i \frac{\partial w}{\partial z} \quad (2.22)$$

$$\sigma_z = (\lambda_i + 2G_i) \frac{\partial w}{\partial z} \quad (2.23)$$

$$\tau_{zx} = G_i \frac{\partial u}{\partial z} \quad (2.24)$$

where  $G_i$  is the shear modulus and  $\lambda_i$  is the Lamé modulus of layer  $i$ :

$$\begin{bmatrix} \tau_{zx} \\ \sigma_z \end{bmatrix} = \begin{bmatrix} G_i \frac{\partial u}{\partial z} \\ (\lambda_i + 2G_i) \frac{\partial w}{\partial z} \end{bmatrix} = \begin{bmatrix} G_i & 0 \\ 0 & \lambda_i + 2G_i \end{bmatrix} \begin{bmatrix} \frac{\partial u}{\partial z} \\ \frac{\partial w}{\partial z} \end{bmatrix} \quad (2.25)$$

Substituting Equation 2.25 into Equation 2.21, we get

$$\int_{z_{i+1}}^{z_i} \frac{\partial \mathbf{N}_i^T}{\delta z} \begin{bmatrix} G_i & 0 \\ 0 & \lambda_i + 2G_i \end{bmatrix} \frac{\partial \mathbf{N}_i}{\delta z} dz \mathbf{U}_i + \int_{z_{i+1}}^{z_i} \mathbf{N}_i^T \mathbf{N}_i \rho_i \frac{\partial^2 \mathbf{U}_i}{\partial t^2} = \begin{bmatrix} T_x|_{z=z_i} \\ T_z|_{z=z_i} \\ T_x|_{z=z_{i+1}} \\ T_z|_{z=z_{i+1}} \end{bmatrix} \quad (2.26)$$

Considering time-harmonic waves in the layered medium, we have

$$\frac{\partial^2 \mathbf{U}_i}{\partial t^2} = -\omega^2 \mathbf{U}_i \quad (2.27)$$

Using the simplification above, the system of equations of motion can be written as

$$\mathbf{K}_i \mathbf{U}_i = \mathbf{P}_i \quad (2.28)$$

where the dynamics stiffness matrix  $\mathbf{K}$  for layer  $i$  is expressed as:

$$\mathbf{K}_i = \int_{z_{i+1}}^{z_i} \frac{\partial \mathbf{N}_i^T}{\delta z} \begin{bmatrix} G_i & 0 \\ 0 & \lambda_i + 2G_i \end{bmatrix} \frac{\partial \mathbf{N}_i}{\delta z} dz - \omega^2 \int_{z_{i+1}}^{z_i} \mathbf{N}_i^T \mathbf{N}_i \rho_i dz \quad (2.29)$$

and, when evaluated, the above integral gives us:

$$\mathbf{K}_i = \frac{1}{(h)} \begin{bmatrix} G_i & 0 & -G_i & 0 \\ 0 & (\lambda_i + 2G_i) & 0 & -(\lambda_i + 2G_i) \\ -G_i & 0 & G_i & 0 \\ 0 & -(\lambda_i + 2G_i) & 0 & (\lambda_i + 2G_i) \end{bmatrix} - \omega^2 \frac{\rho_i}{6} (h) \begin{bmatrix} 2 & 0 & 1 & 0 \\ 0 & 2 & 0 & 1 \\ 1 & 0 & 2 & 0 \\ 0 & 1 & 0 & 2 \end{bmatrix} \quad (2.30)$$

Assuming that there are no externally applied loads at any of the layer interfaces, all components of  $\mathbf{P}$  other than for the end interfaces become zero due to internal tractions cancelling out, and, therefore, the loading vector  $\mathbf{P}$  is expressed as:

$$\mathbf{P}_i = \begin{bmatrix} T_x|_{z=z_i} \\ T_z|_{z=z_i} \\ T_x|_{z=z_{i+1}} \\ T_z|_{z=z_{i+1}} \end{bmatrix} \quad (2.31)$$

and the final system of equations is obtained:

$$\mathbf{K}\mathbf{U} = \mathbf{P} \quad (2.32)$$

The global matrix  $\mathbf{K}$  is a block tridiagonal matrix assembled from the layer matrices  $\mathbf{K}_i$  and the global load vector  $\mathbf{P}$  is given by:

$$\mathbf{P} = \begin{bmatrix} T_x|_{z=z_1} \\ T_z|_{z=z_1} \\ 0 \\ \cdot \\ 0 \\ T_x|_{z=z_{m+1}} \\ T_z|_{z=z_{m+1}} \end{bmatrix} \quad (2.33)$$

where  $m$  denotes the total number of layers.

## 2.2 Inclusions in Layered Media

In the one-dimensional analysis of regular layered media, soil properties are assumed to be constant throughout each layer. Analysis provided in the

previous section does not account for possible inclusions within one or more layers in the domain. Inclusions can represent localized variations of the soil properties within a layer in the domain. Analysis of heterogeneous soil layers is therefore of interest, and will be discussed as follows.

In general, variations of soil properties occur continuously throughout each soil layer. An effective way to model these variations is to divide each soil layer into intervals in the  $x$  direction, and assign representative soil properties for each interval. Analysis of such model would yield a coarse approximation of the site response, but more accurate results can be obtained using smaller intervals.

Such an analysis requires the ability to analyze the effects a single inclusion imposes on the response of the soil. It is therefore of interest to analyze a layered medium with homogeneous soil properties except for one inclusion, as seen in Figure 2.1. The response of a layered medium with multiple inclusions can be obtained as a linear combination of the solutions corresponding to the individual inclusions.

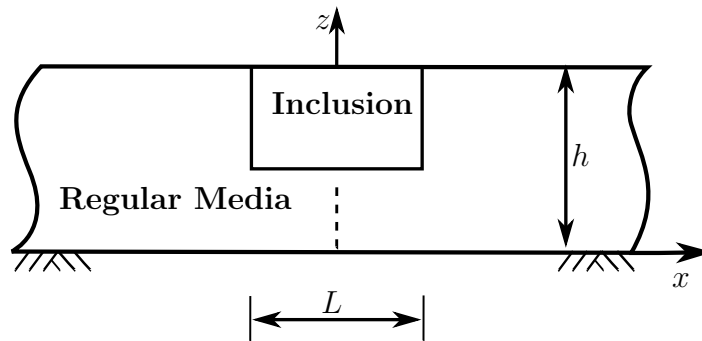


Figure 2.1: Inclusion in Layered Medium

A closed-form approach that can be used to account for variations in the horizontal direction will now be described. The approach is based on the work of Kausel (1981). For a vertically propagating shear wave through a regular layered medium, the modes of wave propagation are found as the eigenvectors,  $\boldsymbol{\phi}$ , of the following problem:

$$(k^2 \mathbf{A} + k\mathbf{B} + \mathbf{C}) \boldsymbol{\phi} = \mathbf{0} \quad (2.34)$$

where  $k$  is the wavenumber (eigenvalue), and  $\mathbf{A}$ ,  $\mathbf{B}$  and  $\mathbf{C}$  are matrices assembled from layer counterparts given by:

$$\mathbf{A}_i = \frac{h}{6} \begin{bmatrix} 2(\lambda + 2G) & 0 & \lambda + 2G & 0 \\ 0 & 2G & 0 & G \\ \lambda + 2G & 0 & 2(\lambda + 2G) & 0 \\ 0 & G & 0 & 2G \end{bmatrix} \quad (2.35)$$

$$\mathbf{B}_i = \frac{1}{2} \begin{bmatrix} 0 & \lambda - G & 0 & -(\lambda + G) \\ \lambda - G & 0 & \lambda + G & 0 \\ 0 & \lambda + G & 0 & -(\lambda - G) \\ -(\lambda + G) & 0 & -(\lambda - G) & 0 \end{bmatrix} \quad (2.36)$$

$\mathbf{C}$  is defined as  $\mathbf{C} = \mathbf{G} - \omega^2 \mathbf{M}$ , where  $\mathbf{G}$  and  $\mathbf{M}$  for layer  $i$  are:

$$\mathbf{G}_i = \frac{1}{h} \begin{bmatrix} G & 0 & -G & 0 \\ 0 & \lambda + 2G & 0 & -(\lambda + 2G) \\ -G & 0 & G & 0 \\ 0 & -(\lambda + 2G) & 0 & \lambda + 2G \end{bmatrix} \quad (2.37)$$

$$\mathbf{M}_i = \frac{\rho h}{6} \begin{bmatrix} 2 & 0 & 1 & 0 \\ 0 & 2 & 0 & 1 \\ 1 & 0 & 2 & 0 \\ 0 & 1 & 0 & 2 \end{bmatrix} \quad (2.38)$$



The formulation above assumes thin-layer discretization, where the layer thickness is much smaller than the length of traveling waves. Linear interpolation is applied for the displacement between layer interfaces.

Solving for the eigenvectors  $\boldsymbol{\phi}$  of Equation 2.34 is achieved by rearranging the rows and columns by the degrees of freedom of the problem. Equation 2.34 can then be expressed as;

$$\bar{\mathbf{A}}\mathbf{Z}\mathbf{K}^2 + \bar{\mathbf{C}}\mathbf{Z} = 0 \quad (2.39)$$

where

$$\bar{\mathbf{A}} = \begin{bmatrix} \mathbf{A}_x & \mathbf{0} \\ \mathbf{B}_{xz}^T & \mathbf{A}_z \end{bmatrix} \quad (2.40)$$

$$\bar{\mathbf{C}} = \begin{bmatrix} \mathbf{C}_x & \mathbf{B}_{xz} \\ \mathbf{0} & \mathbf{C}_z \end{bmatrix} \quad (2.41)$$

$$\mathbf{k} = \text{diag} [k_j] \quad (2.42)$$

$$\mathbf{Z} = \begin{bmatrix} \boldsymbol{\Phi}_x & \mathbf{0} \\ \boldsymbol{\Phi}_z & \mathbf{k} \end{bmatrix} \quad (2.43)$$

Another way of expressing the eigenvalue problem is as:

$$\bar{\mathbf{A}}^T \mathbf{Y} \mathbf{K}^2 + \bar{\mathbf{C}}^T \mathbf{Y} = 0 \quad (2.44)$$

where

$$\mathbf{Y} = \begin{bmatrix} \boldsymbol{\Phi}_x & \mathbf{k} \\ \boldsymbol{\Phi}_z & \mathbf{0} \end{bmatrix} \quad (2.45)$$

$\boldsymbol{\Phi}_x$  and  $\boldsymbol{\Phi}_z$  are the  $x$ - and  $z$ -components of the eigenvectors, respectively. An appropriate normalization of  $\mathbf{Y}$  and  $\mathbf{Z}$  is

$$\mathbf{Y}^T \bar{\mathbf{A}} \mathbf{Z} = \mathbf{k} \quad (2.46)$$

which is substituted into Equation 2.39 to give:

$$\mathbf{Y}^T \bar{\mathbf{C}} \mathbf{Z} = -\mathbf{k}^3 \quad (2.47)$$

The wave-number domain equation for equilibrium is:

$$(\bar{\mathbf{A}}k^2 + \bar{\mathbf{C}}) \begin{bmatrix} \bar{\mathbf{U}}_x \\ k\bar{\mathbf{U}}_z \end{bmatrix} = \begin{bmatrix} \bar{\mathbf{P}}_x \\ k\bar{\mathbf{P}}_z \end{bmatrix} \quad (2.48)$$

If this equation is premultiplied by  $\mathbf{Y}^T$  and an identity matrix is introduced in the form of  $\mathbf{Z}\mathbf{Z}^{-1}$ , we find:

$$(\mathbf{Y}^T \bar{\mathbf{A}} \mathbf{Z} \mathbf{Z}^{-1} k^2 + \mathbf{Y}^T \bar{\mathbf{C}} \mathbf{Z} \mathbf{Z}^{-1}) \begin{bmatrix} \bar{\mathbf{U}}_x \\ k\bar{\mathbf{U}}_z \end{bmatrix} = \mathbf{Y}^T \begin{bmatrix} \bar{\mathbf{P}}_x \\ k\bar{\mathbf{P}}_z \end{bmatrix} \quad (2.49)$$

Rearranging to separate the displacement vector gives:

$$\begin{bmatrix} \bar{\mathbf{U}}_x \\ k\bar{\mathbf{U}}_z \end{bmatrix} = \mathbf{Z} \mathbf{K}^{-1} (\mathbf{I} k^2 - \mathbf{k}^2) \mathbf{Y}^T \begin{bmatrix} \bar{\mathbf{P}}_x \\ k\bar{\mathbf{P}}_z \end{bmatrix} \quad (2.50)$$

If a matrix  $\mathbf{D}$  is defined as:

$$\mathbf{D} = \text{diag} (k^2 - k_j^2)^{-1} \quad (2.51)$$

then substituting Equations 2.43, 2.45 and 2.51 into Equation 2.50, the relationship between the load and displacement of the system can be expressed as:

$$\begin{bmatrix} \bar{\mathbf{U}}_x \\ \bar{\mathbf{U}}_z \end{bmatrix} = \begin{bmatrix} \Phi_x \mathbf{D} \Phi_x^T & k \Phi_x \mathbf{K}^{-1} \mathbf{D} \Phi_z^T \\ k \Phi_z \mathbf{D} \mathbf{K}^{-1} \Phi_x^T & \Phi_z \mathbf{D} \Phi_z^T \end{bmatrix} \begin{bmatrix} \bar{\mathbf{P}}_x \\ \bar{\mathbf{P}}_z \end{bmatrix} \quad (2.52)$$

The matrix appearing in the above expression will be referred to as the flexibility matrix  $\mathbf{F}$ :

$$\mathbf{F} = \begin{bmatrix} \Phi_x \mathbf{D} \Phi_x^T & k \Phi_x \mathbf{K}^{-1} \mathbf{D} \Phi_z^T \\ k \Phi_z \mathbf{D} \mathbf{K}^{-1} \Phi_x^T & \Phi_z \mathbf{D} \Phi_z^T \end{bmatrix} \quad (2.53)$$

The discussion by Kausel (1981) provides a Fourier transformation of  $\mathbf{F}$  in the process of finding Green's function. The Green's function is found for a unit line load applied in the vertical plane at  $x_0 = 0$ , described by

$$\tau = \delta(x - x_0) \quad (2.54)$$

Kausel (1981) developed the integrations below:

$$\frac{1}{2\pi} \int_{-\infty}^{\infty} \mathbf{D} e^{-ikx} dk = \frac{1}{2i} \mathbf{E}_{|x|} \mathbf{K}^{-1} \quad (2.55)$$

$$\frac{1}{2\pi} \int_{-\infty}^{\infty} k \mathbf{D} e^{-ikx} dk = \begin{cases} \frac{1}{2i} \mathbf{E}_x & x > 0 \\ 0 & x = 0 \\ -\frac{1}{2i} \mathbf{E}_{-x} & x < 0 \end{cases} \quad (2.56)$$

where

$$\mathbf{E}_x = \text{diag} \{ e^{-ik_j x} \} \quad (2.57)$$

Equations 2.55, 2.56 can be used in conjunction with Equation 2.53 to produce Green's function:

$$\begin{bmatrix} \bar{\mathbf{U}}_x \\ \bar{\mathbf{U}}_z \end{bmatrix} = \frac{1}{2i} \begin{bmatrix} \Phi_x \mathbf{E}_{|x|} \mathbf{K}^{-1} \Phi_x^T & \pm i \Phi_x \mathbf{E}_{|x|} \mathbf{K}^{-1} \Phi_z^T \\ \mp i \Phi_z \mathbf{E}_{|x|} \mathbf{K}^{-1} \Phi_x^T & \Phi_z \mathbf{E}_{|x|} \mathbf{K}^{-1} \Phi_z^T \end{bmatrix} \quad (2.58)$$

The expression above already accounts for the implicit imaginary factor  $i$  carried by the vertical displacement and load vectors.  $\pm$  and  $\mp$  represent a positive sign for  $x \geq 0$  and a negative for  $x < 0$ , and vice versa. If the line load is applied at  $x_0 = \xi$  instead, then a simple linear translation will provide the displacement solution.

For a layered medium with load applied over a finite interval  $a < x < b$ , Green's function can be integrated to provide the response of the layer:

$$\mathbf{U} = \int_a^b \mathbf{F}(x - \xi) \mathbf{P}(\xi) d\xi \quad (2.59)$$

which can be integrated explicitly.

Calculation of the additional response of layered media due to inclusions can be done using Green's function. The response can be found by representing the difference in soil properties as an equivalent load acting on the regular layered medium. Representation of soil-property variations as equivalent loads can be done by using the perturbation approach discussed in Chapter 4.

The additional response will be equal to the response of the regular layered medium due to the equivalent load.

Green's function along with the perturbation method provides the means to verify solutions obtained from numerical procedures. It provides an exact closed-form solution for site-response analysis. However, the process of calculating the integrations above for each inclusion can become computationally intensive. An extensive study of site-response analysis with numerous soil property variations requires a more efficient numerical procedure. A finite-element based numerical procedure is introduced in the next section to allow for efficient computation.

### **2.3 Finite Element Analysis and Formulation**

A finite element approach to the analysis of soil-structure system response is applied to the near-field region, in the vicinity of the structural foundation. A special treatment of this region is needed to account for the irregularities introduced by the foundation embedment.

Several types of finite elements are needed to fully represent the near-field region. Models that will be used to assist the near-field analysis include a finite-element representation of the soil in the region near the foundation. The soil next to the foundation is discretized using quadrilateral finite elements, whereas soil far away is modeled using hyperelements. The foundation is modeled through the use of rigid elements. A simple mass-spring representation will be used to model the structure.

### 2.3.1 Quadrilateral Elements

The near-field domain is discretized into a number of four-node elements as shown in Figure 2.2. In general, quadrilateral but non-rectangular elements may be required for some geometries. Each node has two degrees of freedom, the total degrees of freedom for a linear rectangular element would be eight.

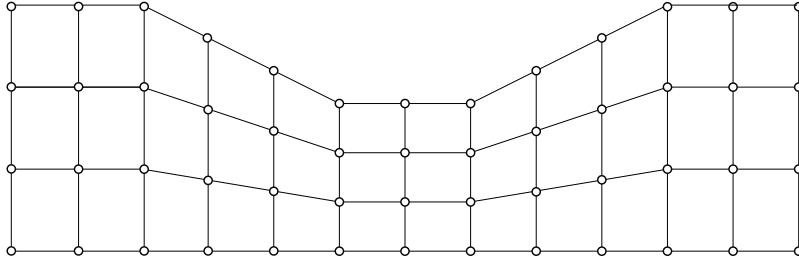


Figure 2.2: Near-Field Discretization with Quadrilateral Elements

For the quadrilateral element we use in our field analysis, we will need to determine both the stiffness and the strain values. The latter are needed to adjust the soil properties with regards to the level of deformation. These are derived below.

The element can be analyzed in either global coordinates or local coordinates where the relationship between the two coordinates systems is as follows:

$$\xi = \frac{1}{a} \left( x - \frac{x_1 + x_2}{2} \right), \quad \eta = \frac{1}{a} \left( z - \frac{z_1 + z_2}{2} \right) \quad (2.60)$$

The shape function matrix for the quadrilateral element is

$$\mathbf{N}(\xi, \eta) = \begin{bmatrix} N_1 & 0 & N_2 & 0 & N_3 & 0 & N_4 & 0 \\ 0 & N_1 & 0 & N_2 & 0 & N_3 & 0 & N_4 \end{bmatrix} \quad (2.61)$$

with the bilinear shape functions expressed as:

$$N_1(\xi, \eta) = \frac{1}{4}(1 - \xi)(1 - \eta) \quad (2.62)$$

$$N_2(\xi, \eta) = \frac{1}{4}(1 + \xi)(1 - \eta) \quad (2.63)$$

$$N_3(\xi, \eta) = \frac{1}{4}(1 + \xi)(1 + \eta) \quad (2.64)$$

$$N_4(\xi, \eta) = \frac{1}{4}(1 - \xi)(1 + \eta) \quad (2.65)$$

The relationship between strain and displacement of the element can be expressed as:

$$\varepsilon = \mathbf{B}\mathbf{d} \quad (2.66)$$

where  $\mathbf{B}$  is known as the strain matrix. The strain can be found by:

$$\mathbf{B}(\xi, \eta) = \begin{bmatrix} \frac{\partial}{\partial x} & 0 \\ 0 & \frac{\partial}{\partial z} \\ \frac{\partial}{\partial z} & \frac{\partial}{\partial x} \end{bmatrix} \mathbf{N}(\xi, \eta) \quad (2.67)$$

which for the four-node quadrilateral elements can be written as:

$$\mathbf{B}(\xi, \eta) = \frac{1}{4ab} \begin{bmatrix} -b(1 - \eta) & 0 & -a(1 - \xi) \\ 0 & -a(1 - \xi) & -b(1 - \eta) \\ b(1 - \eta) & 0 & -a(1 + \xi) \\ 0 & -a(1 + \xi) & b(1 - \eta) \\ b(1 + \eta) & 0 & a(1 + \xi) \\ 0 & a(1 + \xi) & b(1 + \eta) \\ -b(1 + \eta) & 0 & a(1 - \xi) \\ 0 & a(1 - \xi) & -b(1 + \eta) \end{bmatrix}^T \quad (2.68)$$

The constitutive matrix  $\mathbf{D}$  that applies for plane strain is

$$\mathbf{D} = \begin{bmatrix} \lambda + 2G & \lambda & 0 \\ \lambda & \lambda + 2G & 0 \\ 0 & 0 & G \end{bmatrix} \quad (2.69)$$

in which  $G$  is the shear modulus and  $\lambda$  is the Lamé modulus of the soil.

For a quadrilateral element in plane strain assuming unit thickness in the out-of-plane direction, the general expression for the finite element stiffness matrix is

$$\mathbf{K} = \int_{-1}^1 \int_{-1}^1 ab \mathbf{B}^T \mathbf{D} \mathbf{B} d\xi d\eta \quad (2.70)$$

where  $\mathbf{B}$  and  $\mathbf{D}$  are as previously formulated.

The stiffness matrix above can be integrated as a closed form solution, but is more efficiently evaluated using the Gauss numerical integration scheme. Gauss integration scheme consists of taking the weighted sum of the integrand which is evaluated at four representative Gauss points in the element.

Second-order Gauss integration points are located at local coordinates  $\left(\frac{-1}{\sqrt{3}}, \frac{-1}{\sqrt{3}}\right)$ ,  $\left(\frac{1}{\sqrt{3}}, \frac{-1}{\sqrt{3}}\right)$ ,  $\left(\frac{1}{\sqrt{3}}, \frac{1}{\sqrt{3}}\right)$ , and  $\left(\frac{-1}{\sqrt{3}}, \frac{1}{\sqrt{3}}\right)$ , and the weight coefficient of 1 is assigned to all of the points. The stiffness matrix is then equivalent to the sum of the weighted evaluations, and can be expressed as:

$$\mathbf{K} = ab \sum_{j=1}^n \sum_{i=1}^n w_i w_j \mathbf{B}^T(\xi_i, \eta_j) \mathbf{D} \mathbf{B}(\xi_i, \eta_j) \quad (2.71)$$

A second-order Gauss integration scheme will yield exact results for at most degree-3 polynomial integrands. For the stiffness matrix above, the strain matrix  $\mathbf{B}$  is a linear polynomial in  $\xi$  and  $\eta$ . Thus, the integrand is a product



of two linear polynomials which is a quadratic one. Therefore the formulation above provides the exact evaluation of the stiffness matrix.

Mass matrix for a quadrilateral element is evaluated as

$$\mathbf{M} = \int_{-1}^{+1} \int_{-1}^{+1} ab \rho \mathbf{N}^T \mathbf{N} \, d\xi \, d\eta \quad (2.72)$$

which when evaluated explicitly, results in the element mass matrix below

$$\mathbf{M} = \frac{\rho hab}{9} \begin{bmatrix} 4 & 0 & 2 & 0 & 1 & 0 & 2 & 0 \\ 0 & 4 & 0 & 2 & 0 & 1 & 0 & 2 \\ 2 & 0 & 4 & 0 & 2 & 0 & 1 & 0 \\ 0 & 2 & 0 & 4 & 0 & 2 & 0 & 1 \\ 1 & 0 & 2 & 0 & 4 & 0 & 2 & 0 \\ 0 & 1 & 0 & 2 & 0 & 4 & 0 & 2 \\ 2 & 0 & 1 & 0 & 2 & 0 & 4 & 0 \\ 0 & 2 & 0 & 1 & 0 & 2 & 0 & 4 \end{bmatrix} \quad (2.73)$$

The equation of motion for the element is described as

$$\mathbf{M} \frac{\partial^2 \mathbf{U}}{\partial t^2} + \mathbf{K} \mathbf{U} = \mathbf{P} \quad (2.74)$$

where  $\mathbf{U}$  is the element nodal displacement and  $\mathbf{P}$  is the nodal load. Considering that the analysis will be conducted in the frequency domain where  $\frac{\partial^2 \mathbf{U}}{\partial t^2} = -\omega^2 \mathbf{U}$ , we can simplify the above as

$$(\mathbf{K} - \omega^2 \mathbf{M}) \mathbf{U} = \mathbf{P} \quad (2.75)$$

Therefore, the dynamic stiffness of the quadrilateral element can be represented by  $(\mathbf{K} - \omega^2 \mathbf{M})$  where  $\mathbf{K}$  and  $\mathbf{M}$  are as previously defined. Element matrices discussed above can be assembled into the global matrix. The procedure will be discussed in Chapter 4.

### 2.3.2 Rigid-Foundation Elements

In the work presented herein, the interface between the soil and the structure is assumed to be a rigid foundation. The foundation is composed of a horizontal mat and vertical side walls, embedded into the soil layers. The rigid foundation is as shown in Figure 2.3 below:

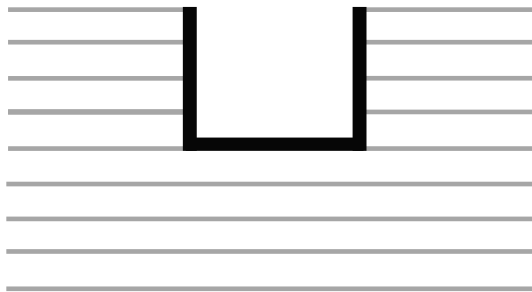


Figure 2.3: Rigid Foundation

The foundation in Figure 2.3 can be represented with rigid elements, which do not deform axially or flexurally. A rigid element ensures a fixed distance between any two nodes of the foundation. As a result, each node is rigidly connected to all of the other nodes. This represents a convenient simplification for the purposes of this study. Flexible connection elements may be used for other cases as needed.

In order to model the rigid foundation mat and walls, we need to implement some conditions to the foundation nodes in order to ensure rigid-body behavior. This implies that the distance between any two nodes within the foundation is constant at all times. Alternatively, one reference node, e.g.,

central node of the foundation, can be connected by rigid elements to all the other nodes.

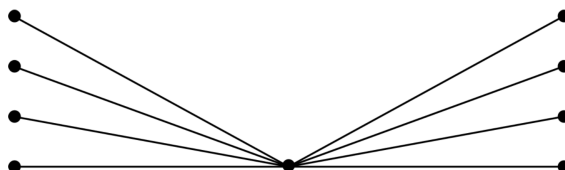


Figure 2.4: Representation of Foundation using Rigid Links

The reference node can be different from the center of mass of the foundation. It should be chosen on the basis of convenience.

Let us examine the connection between one pair of nodes of the foundation.

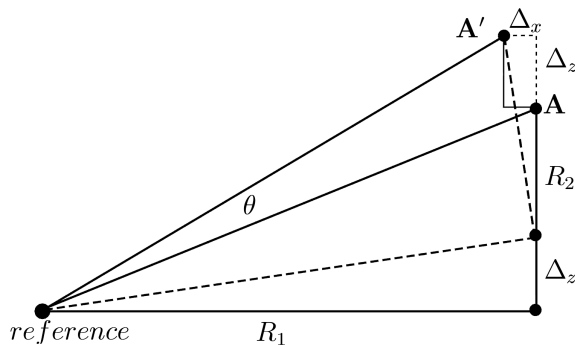


Figure 2.5: Rigid Connection

The motion of both nodes is governed by the overall translation of the foundation as well as the rotation of the foundation with respect to the reference node.

A purely translational motion will not change the distance between the two nodes in either the horizontal  $x$  or vertical  $z$  directions. Therefore, the displacements of both nodes in the  $x$  and  $z$  direction remains the same, i.e  $u_{ax} = u_{cx}$  and  $u_{ay} = u_{cy}$ .

A rotation of the foundation however will cause a change in the distance between the two nodes in terms of the  $x$  and  $z$  directions. The changes are  $\Delta_x$  and  $\Delta_z$ , respectively. Positive counterclockwise rotation convention is assumed. As seen in Figure 2.5, a rotation of  $\theta$  will induce a change of distance of:

$$\Delta_x = -R_2\theta \quad (2.76)$$

$$\Delta_z = R_1\theta \quad (2.77)$$

Using the above relationships to express the overall change of coordinates between the two nodes, we get:

$$u_{ax} - u_{cx} + R_2\theta = 0 \quad (2.78)$$

$$u_{ay} - u_{cy} - R_1\theta = 0 \quad (2.79)$$

Additionally, we have equilibrium of external forces that act on the two nodes. In essence,

$$\mathbf{F}_{ax} = -\mathbf{F}_{cx} \quad (2.80)$$

$$\mathbf{F}_{ay} = -\mathbf{F}_{cy} \quad (2.81)$$

Combining all the relationships defined above together with identity properties allows for expression of the rigid connection as a 7-by-7 system of equations expressed in matrix form.

$$\begin{bmatrix} 0 & 0 & -1 & 0 & 0 & 0 & 0 \\ 0 & 0 & 0 & -1 & 0 & 0 & 0 \\ -1 & 0 & 0 & 0 & +1 & 0 & -R_2 \\ 0 & -1 & 0 & 0 & 0 & +1 & R_1 \\ 0 & 0 & +1 & 0 & 0 & 0 & 0 \\ 0 & 0 & 0 & +1 & 0 & 0 & 0 \\ 0 & 0 & -R_2 & R_1 & 0 & 0 & 0 \end{bmatrix} \begin{bmatrix} u_{1x} \\ u_{1y} \\ F_{1x} \\ F_{1y} \\ u_{2x} \\ u_{2y} \\ u_{2\theta} \end{bmatrix} = \begin{bmatrix} -F_{1x} \\ -F_{1y} \\ 0 \\ 0 \\ -F_{2x} \\ -F_{2y} \\ M_2 \end{bmatrix} \quad (2.82)$$

This matrix is singular, which is acceptable because the rigid link is not anchored down by boundary conditions.

The choice of expressing the rigid connection as an 7-by-7 matrix as opposed to the minimum required five degree of freedom matrix is for ease of assembly into the global matrix. Mapping of the stiffness matrix to the global matrix will be optimized for an 8-by-8 quadrilateral element matrix. Details of this optimization will be discussed in Chapter 4. Representing the rigid foundation as an 8-by-8 matrix with an eighth row and an eighth column of zeros, the efficient mapping and assembly procedures developed for quadrilateral elements can also be applied to rigid elements.

Mapping procedures used in later analysis assume eight degrees of freedom in the rigid element stiffness matrix. The degrees of freedom are contributions from four nodes with two degrees of freedom in each node (for  $x$  and

$z$  directions). The first and second node is associated with the actual node A. Node 1 represents the displacements of node A, and node 2 represents the loading on node A. Contributions of node 2 to the system of equations are the force equilibrium equations of Equations 2.80 and 2.81.

The third and fourth nodes are associated with the reference node, which in this case is the actual center node of the foundation. The third node represents displacements of the actual center node. The fourth node represents rotation of the actual center node and a dummy placeholder.

### 2.3.3 Hyperelements

Hyperelements provide equivalent representations of the regions bordering the near field. The role of the hyperelement is to provide consistent transmitting boundaries which accurately represent the far field. It contributes both an equivalent stiffness to the overall soil structure system, as well as consistent nodal forces which represent the internal forces at the boundary of the near field.

Consistent nodal forces are given by

$$\mathbf{F} = \int_{z_{i+1}}^{z_i} \begin{bmatrix} T_x(x, z) \\ T_z(x, z) \end{bmatrix} dz \quad (2.83)$$

where  $T_x(x, z)$  and  $T_z(x, z)$  are the  $x$  and  $z$  components of the traction acting on the vertical plane. Based on the constitutive relationship, the tractions are

defined as:

$$T_x(x, z) = -(\lambda + 2G) \frac{\partial u}{\partial x} - \lambda \frac{\partial w}{\partial z} \quad (2.84)$$

$$T_z(x, z) = -G \left( \frac{\partial w}{\partial x} + \frac{\partial u}{\partial z} \right) \quad (2.85)$$

Semidiscretization of the layers leads to approximation of soil layer response as:

$$\begin{bmatrix} u(x, z) \\ w(x, z) \end{bmatrix} = \mathbf{N}_i(z) \mathbf{U}_i(x) \quad (2.86)$$

where  $\mathbf{U}_i(x)$  is the vector of nodal displacements. The nodal interpolation function matrix  $\mathbf{N}_i(z)$  is defined in Equation 2.18. By combining Equations 2.84, 2.85 and 2.86, the traction can be written as:

$$\begin{aligned} \begin{bmatrix} T_x(x, z) \\ T_z(x, z) \end{bmatrix} &= - \begin{bmatrix} (\lambda_i + 2G_i) & 0 \\ 0 & G_i \end{bmatrix} \mathbf{N}_i(z) \frac{d\mathbf{U}_i(x)}{dx} \\ &\quad - \begin{bmatrix} 0 & \lambda_i \\ G_i & 0 \end{bmatrix} \frac{\partial \mathbf{N}_i(z)}{\partial z} \mathbf{U}_i(x) \end{aligned} \quad (2.87)$$

Consistent nodal forces acting on layer  $i$  at the vertical boundary ( $x = 0$ ), are expressed as:

$$\mathbf{F}_i = \int_{z_{i+1}}^{z_i} (\mathbf{N}_i(z))^T \begin{bmatrix} T_x(x, z) \\ T_z(x, z) \end{bmatrix} dz \quad (2.88)$$

$$\begin{aligned} &= - \int_{z_{i+1}}^{z_i} (\mathbf{N}_i(z))^T \begin{bmatrix} (\lambda_i + 2G_i) & 0 \\ 0 & G_i \end{bmatrix} \mathbf{N}_i(z) dz \left( \frac{d\mathbf{U}_i(x)}{dx} \right) \Big|_{x=0} \\ &\quad - \left( \int_{z_{i+1}}^{z_i} (\mathbf{N}_i(z))^T \begin{bmatrix} 0 & \lambda_i \\ G_i & 0 \end{bmatrix} \frac{\partial \mathbf{N}_i(z)}{\partial z} dz \mathbf{U}_i(x) \right) \Big|_{x=0} \end{aligned} \quad (2.89)$$

The unbounded medium of the hyperelement is to the right of the vertical boundary (in the positive  $x$ -direction).

Evaluating the above integral, we can rewrite the consistent nodal forces as

$$\mathbf{F} = -\mathbf{A} \left. \frac{d\mathbf{U}(x)}{dx} \right|_{x=0} + \mathbf{D}\mathbf{U}(0) \quad (2.90)$$

where

$$\mathbf{A}_i = \frac{h}{6} \begin{bmatrix} 2(\lambda_i + 2G_i) & 0 & (\lambda_i + 2G_i) & 0 \\ 0 & 2G_i & 0 & G_i \\ (\lambda_i + 2G_i) & 0 & 2(\lambda_i + 2G_i) & 0 \\ 0 & G_i & 0 & 2G_i \end{bmatrix} \quad (2.91)$$

$$\mathbf{D}_i = \frac{1}{2} \begin{bmatrix} 0 & -\lambda_i & 0 & \lambda_i \\ -G_i & 0 & G_i & 0 \\ 0 & -\lambda_i & 0 & \lambda_i \\ -G_i & 0 & G_i & 0 \end{bmatrix} \quad (2.92)$$

The displacement vector  $\mathbf{U}(x)$  is represented in terms of a linear combination of semidiscrete modes as seen in Equation 2.58. Both the displacement vector and its rate of change with respect to  $x$  as evaluated at  $x = 0$  can be reexpressed as:

$$\mathbf{U}(0) = \mathbf{X} \mathbf{\Gamma} \quad (2.93)$$

$$\left. \frac{d\mathbf{U}(x)}{dx} \right|_{x=0} = -i \mathbf{X} \mathbf{K} \mathbf{\Gamma} \quad (2.94)$$



$\mathbf{\Gamma}$  is the vector of the modal participation factors, and  $\mathbf{K}$  is the diagonal matrix of the plane-strain wave numbers. The wavenumbers are eigenvalues of Equation 2.34.

The columns of the modal matrix  $\mathbf{X}$  contain the mode shapes for the plane-strain case. For  $n$ , the number of modes is  $2n$ . The modal matrix is expressed as:

$$\mathbf{X} = [\mathbf{\Delta}_1, \mathbf{\Delta}_2, \dots, \mathbf{\Delta}_{2n}] \quad (2.95)$$

The mode shapes  $\mathbf{\Delta}_i$  can be obtained as the eigenvectors of Equation 2.34. Further details and discussions can be found in the works of Kausel (1981) and Ikeda (2008).

The vector of consistent nodal forces  $\mathbf{F}$  at the vertical boundary can then be calculated by substituting Equations 2.93 and 2.94 into Equation 2.90. The final form is:

$$\mathbf{F} = (i\mathbf{A} \mathbf{X} \mathbf{K} \mathbf{X}^{-1} + \mathbf{D}) \mathbf{U} \quad (2.96)$$

With the above expression of the consistent nodal forces as a matrix product of a certain stiffness matrix multiplied by displacement vector, we can conclude that the stiffness matrix associated with the hyperelement can be expressed as:

$$\mathbf{S} = i\mathbf{A} \mathbf{X} \mathbf{K} \mathbf{X}^{-1} + \mathbf{D} \quad (2.97)$$

The stiffness matrix corresponding to the hyperelement of opposite configuration (extending in the negative  $x$ -direction) can be found by changing

the signs of the coupling terms between the horizontal and vertical degrees of freedom.

## 2.4 Soil-Structure System Model

Near-field analysis accounts for the variation of soil properties that occur near an embedded foundation. A complete site-response analysis must also account for the effects the structure imposes on the soil. The structural response during an earthquake event depends on the response of the soil, and motion of the structure also provides feedback that affects the soil. Soil-structure interaction represents an important part of the site-response analysis, and is discussed in this section.

The motion of the structural mass imposes an inertial load on the soil which affects the response of the soil. The inertial interaction can be represented by including the effects of the structural mass into the analysis of the soil layer. The presence of the structure can be combined into the soil analysis by presenting an equivalent stiffness and mass representation into the soil system of equations.

A representation of a structure with an embedded foundation is shown in Figure 2.6. In general, a structure is a complex system with numerous vibration modes and variability in terms of both the mass distribution and the stiffness. Modeling the complexity of actual structures is not necessary in studying the effects of soil-property adjustments on the site response.

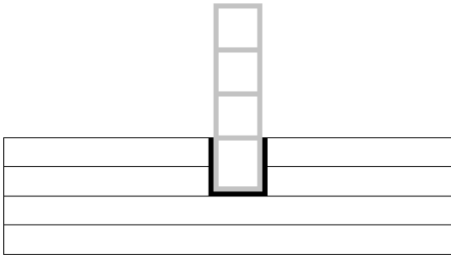


Figure 2.6: Structure Embedded in a Soil Layer

A simple representation of the structure used for the purposes of this study is shown in Figure 2.7. The representative structure is a single point mass located at the top of a structural beam, the mass of the structure being  $m$  and the stiffness  $k$ . The connection between the structure and the foundation is assumed to be rigid. Translation and rotation that occur at the base of the structure are only due to the motion of the soil.

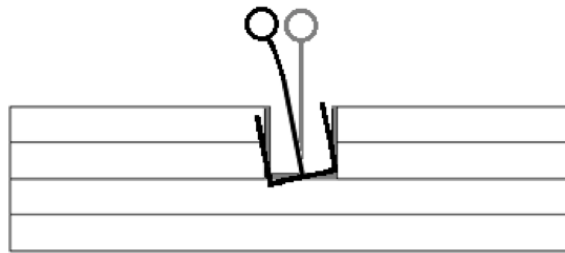


Figure 2.7: Simple Structure Representation

A way to incorporate the structure into the soil response calculation is to introduce an equivalent stiffness to the soil system. A spring-mass system

is used to model the structure, and analysis of equilibrium of the structure is carried out for the direction of structural movement. The analysis will produce the equivalent stiffness of the structure which will be added to the soil stiffness. Calculating the response of the soil system with the additional equivalent stiffness from the structure will produce the response of the soil-structure system.

The equivalent horizontal stiffness of the structure is determined for the representation in Figure 2.8.

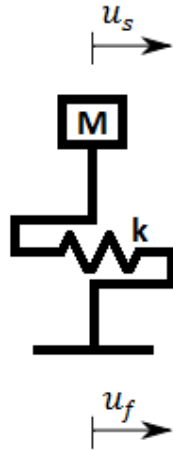


Figure 2.8: Equivalent Horizontal Stiffness of the Structure

Hysteretic damping is assumed for the structure. The dynamic stiffness can then be expressed as:

$$k = k_o(1 + 2i \beta_{str}) \quad (2.98)$$

where  $k_o$  is the stiffness of the structure and  $\beta_{str}$  is its damping ratio. Denoting the global displacement of the structure by  $u_s$  and the foundation displacement

by  $u_f$ , the equation of motion for the structural mass is:

$$m\ddot{u}_s + ku_s = ku_f \quad (2.99)$$

Assuming time-harmonic response, we have:

$$\ddot{u}_s = -\omega^2 u_s \quad (2.100)$$

Substituting Equation 2.100 into Equation 2.99 and rearranging gives an expression for the displacement of the structure in terms of the foundation displacement:

$$u_s = \frac{ku_f}{-\omega^2 m + k} \quad (2.101)$$

The lateral force that occurs on the spring is therefore:

$$F = k(u_s - u_f) \quad (2.102)$$

$$= k \left( \frac{ku_f}{k - \omega^2 m} - u_f \right) \quad (2.103)$$

$$= k \left( \frac{k}{k - \omega^2 m} - 1 \right) u_f \quad (2.104)$$

and, if the force acting on the foundation is expressed as

$$F = k_{eq} u_f \quad (2.105)$$

then the equivalent horizontal stiffness is

$$k_{eq} = k \left( \frac{k}{k - \omega^2 m} - 1 \right) \quad (2.106)$$

For a nearly rigid structure, the equivalent stiffness approaches  $\omega^2 m$  which is the equivalent of applying the inertia of the mass directly to the soil system.

If foundation rotation is considered, additional modification is needed to incorporate both the horizontal and rotational effects of the structure on the soil. Effects of rotation can be analyzed by examining the moment equilibrium of the structural mass. The mass displacement and rotation are as shown in Figure 2.9:

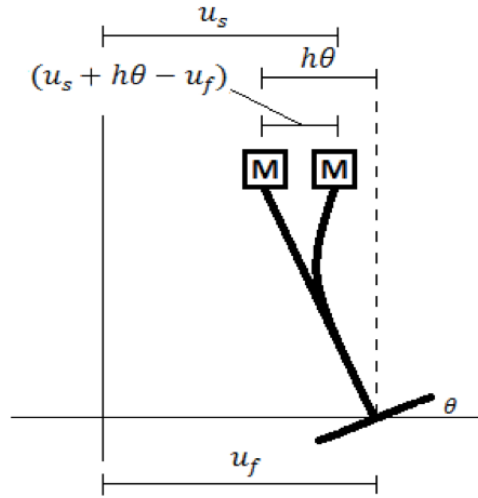


Figure 2.9: Displacement of Structural Mass and Foundation

In Figure 2.9,  $\theta$  is the counterclockwise-positive rotation of the foundation base and  $h$  is the height of the structure. Small rotation is assumed. The displacement of the structure due to rotation is  $h\theta$  and the displacement due to bending is:

$$u_{flex} = u_s - u_f + h\theta \quad (2.107)$$

Considering equilibrium of forces in the horizontal direction leads to:

$$m\ddot{u}_s = (-\omega^2 m) u_s = -k(u_s - u_f + h\theta) \quad (2.108)$$

The displacement of the structural mass can be determined by rearranging Equation 2.108. The structural displacement is found to be:

$$u_s = \frac{ku_f - kh\theta}{-\omega^2m + k} \quad (2.109)$$

The horizontal force exerted on the mass is equal to the force of the spring undergoing a displacement  $u_{flex}$ . Therefore, the lateral force that occurs on the spring is:

$$F = k(u_s - u_f + h\theta) \quad (2.110)$$

$$= k\left(\frac{ku_f - kh\theta}{-\omega^2m + k} - u_f + h\theta\right) \quad (2.111)$$

$$= k\left(\frac{k}{k - \omega^2m} - 1\right)u_f - k\left(\frac{kh}{-\omega^2m + k} - h\right)\theta \quad (2.112)$$

Equation 2.112 provides the same horizontal equivalent stiffness as previously derived in Equation 2.106.

Additionally, Equation 2.112 establishes the coupling components between the rotation and displacement of the soil-structure system. The relationship between rotation and the horizontal force is observed as the coefficient of  $\theta$  in equation 2.112.

The moment acting at the base of the foundation is:

$$M = -ku_{flex}h \quad (2.113)$$

$$= -k\left(\frac{ku_f - kh\theta}{-\omega^2m + k} - u_f + h\theta\right)h \quad (2.114)$$

$$= -k\left(\frac{kh}{-\omega^2m + k} - h\right)hu_f + kh\left(\frac{kh}{-\omega^2m + k} - h\right)\theta \quad (2.115)$$

Combining Equation 2.112 and Equation 2.115, the force and moment acting on the foundation due to the structural displacement can be expressed in matrix form:

$$\begin{bmatrix} \mathbf{F} \\ \mathbf{M} \end{bmatrix} = \begin{bmatrix} k \left( \frac{k}{k - \omega^2 m} - 1 \right) & -k \left( \frac{kh}{-\omega^2 m + k} - h \right) \\ -k \left( \frac{kh}{-\omega^2 m + k} - h \right) & kh \left( \frac{kh}{-\omega^2 m + k} - h \right) \end{bmatrix} \begin{bmatrix} u_f \\ \theta \end{bmatrix} \quad (2.116)$$

Therefore, the equivalent stiffness of the structure to be added to the soil is:

$$\mathbf{K}_{eq} = \begin{bmatrix} k \left( \frac{k}{k - \omega^2 m} - 1 \right) & -k \left( \frac{kh}{-\omega^2 m + k} - h \right) \\ -k \left( \frac{kh}{-\omega^2 m + k} - h \right) & kh \left( \frac{kh}{-\omega^2 m + k} - h \right) \end{bmatrix} \quad (2.117)$$

The structural mass will not be explicitly represented by a degree of freedom in the analysis. Instead, the equivalent dynamic stiffness is included in the system in the process of evaluating the foundation response. Once the foundation displacement is obtained, the structural acceleration can be computed as:

$$\ddot{u}_s = -\frac{k}{m} (u_s - u_f + h\theta) \quad (2.118)$$

where the structural displacement  $u_s$  is computed by substituting the foundation response into Equation 2.109. The relative structural displacement can be found by subtracting the foundation displacement from  $u_s$ .



## Chapter 3

### Soil Properties Consistent with Deformation

The site-response analysis that will be conducted in this research is based on two alternative sets of soil properties: hypothetical and actual. The latter are those of a site in Mexico City subjected to the 1985 earthquake. The soil properties and their adjustments with respect to the site response will be discussed in this chapter.

The underlying assumption in site-response analysis is that the soil is made up of stratified layers. A one-dimensional site characterization is typically considered sufficient as the soil layers are assumed to be homogeneous in the horizontal direction. In the context of equivalent linear analysis, the soil is assumed to be a linear viscoelastic solid and can be represented as a combination of elastic springs and viscous dashpots (Kramer, 1996).

Soil properties initially assigned to each layer correspond to small strain levels. Soil properties of interest include the shear modulus, damping ratio, Poisson's ratio and mass density. Many other soil properties contribute to site characterization but only the properties listed are considered for the present analysis.

Determination of soil properties can be achieved by different means, for example, lab testing of soil samples taken from the site. Different methods of determining the shear modulus from samples are available (Kramer, 1996).

For a vertically propagating wave of frequency  $\omega$ , the soil response can be expressed as a function of location and time as:

$$u(z, t) = A e^{i(\omega t + kz)} + B e^{i(\omega t - kz)} \quad (3.1)$$

where  $A$  is the amplitude of the upward wave,  $B$  is the amplitude of the downward wave and  $k$  represents the wavenumber. The wavenumber can be expressed in terms of shear-wave velocity as:

$$k = \frac{\omega}{C_s} \quad (3.2)$$

where  $C_s$  is the measured shear-wave velocity. The shear-wave velocity also characterizes the fundamental frequency of the soil deposit, given by

$$\omega_{fund} = \frac{2\pi C_s}{4H} \quad (3.3)$$

The measured shear wave velocity provides the shear modulus for the soil. The small-strain shear modulus is expressed as:

$$G_{max} = \rho C_s^2 \quad (3.4)$$

where  $\rho$  is the density of the soil.

Poisson's ratio for clayey soil is typically 0.3 to 0.4 and about 0.25 for sandy soil. Combined with the shear modulus, Poisson's ratio defines the Lamé

modulus to be used in constructing the stiffness matrices described in Chapter 2. The Lamé modulus is expressed as:

$$\lambda = \frac{2G\nu}{1 - 2\nu} \quad (3.5)$$

Damping of the soil is determined by either a cyclic triaxial test or a resonant column test. Generally accepted values range from 1-5% for small strain and up to 20% for high magnitude excitations.

Presence of damping in the soil is integrated into the site-response analysis through the use of complex shear modulus. The latter can represent hysteretic damping approximately, and is evaluated according to Kramer (1996) as:

$$G^* = G \left( 1 - 2\beta^2 + i2\beta\sqrt{1 - \beta^2} \right) \quad (3.6)$$

where  $\beta$  is the soil's damping ratio.

For damping ratio values normally encountered in practice (up to 20%), the complex shear modulus expression can be simplified as:

$$G^* \approx G(1 + i2\beta) \quad (3.7)$$

Determination of related parameters, including the Lamé modulus, complex wavenumber and complex shear-wave velocity will be based on the complex shear modulus given in Equation 3.7.

### 3.1 Theoretical Site Characterization

The first part of the soil-structure system analysis involves an idealized soil layer supporting a massive structure. This case study can be representative of a nuclear power plant with embedded foundation. The soil is assumed to be homogeneous for the small-strain case. However, the soil properties will eventually vary due to deformation.

A set of parameters to be used in this case study is chosen based on values commonly observed in practice for similar situations. The soil parameters are:

$$G = 8 \cdot 10^7 N/m^2 \quad (3.8)$$

$$\rho = 2000 \text{ kg}/m^3 \quad (3.9)$$

$$\beta_{SOIL} = 0.05 \quad (3.10)$$

$$\nu = 0.4 \quad (3.11)$$

The corresponding shear-wave velocity of the layer is 200 m/s, and the height of the soil medium is chosen to be 240 meters. Analysis of the soil requires division of the domain into layers; the number of layers is chosen to be 24. The layers will further be divided into a number of sublayers to satisfy the thin layer requirements previously described. An appropriate number of sublayers can be determined based on the maximum sublayer thickness allowed by the analysis, which will be discussed in Chapter 4.

Input ground motion deemed appropriate for the theoretical case study is the El Centro earthquake motion. Data used in the analysis represents the

corrected North-South component of the El Centro ground motion, which is shown in Figure 3.1. The El Centro input motion has several advantages as a representative ground motion which leads to its wide use in earthquake research.

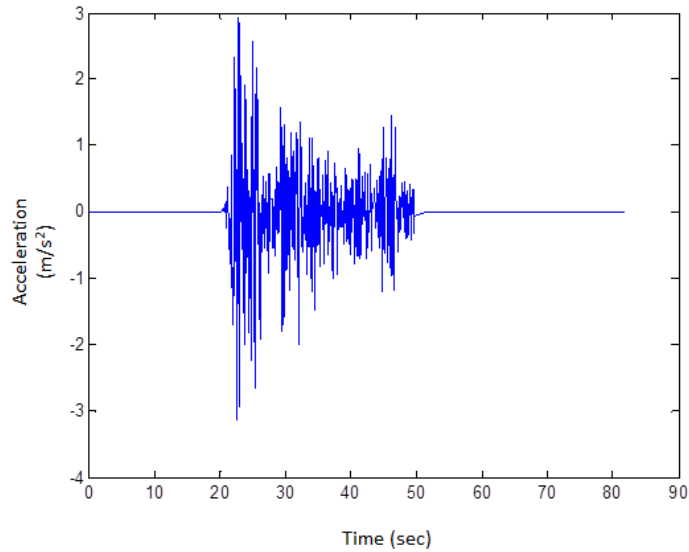


Figure 3.1: El Centro Recorded Ground Motion

## 3.2 Mexico City Site Characterization

Soil-structure system analysis will also be conducted using soil properties adjusted for the level of deformation in the near field during actual earthquake events. Soil-structure system response varies widely depending on local soil properties and site-specific conditions. The effects of soil-structure interaction are especially pronounced in locations with soft soils.

Natural frequencies of the soil layer also determines the dominant frequencies of wave motion that will be propagated from the base of the soil layer to the foundation and structure. Relationships between the frequencies of motion and the frequencies of the soil-structure system can significantly affect the structural response. This is especially important for soil layers with natural periods comparable to the structural period.

A suitable choice for an actual case study is the Mexico City earthquake of September 19, 1985. The Mexico City event is especially interesting to examine because of the level of damage that occurred during the earthquake. The level of motion was substantially amplified due to the dominant periods of the soil layer. Excitation frequencies were close to the range of the natural frequencies of many structures in the region. Amplification that occurred due to resonance caused significant damage to Mexico City's high-rise buildings.

### **3.2.1 General Site Conditions**

An important aspect of the Mexico City site is its location on lake deposits. Development of Mexico City occurred on the former lakebed of Lake Texcoco, and the city is situated on top of the lakebed's soft clay deposits. The earthquake site encompasses both the Texcoco lakebed composed of softer clays and the Xochimilco-Chalco lakebed composed of stiffer clays. Locations of recording stations relative to the lakebeds of the Mexico City site are shown in a map by Seed et al. (1988) and provided below.

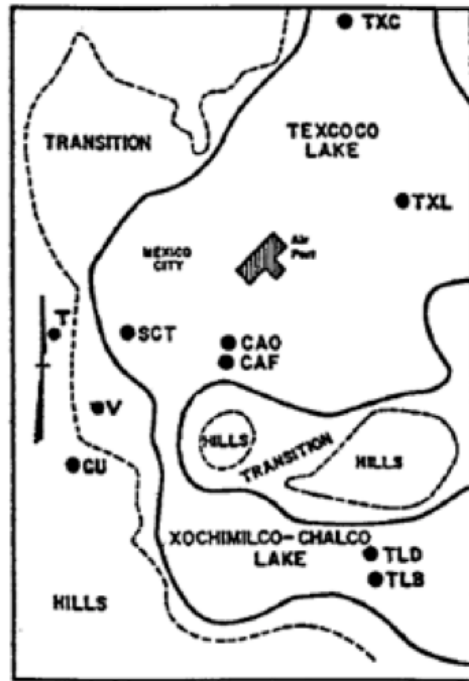


Figure 3.2: Recording Stations and Lakebeds of Mexico City (from Seed et al., 1988)

Soft clay deposits of the Texcoco lakebed exhibits shear-wave velocities ranging from 40-90 m/s, with layer depth ranging from 26-44 meters. Underneath the soft deposits lie stiff rock formations with shear-wave velocities upwards of 500 m/sec. Mexico City's earthquake damage is most prominent in structures of 6 to 18 stories. The level of damage is consistent with the natural periods that correspond to the the shear-wave velocities of the soft deposit.

Make up of the soil characteristics in the Texcoco lakebed can be seen in the soil profile provided by Seed et al. (1988) in Figure 3.3.

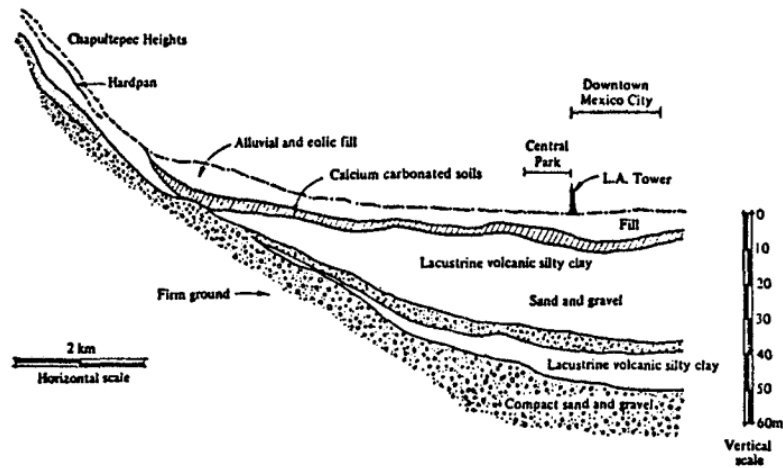


Figure 3.3: Basin of Valley of Mexico (from Zeevaert, 1971)

The epicenter of the Michoacan earthquake was located in the Cocos Plate subduction zone in the Pacific Ocean, more than 350 km away from Mexico City. Seismic waves propagated east towards Mexico City, initially being recorded at Caleta de Campos, and also recorded in various stations in the Mexico City area. A schematic drawing of the locations of the earthquake epicenter and recording stations by Celebi et al. (1987) is shown in Figure 3.4.



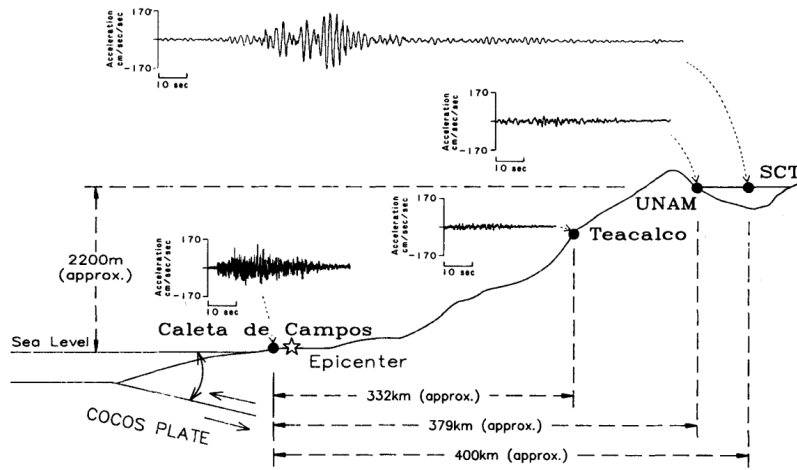


Figure 3.4: East-West Profile of Mexico City (from Celebi et al., 1987)

### 3.2.2 Site Conditions at Recording Stations

One of the most critical recordings of the earthquake event were recorded at the UNAM station seen in Figure 3.4. The site of the UNAM (Universidad Nacional Autónoma de México) recording station is located on rock and hard soil deposit in the hills zone of Mexico City. The deposit consists of a layer of fractured lava with soft rock underneath with an estimated shear wave velocity between 450 m/s to 600 m/s. The fractured lava layer varies in depth and outcrops of the soft rock are apparent near the recording site. Discussions by Seed et al. (1988) conclude that these conditions represent the hard layer of the Mexico City area.

Three stations (CU01, CUMV, CUIP) recorded the ground motions at the UNAM site. Recordings from all three stations exhibited similar prop-

erties, with the spectral peaks of all recordings having periods of about 0.9 seconds and 2 seconds. The recordings of the CUMV station are considered representative of the rock ground motions of Mexico City, and will be used as the input motion for the Texcoco site-response analysis.

Another recording site of great interest is the SCT recording station. Although six recording stations were located in the Mexico City lakebed regions, the SCT station was the only one situated in the heavily damaged regions (Tena-Colunga et al., 2007). The SCT (Secretariat of Communications and Transportation) station is positioned in the Texcoco lakebed area as seen in Figure 3.4. Recordings at the SCT represent ground motion recordings at the surface of the Texcoco lakebed deposit.

The first 4 meters of the SCT soft deposit consist of mostly sand and silt. Underneath the sand layer lies a thick layer of clay in addition to silty sand, volcanic glass and fly ash. The 27 meter clay layer has a very high water content (up to 450%) with an undrained shear strength up to  $0.8 \text{ kg/cm}^2$ . The last 7 meters of the soft deposit consists of stiff clay and sandy silt, which is then followed by hard rock layer.

A suspension logging test performed in 1986 was reported by Ovando-Shelley et al. (2007). Shear-wave velocities of the SCT site tests are shown in Figure 3.5. Test results demonstrate that the shear-wave velocities of the soft deposit range between 50-100 m/s. They also confirm the presence of the hard layer at a depth of about 38 meters.

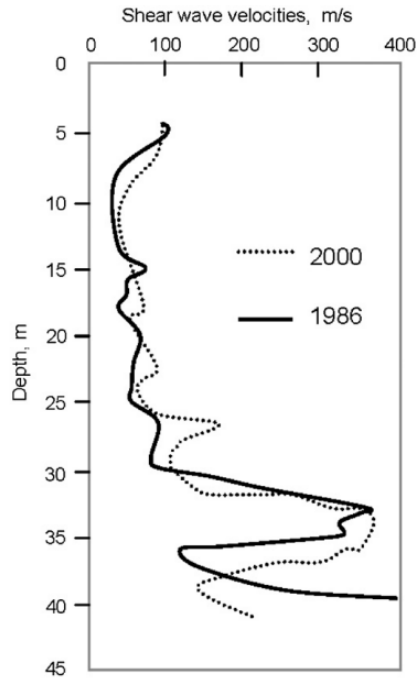


Figure 3.5: SCT Suspension Logging Test (from Ovando-Shelley et al., 2007)

Seed et al. (1988) determined the average shear-wave velocity of the SCT site to be about 75 m/s, and the soil density was estimated to be around 1200 kg/m<sup>3</sup>. A representative soil profile was constructed as shown in Figure 3.6a. Seed et al. (1988) also developed a representative shear-wave velocity profile from the results of CPT procedures and direct borehole measurements, as shown in Figure 3.6b.

A study of the performance of flexible foundations in Mexico City by Avilés and Pérez-Rocha (2005) provides additional information regarding the SCT lakebed soil properties. The study proposed a representative shear mod-

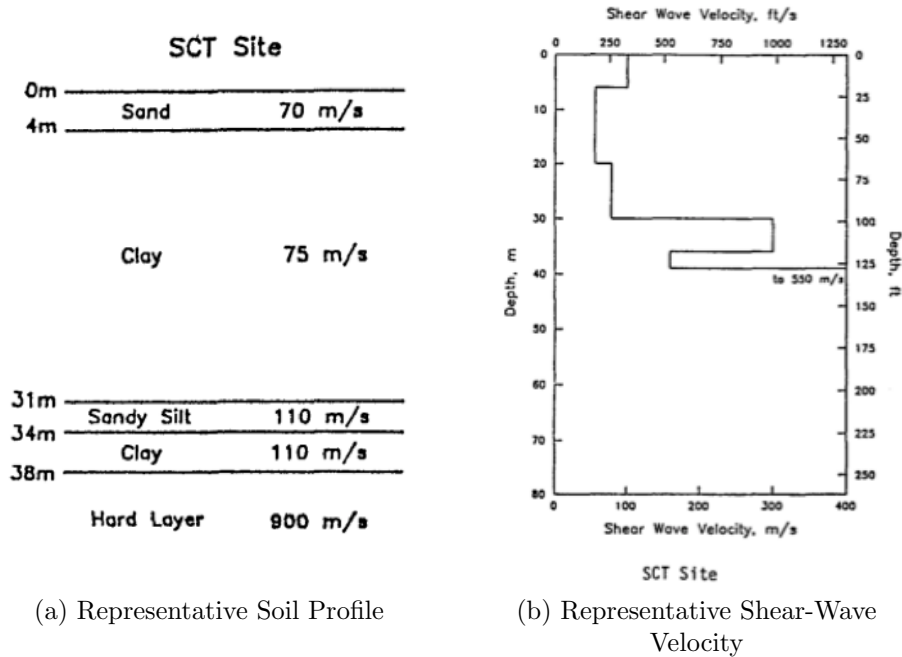


Figure 3.6: Representative Soil Profile (from Seed et al., 1988)

ulus of  $7.8 \cdot 10^6 \text{ N/m}^2$ . It also suggested ratio values between properties of the soft deposit and the underlying hard rock layer. Ratio of the soil densities of the soft layer and the hard layer is assumed to be 0.8. Ratio of the shear-wave velocities of the soft layer and the hard layer is approximately 0.2. Additionally, the initial damping ratio is assumed to be 0.05 for the soft soil and 0.03 for the hard layer. Poisson's ratio is determined to be 0.45 for the soft soil and 0.33 for the hard layer (Avilés and Pérez-Rocha, 2005).

Recorded input motion data used in this research is provided by the National Oceanic and Atmospheric Administration. Data available for the

UNAM and SCT recording stations include the North-South and East-West directions. The UNAM and SCT recorded ground motions shown in Figures 3.7 are for the East-West direction. It is important to note that the recordings at the two stations did not start at the same time nor did they have the same duration lengths. The SCT recording started approximately 14 seconds before the UNAM recording, and its duration is 180 seconds compared to 60 seconds for UNAM.

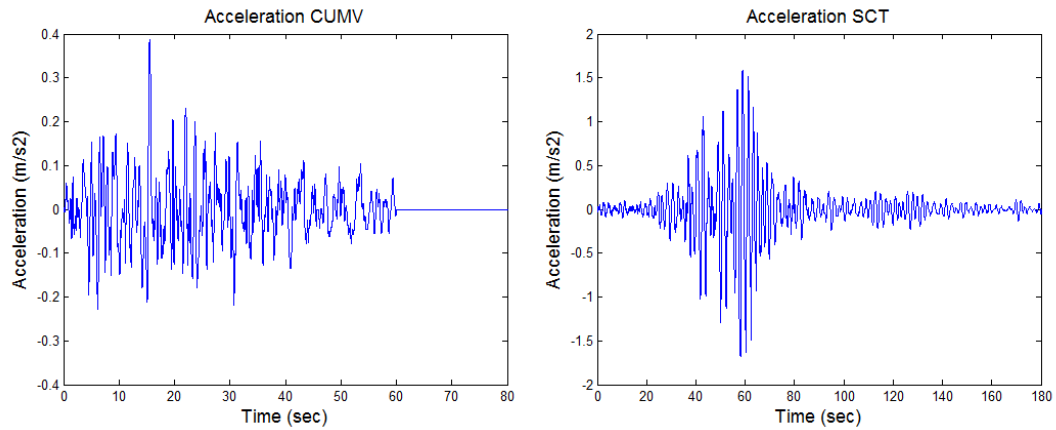


Figure 3.7: UNAM and SCT Recorded Motion

Frequency-domain representations of these two motions are shown in Figure 3.8. Examination of the UNAM motion shows it has significant but distributed frequency content up to 2 Hz. Frequency content of the SCT motion is significantly more localized near the 0.5 Hz range, which can be attributed to the site amplification by the lakebed deposit.

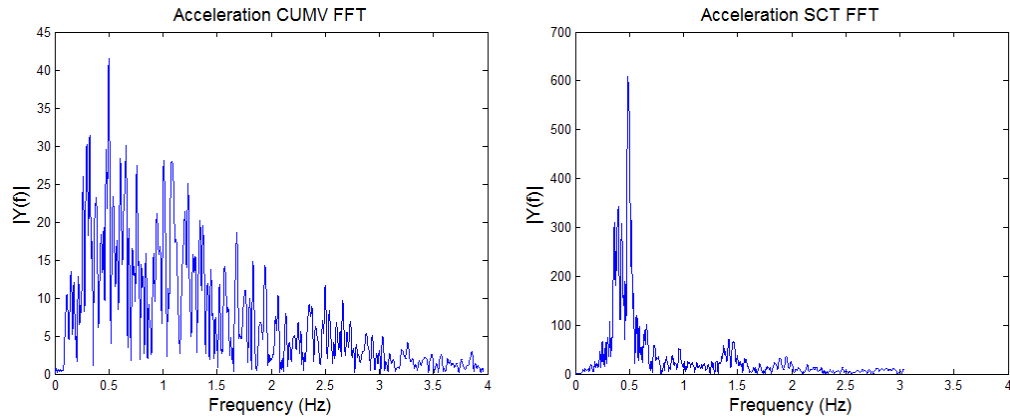


Figure 3.8: Frequency Domain Representations

The amplification that occurred at the SCT site is well documented and a summary is provided by Celebi et al. (1987). Peak ground acceleration for the UNAM recorded motion is 0.035 g and for the SCT motion is 0.17 g. Amplification of motion in the 0.4 to 0.5 Hz range is most significant with amplifications of up to a factor of 10 in the horizontal direction (Celebi et al., 1987). Other sites in Mexico City experienced significant amplification as well but to lesser extents compared to the SCT site.

The highest level of amplification is observed in the East-West recording at the SCT site. A comparison of the response spectra for the East-West motions of UNAM and SCT further highlights the amplification of motion especially for low frequencies. High amplification levels are observed for periods between 1 to 3 seconds. These periods correspond to structural heights of 10 to 30 stories, and provide justification to the level of damage seen in Mexico City structures of these heights.

The range of period with significant amplification is seen in the spectral ratio shown in Figure 3.9. The significant amplification periods correspond to the shear-wave velocity profile in Figure 3.6b. Determination of the natural periods of soil layers can be done using Equation 3.3. For a soft deposit thickness of about 38 meters, these periods corresponds to a shear-wave velocity range between 50 to 150 m/s. The representative shear-wave velocity of 75 m/s produces the highest amplification at a period of 2 seconds which corresponds to the peak spectral acceleration observed in Figure 3.9.

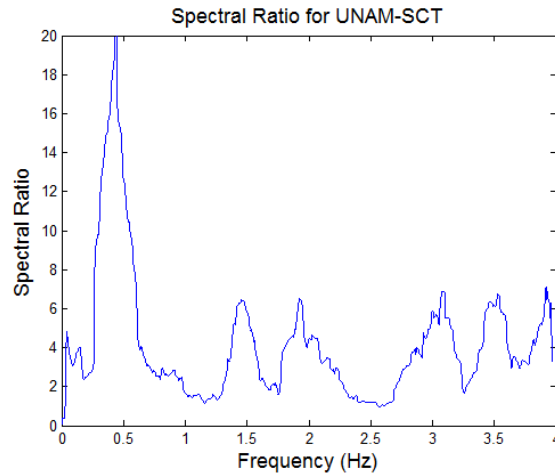


Figure 3.9: Spectral Ratio for UNAM-SCT

Significant amplification levels at the SCT site indicate high levels of deformation in the Texcoco lakebed deposits. Site-response analysis will provide insights into the deformation levels and soil-property adjustments of the SCT site. The East-West ground motions at the SCT site will be used to study the effects of soil-property adjustments in the Texcoco lakebed.

### **3.3 Adjustments of Soil Properties**

The dynamic analysis of dynamic soil-structure system requires accurate representation of soil nonlinearities. The true nonlinear behavior of soil can be characterized by the soil's hysteretic stress strain relationship. An analysis in the time domain would incorporate this relationship into the site-response analysis. An equivalent linear analysis in the frequency domain otherwise requires a representation of the nonlinear behavior through the determination of shear modulus and damping consistent with the level of deformation.

#### **3.3.1 Reduction Curves**

Theoretical and experimental relationships between levels of strain and corresponding soil properties are provided by reduction curves. Variation of the secant modulus in terms of shear strain is characterized by normalized modulus reduction curves.

Loss of energy due to hysteretic dissipation is represented by material damping curves. Numerous research and laboratory tests have been conducted for different types of soil, and empirical curves to be used in site-response analysis have been documented by Vucetic and Dobry (1991) for clays and Seed and Idriss (1970) for sands.

A factor that significantly affects the modulus reduction and damping characteristics of soil is the plasticity index. Site-response analysis of soft clay deposits with different plasticity index values resulted in significant differences in peak spectral acceleration and period, as shown in Figure 3.10.



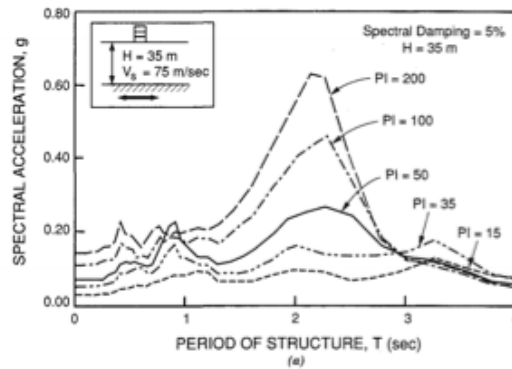


Figure 3.10: Effect of Plasticity Index on Site Response (from Vucetic and Dobry, 1991)

Soils with high plasticity index exhibit more linear behavior and less damping for higher strain levels. The linear behavior of highly plastic soils contribute to significant ground motion amplifications seen in Figure 3.10. Modulus reduction and damping curves corresponding to the different plasticity index values in Figure 3.10 are shown in Figure 3.11.

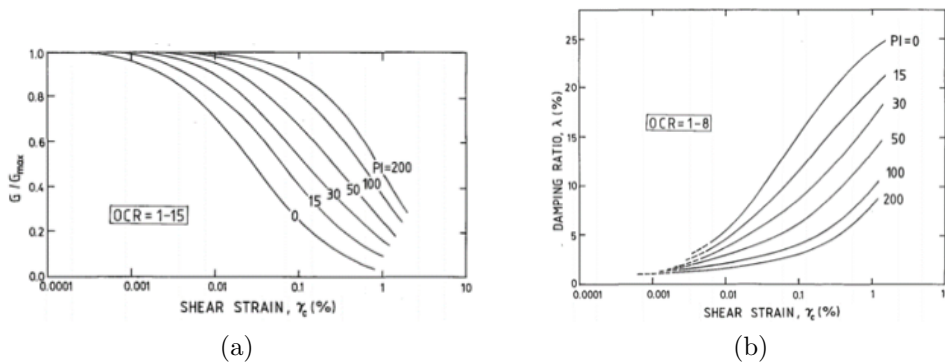


Figure 3.11: Modulus Reduction and Damping of Clays of Various Plasticity Index Values (from Vucetic and Dobry, 1991)

### 3.3.2 Hyperbolic Model

Reduction curves obtained from experimental results can be categorized based on various site characteristics, and correlation of the reduction curves to these site characteristics has been determined. These correlations were initially used to develop hyperbolic models that predicted the reduction curves (Hardin and Drnevich, 1972).

The hyperbolic model provided a relationship between shear-stress and strain as:

$$\tau = \frac{\gamma}{\frac{1}{G_{max}} + \frac{\gamma}{\tau_{max}}} \quad (3.12)$$

The reference strain in the hyperbolic model is defined in terms of the small-strain modulus. It is expressed as:

$$\gamma_r = \frac{\tau_{max}}{G_{max}} \quad (3.13)$$

The hyperbolic relationship is illustrated in Figure 3.12.

Both sides of Equation 3.12 can be divided by the strain and rearranged to produce the normalized shear modulus. The formulation for the normalized shear modulus reduction curve is expressed as:

$$\frac{G}{G_{max}} = \frac{1}{1 + \gamma_h} \quad (3.14)$$

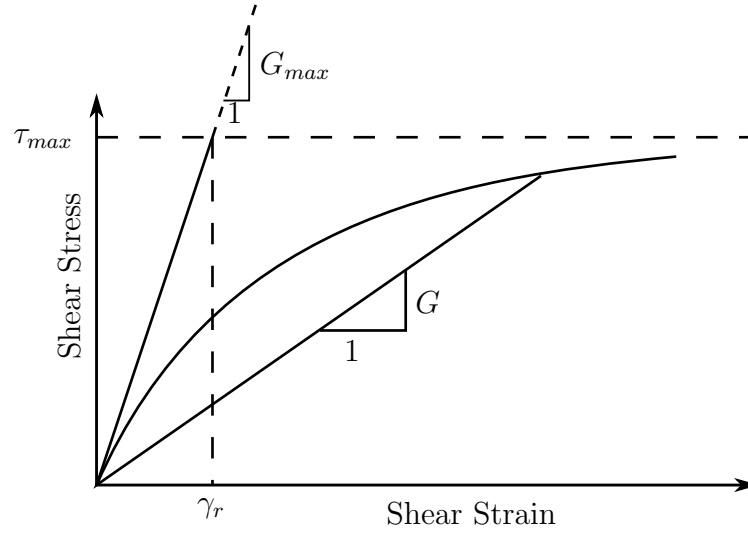


Figure 3.12: Stress-Strain Curve based on the Hyperbolic Model

The hyperbolic strain  $\gamma_h$  is found by:

$$\gamma_h = \frac{\gamma}{\gamma_r} \left[ 1 + a \cdot \exp \left( -b \left( \frac{\gamma}{\gamma_r} \right) \right) \right] \quad (3.15)$$

where reference strain  $\gamma_r$  is as defined above (depends on material soil types), and  $a$  and  $b$  are coefficients that corrects the stress-strain curve shape based on soil types. The normalized material damping curve is also described in terms of the hyperbolic strain as:

$$\frac{D}{D_{max}} = \frac{\gamma_h}{1 + \gamma_h} \quad (3.16)$$

where  $D_{max}$  is the upper limit for damping determined based on soil types

and saturation levels. Both the shear modulus reduction and damping curves are plotted semi-log in terms of strain. The reduction curves predicted by the hyperbolic model is shown in Figure 3.13.

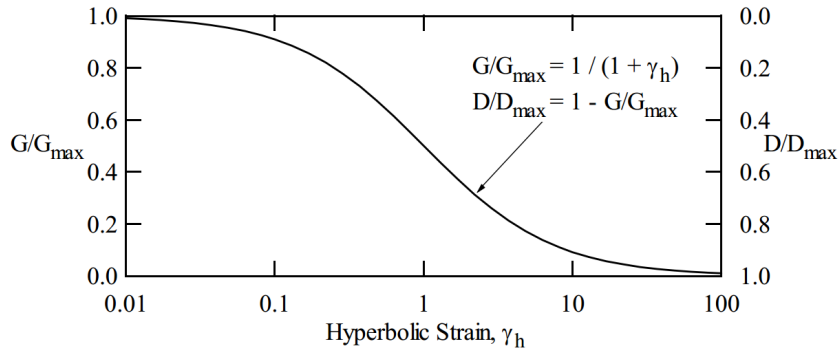


Figure 3.13: Hyperbolic Model (from Darendeli, 2001)

### 3.3.3 Darendeli Model

An alternative to the hyperbolic model based on empirical reduction curves was developed by Darendeli (2001). The Darendeli model for modulus reduction expands on the hyperbolic form of Equation 3.14 by introducing a curvature coefficient. The coefficient adjusts the curvature of the predicted curves closer to the empirical curves. Normalized modulus curves predicted by the Darendeli model are defined by the following expression (Darendeli, 1997).

$$\frac{G}{G_{max}} = \frac{1}{1 + \left(\frac{\gamma}{\gamma_r}\right)^a} \quad (3.17)$$

Reference strain  $\gamma_r$  can be determined based on previously established relationships with the plasticity index (PI) and overconsolidation ratio (OCR) of the soil. It is also affected by the mean effective confining pressure  $\sigma'_0$ . Darendeli expressed the reference strain as:

$$\gamma_r = \left(\sigma'_0\right)^{0.3483} (0.0352 + 0.0010 \cdot PI \cdot OCR^{0.3246}) \quad (3.18)$$

where  $\sigma'_0$  is expressed in atmospheric-pressure units. The mean effective stress in Equation ( $D_{min}$ ) and ( $\gamma_r$ ) can be calculated as:

$$\sigma'_0 = \sigma'_v \left( \frac{1 + 2K_o}{3} \right) \quad (3.19)$$

where  $K_o$  is the at-rest earth pressure coefficient and  $\sigma'_v$  is the vertical effective stress of the soil layer.  $K_o$  is generally assumed to be 0.5 for most clays.

The relationship between  $G$  and  $G_{max}$  can be inserted in the stress-strain constitutive relation to express the shearing stress as:

$$\tau = \frac{\gamma}{1 + \left(\frac{\gamma}{\gamma_r}\right)^a} \cdot G_{max} \quad (3.20)$$

Energy dissipation due to nonlinear soil behavior contributes a significant portion of damping. Nonlinearity of the stress-strain relationship is assumed to follow the Masing behavior (Masing, 1926) with an assumed hysteresis loop as shown in Figure 3.14. The cyclic stress-strain path of the hysteresis loop is assumed to be constructed by scaling the monotonic loading path by two.

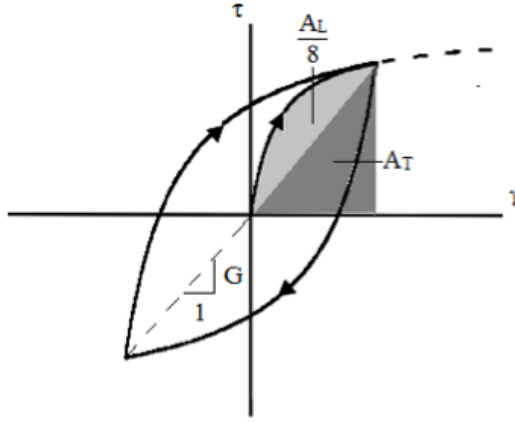


Figure 3.14: Masing Behavior Hysteresis Loop

The assumption of Masing behavior can be used to estimate the equivalent viscous damping (Darendeli, 2001). Dissipation of energy  $A_L$  is the area inside the hysteresis loop which, based on Masing behavior, is equal to 8 times the area enclosed by the backbone curve. It is calculated to be:

$$A_L = 8 \int \tau d\gamma - A_T \quad (3.21)$$

where the stored strain energy  $A_T$  is

$$A_T = \frac{\tau\gamma}{2} \quad (3.22)$$

Thus, the viscous damping of the hysteretic system can be written as:

$$D = \frac{A_L}{4\pi A_T} \quad (3.23)$$

The Masing damping can be calculated by evaluating the dissipated energy and the stored energy using Equation 3.21 and 3.22 and substituting

the results into Equation 3.23. For a curvature coefficient  $a = 1$ , the Masing damping is evaluated as:

$$D_{Masing,a=1.0}(\%) = \frac{400}{\pi} \frac{\gamma_r \left[ \gamma - \gamma_r \ln \left( \frac{\gamma + \gamma_r}{\gamma_r} \right) \right] - \frac{1}{2} \frac{\gamma^2}{1 + \frac{\gamma}{\gamma_r}}}{\frac{\gamma^2}{1 + \frac{\gamma}{\gamma_r}}} \quad (3.24)$$

The integration in Equation 3.21 does not have a closed-form solution for curvature coefficients other than 1. Equation 3.21 has been evaluated numerically for curvature coefficients between 0.7 to 1.3. The results were used to provide a relationship between the Masing damping for coefficient  $a$  in terms of the damping for coefficient of 1.

$$D_{Masing} = c_1 D_{Masing,a=1.0} + c_2 D_{Masing,a=1.0}^2 + c_3 D_{Masing,a=1.0}^3 \quad (3.25)$$

where  $D_{Masing,a=1.0}$  represents the Masing damping for  $a = 1$ . Coefficients  $c_1$ ,  $c_2$  and  $c_3$  were determined by fitting the damping predicted in Equation 3.25 to the damping calculated numerically. Expressions for the coefficients are provided below:

$$\begin{aligned} c_1 &= -1.1143a^2 + 1.8618a + 0.2523 \\ c_2 &= 0.0805a^2 - 0.071a - 0.0095 \\ c_3 &= -0.0005a^2 + 0.0002a + 0.0003 \end{aligned} \quad (3.26)$$

The Masing damping does not account for small strain damping, and tends to overestimate experimental damping values for higher strains.

Correction factors in terms of the shear modulus reduction were determined by Darendeli as:

$$F = b \cdot \left( \frac{G}{G_{max}} \right)^{0.1} \quad (3.27)$$

The scaling coefficient  $b$  is a function of the number of cycles of loading ( $N$ ). Darendeli determined the coefficient  $b$  to be:

$$b = 0.6329 - 0.0057 \ln N \quad (3.28)$$

The expression for the strain-consistent damping which limits the damping at higher strains and incorporates minimum damping is provided below:

$$D = b \left( \frac{G}{G_{max}} \right)^{0.1} D_{Masing} + D_{min} \quad (3.29)$$

Determination of the minimum damping is based on experimental data. Small-strain damping observed in laboratory tests is correlated with the plasticity index, overconsolidation ratio, and excitation frequency of soil samples. The relationship between these factors and the minimum damping is determined to be:

$$D_{min}(\%) = \left( \sigma'_0 \right)^{-0.2889} \left( 0.8005 + 0.0129 \cdot PI \cdot OCR^{-0.1069} \right) \left( 1 + 0.2919 \ln f \right) \quad (3.30)$$

In Equation 3.30, the mean effective stress  $\sigma'_0$  is expressed in atmospheric-pressure units, and excitation frequency  $f$  is in units of Hertz. Excitation frequency is included in Equation 3.30 although it is noted that its effects are



less significant compared to the mean effective stress and soil plasticity. Further details concerning the derivation of the equations above and parameter determination can be found in the discussions by Darendeli (2001).

The Darendeli model is used to determine the reduction curves for the purposes of the theoretical case study. For most site-response computations under earthquake loading, the number of cycles is assumed to be 10 and the excitation frequency is assumed to be 1 Hz (Kottke, 2010). Additionally, the curvature coefficient  $a$  can be taken to be 0.919.

Site conditions assumed for the theoretical case study has a plasticity index of 0, and the soil is normally consolidated ( $\text{OCR} = 0$ ). The shear modulus reduction and damping curves generated by the Darendeli model for the theoretical case study are shown in Figure 3.15.

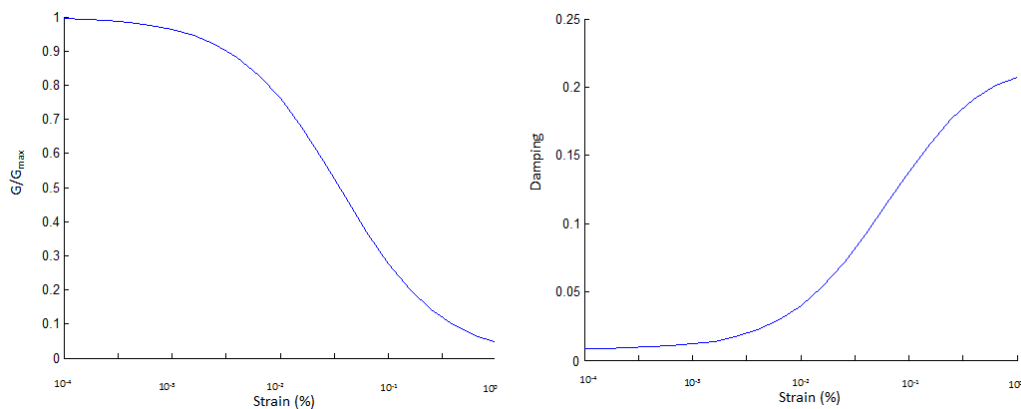


Figure 3.15: Reduction Curves for Theoretical Case Study based on Darendeli Model

### 3.3.4 Site-Specific Reduction Curves

Reduction curves applicable for the SCT response analysis are determined based on the site characteristics of Mexico City. A contributing factor affecting the dynamic soil properties of the SCT site is the plasticity of the Mexico City clays. Soft clay deposits at the site have very high plasticity levels with index values ranging between 150 to 250. Reduction curves based on experimental data on Mexico City clays were constructed as shown in Figure 3.16 (Leon et al., 1974; Romo and Jaime, 1986).

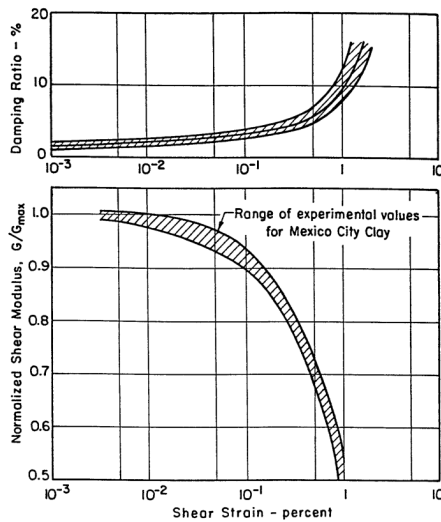


Figure 3.16: Mexico City Empirical Reduction Curves (from Leon et al., 1974; Romo and Jaime, 1986)

The Mexico City empirical curves closely resemble the reduction curves shown in Figure 3.11 corresponding to plasticity index of 200. High-plasticity

lacustrine deposits exhibit a more-nearly linear soil behavior compared to other clays in Figure 3.11. The linear behavior for lower strains caused high levels of amplification of the UNAM ground motion at the SCT site. Nevertheless, nonlinear behavior does significantly affect the SCT site response at higher strains observed during the Mexico City earthquake.

Another important factor affecting the dynamic soil properties of Mexico City clay is the loading condition of the region. Mexico City was initially built on an island on the western part of Lake Texcoco. Throughout its history, the original site of Mexico City has experienced more urbanization compared to its surrounding area. The development of Mexico City led to intense pumping of water from its aquifers as well as the draining of Lake Texcoco to prevent flooding of the city.

Development levels of the western part of Lake Texcoco along with its history of water withdrawal contribute to higher effective stresses. The lakebed is categorized into two zones based on this distinction: the Preloaded zone and the Virgin zone. Higher effective stresses of the Preloaded zone generated more clay consolidation compared to the Virgin zone. Preloaded zone clays are less compressible and more resistant than Virgin zone clays due to lower water content in the Preloaded zone (Romo et al., 1988)

Both the Preloaded and Virgin zones are underlain by hard formations. The thickness of the Preloaded zone clay deposits is less than 50 meters, whereas the softer clay of the Virgin zone has a thickness of 50 to 75 meters (Jaime and Romo, 1988). A contour map of the depths to hard formation was

constructed by Jaime (1987) and is shown in Figure 3.17. The Preloaded zone is determined to be the region between the 25-meter and the 50-meter contour lines. The Virgin zone is determined to be the region east of the 50-meter contour line.

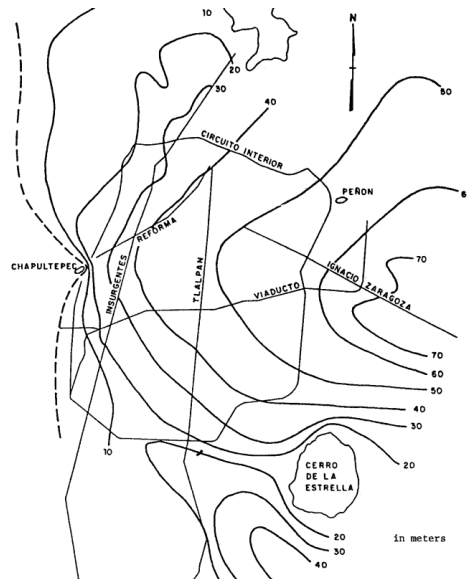


Figure 3.17: Depth to Hard Formation (from Jaime, 1987)

The SCT recording station is located in the Preloaded zone, and soil properties corresponding to this region will be used for the SCT site-response analysis. Stratigraphical profile of the Preloaded zone is shown in Figure 3.18 (Romo et al., 1988). Depth of the ground water table is estimated at 4 meters. The soil profile measured in the Preloaded zone matches the soil profile determined by Seed et al. (1988).

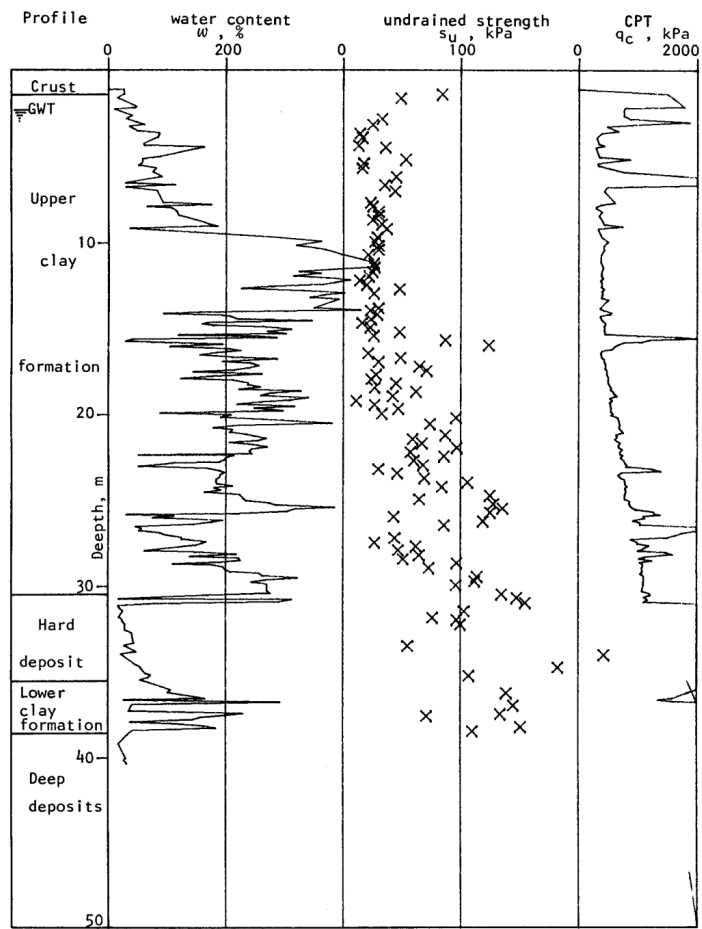


Figure 3.18: Texcoco Lakebed Stratigraphic Profile (from Romo et al., 1988)

The effective stress at the SCT site can be determined using the same approach used for the theoretical case study. A Darendeli model for the reduction curves of the SCT site can be constructed using characteristics of the Lake Texcoco deposits as input parameters. The Darendeli reduction curves can be fitted on the basis of the soil properties of Lake Texcoco.

Applicability of the Darendeli model can be justified by examining laboratory test results for the Preloaded zone. Triaxial compression tests were carried out on Preloaded-zone clay samples to produce the stress-strain curves shown in Figure 3.19 (Romo et al., 1988). Stress-strain curves of the Preloaded zone exhibit a near-hyperbolic shape. The Darendeli model was derived as an extension of the hyperbolic model, and thus is promising as the model for the reduction curves.

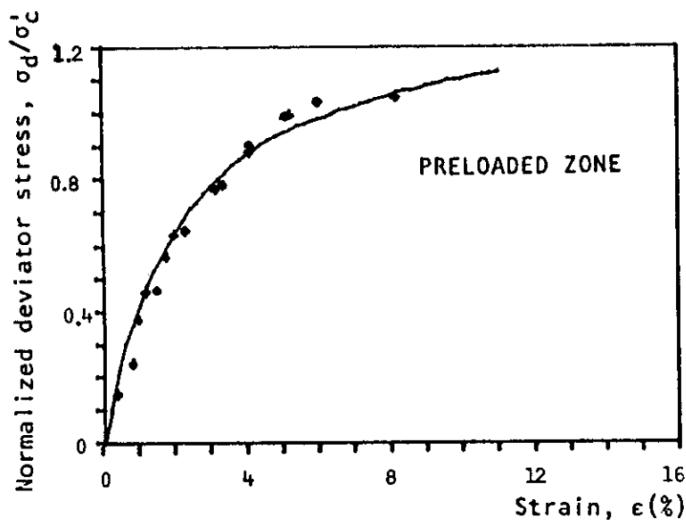


Figure 3.19: Stress-Strain Relationship for Preloaded Texcoco Lakebed (from Romo et al., 1988)

Furthermore, the Darendeli model can be justified by comparing the Darendeli reduction curves to empirical curves for the Preloaded zone. Results of the cyclic triaxial and resonant column tests were used to generate a range of shear modulus reduction curves for the Preloaded zone (Romo et al., 1988).

The range of empirical reduction curves in Figure 3.20 are compared to the range of curves predicted by the Darendeli model for the different layers of the SCT site.

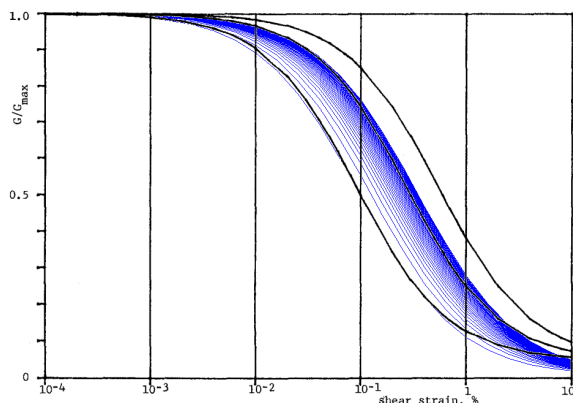


Figure 3.20: Shear Modulus Reduction Curves for SCT Site (from Romo et al., 1988)

Comparison between the empirical modulus reduction curve and the curves predicted by the Darendeli model shows good agreement. Reduction curves on the left correspond to smaller depths and the reference strains increase for higher mean effective stresses. Reference strain for the Preloaded zone ranges between 0.1% and 0.6% with an average of approximately 0.3%.

The damping level determined from the Preloaded zone samples is shown in Figure 3.21 (Romo et al., 1988). The Darendeli damping curve corresponding to the  $D_{min}$  of the Preloaded zone is plotted for comparison.

The damping curve predicted by Darendeli reasonably matches the damping curve obtained from empirical results for lower strain levels. The

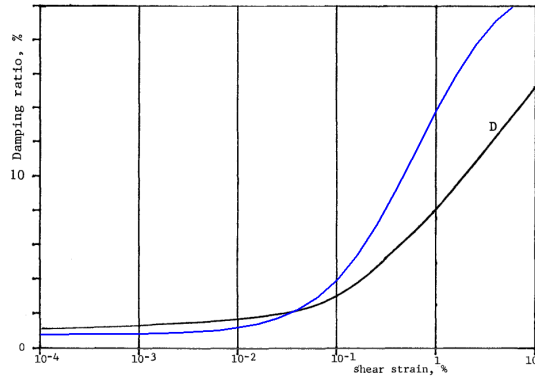


Figure 3.21: Damping Curves for SCT Site (from Romo et al., 1988)

Darendeli model does not match the empirical curves for strains higher than 0.1%. It more closely resembles the damping curve expected for normal clays, whereas the Mexico City clay exhibits aberrant behavior and unusually low damping. Comparison between Mexico City damping level and damping levels of other clays measured can be seen in Figure 3.22.

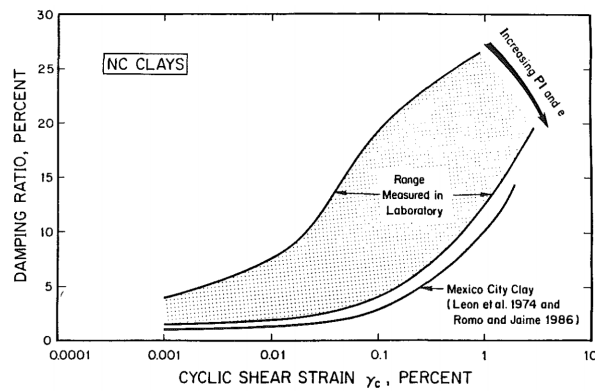


Figure 3.22: Measured Damping Level of Normally Consolidated Clay (from Dobry and Vucetic, 1987)



Discrepancy in the damping curves may be attributed to the fact that the assumption of Masing behavior overestimates the higher-strain damping. The correction factor applied to the Masing damping is derived empirically based on normal clay, and does not adequately predict the Lake Texcoco case. Damping curve obtained from the Preloaded zone test results will be used for the SCT site-response analysis.

## Chapter 4

# Equivalent Linear Analysis with Perturbation Method

### 4.1 Process of Equivalent Linear Analysis

In previous chapters, the ingredients of both the free-field and near-field analyses have been established. Models have been formulated for each of the components of the analysis. The soil properties and characteristics to be applied in the analysis have also been previously determined. In this chapter, we put to use the results of the previous discussions in order to provide an overall analysis of soil-structure systems.

Numerous methods of conducting site-response analysis are available. A comprehensive review has been done detailing the different approaches and possible analysis techniques, including linear analysis, equivalent linear analysis, and fully nonlinear analysis (Kramer, 1996).

Nonlinear analysis is considered to be the most detailed and accurate approach, as it accounts for the entire hysteretic behavior of the soil. As described by Stewart et al. (2008), a fully nonlinear analysis conducted in the time domain would include the true hysteretic properties for the duration of the earthquake event. Soil layers are modeled as lumped masses and nonlinear

springs. In this case, the response of the soil-structure system is calculated for each time step. The shear springs behave according to the actual shear stress-strain relationship of the soil. There is no need for ad hoc strain-consistent adjustment of the soil-properties in a fully nonlinear time-domain analysis.

Although the time-domain analysis described produces accurate results, many drawbacks of the method prevent it from being a practical approach to the solution. As discussed by Stewart et al. (2008), a time-domain analysis can become very computationally intensive. The process of incorporating the entire shear stress-strain relationship into the site response calculation is not practical for a detailed analysis consisting of many elements. This leads to the need for an alternate approach.

Equivalent linear analysis conducted in the frequency domain obviates the need to repetitively conduct site-response analysis for a given set of soil properties. Instead, the soil properties are assumed to be linear by approximating the nonlinear stress-strain curve as a linear secant modulus. An approximate site response can be generated using the linear set of soil properties. The initial set of properties correspond to the small strain shear modulus  $G_{max}$  and small strain damping  $D_{min}$ .

Results of the initial analysis are accurate only if the response calculated in the analysis represents negligible strain levels. Cyclic tests on most soils show that strain levels under  $10^{-6}$  exhibits linear behavior. However, strain levels between  $10^{-6}$  to  $10^{-2}$  are expected during earthquake events, and assumption of small strains is no longer appropriate.

Further iterations of the site-response analysis are needed to ensure compatibility between the strain-dependent properties and the level of strain experienced. Representative strain levels of the initial analysis are estimated after each analysis, and a new set of soil properties is applied to the domain consistently with the level of deformation of the previous analysis. Another linear analysis is conducted using the updated soil properties, and the process is repeated until convergence of the soil properties. A criterion for acceptable level of convergence can be defined with respect to the level of accuracy desired. Once convergence is achieved, the strain-consistent properties are used to output the dynamic response of the system. The process for a one-dimensional equivalent linear analysis is illustrated in Figure 4.1 below.

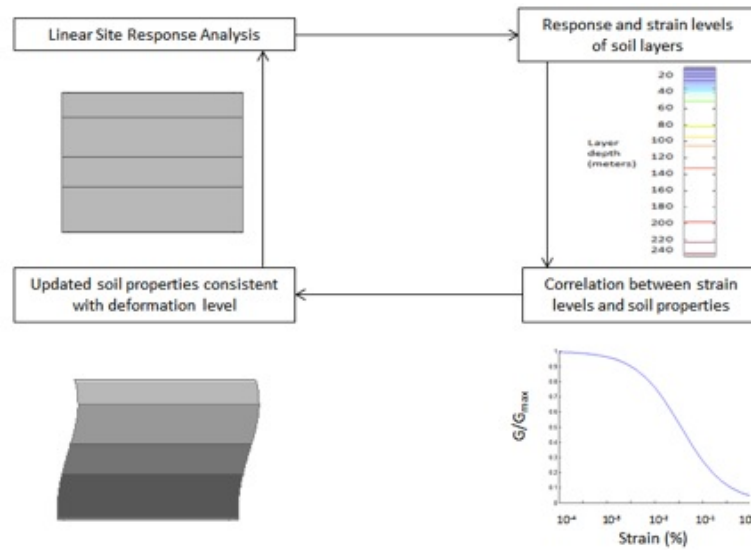


Figure 4.1: Process for a One-Dimensional Equivalent Linear Analysis

In the process above, a regular layered medium is analyzed using an initial set of properties for each layer. The modulus reduction and damping curves discussed in the previous chapter are used. Shear strain of a soil layer with constant height can simply be calculated as the difference of displacement of the top and bottom of the layers divided by the height. Shear strain for the  $i^{th}$  soil layer can be calculated as follows:

$$\begin{aligned}
\gamma_{zx} &= \left[ \frac{\partial}{\partial z} \quad \frac{\partial}{\partial x} \right] \mathbf{N}_i \mathbf{U}_i \\
&= \left[ \frac{\partial \mathbf{N}_i}{\partial z} \quad 0 \quad \frac{\partial \mathbf{N}_{i+1}}{\partial z} \quad 0 \right] \mathbf{U}_i \\
&= \left[ \frac{1}{h} \quad 0 \quad \frac{-1}{h} \quad 0 \right] \mathbf{U}_i
\end{aligned} \tag{4.1}$$

Representative strain can be measured as two-thirds of the root-mean-square. The effective strain is usually about 60-70% of the maximum strain value. As the analysis is done in the frequency domain, the root mean square is evaluated using Parseval's theorem and the effective strain is expressed below:

$$\gamma_{eff} = \frac{2}{3} \sqrt{\frac{1}{n^2} \sum_n |X(f)|^2} \tag{4.2}$$

Results obtained from the one-dimensional equivalent linear analysis adequately characterize the nonlinear nature of the regular soil layer. However, any inclusion or embedded foundation in the soil layer will change the soil response near that inclusion. Deviation of the strain level from the regular layered values indicates the properties of soil elements in the near-field will no

longer be consistent with the level of deformation. Further adjustments of the soil properties are needed to ensure consistency with the strain levels.

Analysis for a two-dimensional case can be initiated using the converged properties of the free-field counterpart. Regions far away from the inclusion behave the same way as a regular layered medium. Therefore, soil properties in this region are no longer adjusted in the near field analysis. For the region near the inclusion, additional iterations are performed to further estimate the compatible values of strain level and soil properties. The process a two-dimensional analysis is illustrated in Figure 4.2.

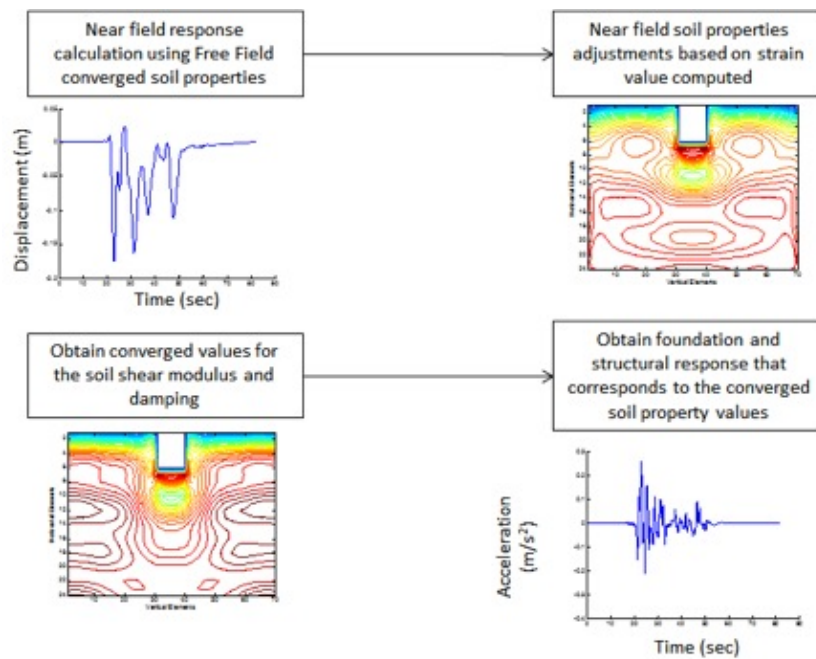


Figure 4.2: Process for a Two-Dimensional Equivalent Linear Analysis

In the process outlined above, a near-field equivalent linear analysis is conducted once to obtain a first approximation of the near-field response. In many applications in geotechnical engineering, the first approximation obtained for the near-field is considered adequate, and no further adjustments are done. However, we sought to analyze the effects of further adjustments to the soil properties beyond the free-field analysis. Therefore, further iterations are conducted by adjusting the near-field properties with respect to the updated strain levels, and recalculating the system response using the updated properties. The same criterion for convergence used in the free-field analysis can be employed in the near-field analysis.

In the finite element analysis for the near-field region, additional soil property adjustments are applied to the quadrilateral elements. The shear strain for a quadrilateral element varies within the element, and a representative shear strain is calculated as the average of shear strains evaluated at the integration points.

The effective shear strain for an  $i^{th}$  quadrilateral element can be calculated as follows:

$$\gamma_{eff} = \frac{1}{4} \sum_{j=1}^4 \left[ \frac{\partial}{\partial z} \quad \frac{\partial}{\partial x} \right] \mathbf{N}_i(\xi_j, \eta_j) \mathbf{U}_i(\xi_j, \eta_j) \quad (4.3)$$

where  $\mathbf{N}_i(\xi_j, \eta_j)$  is the shape function defined in Equation 2.61, and  $\xi$  and  $\eta$  are the local coordinates of the element. Substituting the shape functions into Equation 4.3 and calculating the partial derivatives produces the following

expression for effective strain:

$$\gamma_{eff} = \frac{1}{16ab} \sum_{j=1}^4 \begin{bmatrix} -a(1 - \xi_j) \\ -b(1 - \eta_j) \\ -a(1 + \xi_j) \\ b(1 - \eta_j) \\ a(1 + \xi_j) \\ b(1 + \eta_j) \\ a(1 - \xi_j) \\ -b(1 + \eta_j) \end{bmatrix}^T \mathbf{U}_i \quad (4.4)$$

where  $a$  and  $b$  are the dimensions of the rectangular element.

As previously discussed, the evaluation points for a second order Gauss integration scheme are at  $\left(\frac{-1}{\sqrt{3}}, \frac{-1}{\sqrt{3}}\right)$ ,  $\left(\frac{1}{\sqrt{3}}, \frac{-1}{\sqrt{3}}\right)$ ,  $\left(\frac{1}{\sqrt{3}}, \frac{1}{\sqrt{3}}\right)$ , and  $\left(\frac{-1}{\sqrt{3}}, \frac{1}{\sqrt{3}}\right)$ . The Gauss integration points are chosen as the representative strain locations because the components of the strain matrix at these points were already computed in the stiffness matrix calculation, thus reducing the computational effort.



## 4.2 Equation of Motion

For the purposes of this study, the equivalent linear analysis done can be represented in the form of:

$$\mathbf{K}\mathbf{U} = \mathbf{P} \quad (4.5)$$

where  $\mathbf{K}$  is the global stiffness matrix,  $\mathbf{U}$  is the global displacement vector, and  $\mathbf{P}$  is the global force vector. All of these quantities are formed through assembly of element stiffness matrices and loads.  $\mathbf{K}$  is the dynamic stiffness matrix of the system, which already includes the inertial contribution to the dynamic stiffness. The shear modulus used to construct the global stiffness matrix is the complex shear modulus, which accounts for material damping of the system. Hysteretic damping is assumed.

Input ground motion used in the analysis is converted using an FFT algorithm into the frequency domain, and the transform is applied as a boundary condition on the domain of the system. Once the ground motion is applied, the system of equations is solved for each frequency to produce both the soil and structural response in the frequency domain. Time history of the structural response as well as the surface response of the soil medium can be generated by calculating the inverse FFT of the analysis results.

A limitation of frequency-domain computations is that the frequency range must be extended to the maximum usable frequency for the analysis. Several factors affect the usable frequency. The time step of the time series

provides a limitation in the form of the Nyquist frequency. A detailed discussion regarding the usable-frequency limitation was reported by (Kottke, 2010), with the generally accepted result that the frequency of 25 Hz serves as an acceptable upper boundary. Therefore, for practical site-response analysis, input motions above 25 Hz can be neglected through the use of a low-pass filter.

Additionally, it is known that the fundamental frequency of a single homogeneous soil layer is given by:

$$f_{fund} = \frac{C_s}{4H} \quad (4.6)$$

where  $C_s$  is the shear wave velocity of the soil and  $H$  is the thickness of the layer. The shear wave velocity is defined as:

$$C_s = \sqrt{\frac{G_{max}}{\rho}} \quad (4.7)$$

A suitable layer height must be smaller than  $\frac{1}{4}$  of the minimum wavelength of traveling waves. The minimum wavelength is defined by the following equation:

$$\lambda_{min} = \frac{2\pi \cdot C_s}{\omega_{max}} \quad (4.8)$$

However, it is often desirable that the layer height represent a finer discretization, between  $\frac{1}{8}$  to  $\frac{1}{32}$  of the minimum wavelength. Therefore, the maximum soil layer height allowed which ensures adequate discretization is:

$$h_{max} = \frac{1}{8} \frac{2\pi C_s}{\omega_{max}} = \frac{\pi}{4} \frac{1}{\omega_{max}} \quad (4.9)$$

Soil layer heights in the site-response analysis must be at most  $h_{max}$  as defined in Equation 4.9. The height requirement applies for both the free-field and near-field analyses. It is important to consider that  $h_{max}$  is a function of  $C_s$ , which in turn depends on the shear modulus. As iterations of the equivalent linear analysis progress, reductions are made to the shear modulus which translate to smaller maximum layer height requirements. This issue can be accounted for by either adjusting the layer heights after each iteration to ensure consistency with the reduced shear modulus, or by defining set layer heights that meet the requirement in the extreme shear modulus case. The latter option is used in this research.

Several simplifications can be implemented to improve the analysis process and reduce the computational effort. As mentioned above, the highest frequency that can be correctly analyzed is limited by the thickness of the soil layer. This reduces the number of frequencies analyzed, as the contribution of frequencies higher than the determined limit will be set to zero. Additionally, site-response calculations are only carried out for positive frequencies; site response for negative frequencies can easily be found by taking the complex conjugate of the positive frequency responses.

### 4.3 Boundary Conditions

Response of the soil-structure system due to input ground motion is found by solving the system of equations above. Before the solution can be computed, the matrices must be arranged in a certain way to ensure an efficient process of solution.

The global matrices are formed through assembly of the individual element matrices. For a free-field analysis, the assembly is simply a series of connections of the consecutive layer matrices. For a near-field analysis, the assembly is done based on contributions of the finite element matrices to the global nodes of the domain. The contributions are pictured in Figure 4.3 .

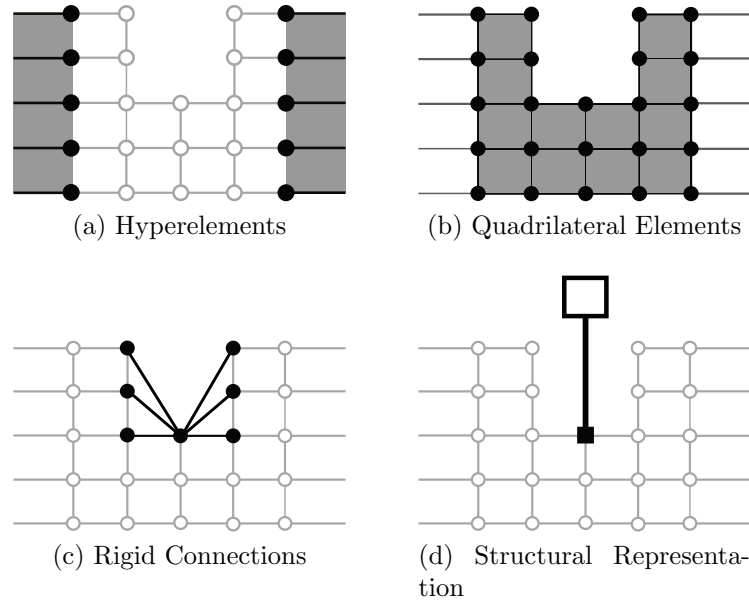


Figure 4.3: Element Contributions to the Global Dynamic Stiffness Matrix

In addition to assembly of the global stiffness matrix, appropriate boundary conditions must be applied to the system. Input displacement ground motion applied at the bottom of the soil layer serves as a boundary condition that represents the source of wave motion propagating through the soil. The displacement of each of the nodes at the bottom of the layer is fixed to the frequency-domain value of the specified ground motion.

The recorded ground motion previously described in Chapter 3 will be used for the site-response analysis. Zero padding of the recorded time history is done to ensure an efficient FFT process and to allow dissipation of the transient motion. The resulting frequency-domain motion is divided by  $-\omega^2$  to produce the displacement input motion, as the recorded input motion was originally an acceleration recorded motion.

Actual earthquake motions are often recorded at the surface of the soil. An input ground motion at the bottom of the layer that would produce the recorded motion at the top must first be determined through a one-dimensional analysis. The process of determining the base motion that corresponds with a recorded surface motion for a fixed set of soil properties is shown in Figure 4.4.

A white noise of unit magnitude is applied at the bottom and the corresponding surface motion is calculated using the free-field analysis (Figure 4.4a). The site response solution is then normalized by dividing the site response by the surface response (Figure 4.4b). The site response corresponding to a unit motion at the top is then scaled by the actual recorded surface motion

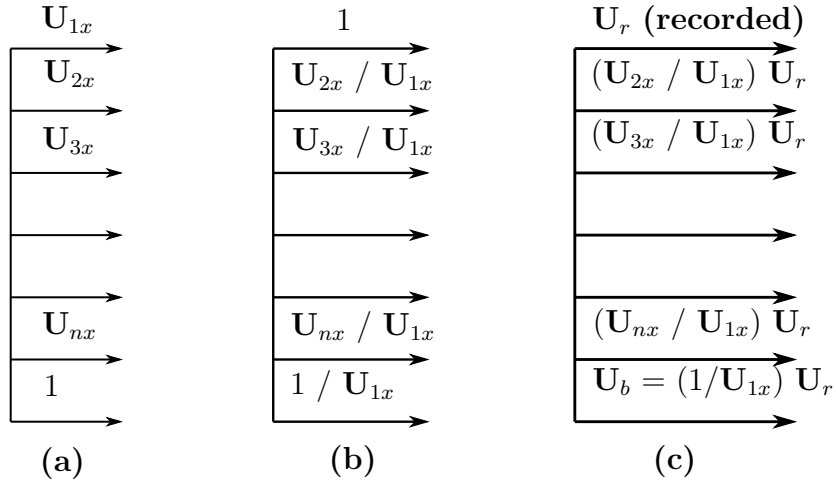


Figure 4.4: Determination of Base Motion

(Figure 4.4c). The resulting response of the bottom of the soil layer represents the input ground motion that corresponds to the recorded surface motion.

The bottom input (bedrock) ground motion is then applied as the boundary condition for subsequent analysis. Removing the last rows and columns of the matrix equation that corresponds to the degree of freedom of the boundary enforces a zero-displacement boundary condition. Additional modification to the matrix equation is needed for non-zero displacement boundary conditions.

This modification can be achieved by adding an additional degree of freedom to the system of equations for each prescribed displacement boundary condition.

In essence, a matrix system of equations of the form:

$$\begin{bmatrix} K_{1,1} & \cdot & \cdot & K_{1,n-1} & K_{1,n} \\ \cdot & \cdot & \cdot & \cdot & \cdot \\ \cdot & \cdot & \cdot & \cdot & \cdot \\ K_{n-1,1} & \cdot & \cdot & K_{n-1,n-1} & K_{n-1,n} \\ K_{1,n} & \cdot & \cdot & K_{n,n-1} & K_{n,n} \end{bmatrix} \begin{pmatrix} U_1 \\ \cdot \\ \cdot \\ U_{n-1} \\ U_n \end{pmatrix} = \begin{pmatrix} P_1 \\ \cdot \\ \cdot \\ P_{n-1} \\ P_n \end{pmatrix} \quad (4.10)$$

is written as

$$\begin{bmatrix} K_{1,1} & \cdot & \cdot & K_{1,n-1} & K_{1,n} & 0 & 0 \\ \cdot & \cdot & \cdot & \cdot & \cdot & 0 & 0 \\ \cdot & \cdot & \cdot & \cdot & \cdot & 0 & 0 \\ K_{n-1,1} & \cdot & \cdot & K_{n-1,n-1} & K_{n-1,n} & -1 & 0 \\ K_{1,n} & \cdot & \cdot & K_{n,n-1} & K_{n,n} & 0 & -1 \\ 0 & 0 & 0 & -1 & 0 & 0 & 0 \\ 0 & 0 & 0 & 0 & -1 & 0 & 0 \end{bmatrix} \begin{pmatrix} U_1 \\ \cdot \\ \cdot \\ U_{n-1} \\ U_n \\ P_{n-1} \\ P_n \end{pmatrix} = \begin{pmatrix} 0 \\ \cdot \\ \cdot \\ 0 \\ 0 \\ -\hat{U}_{n-1} \\ -\hat{U}_n \end{pmatrix} \quad (4.11)$$

In Equation 4.11, the loading of layer  $n$  is carried to the left-hand side of the equation, because the actual load acting on the bottom of the domain is unknown. No other loads are applied on the other interfaces including the surface. The known displacement motion of the bottom node is represented by  $U_{n-1}$  for the  $x$  direction and  $U_n$  for the  $y$  direction. The choice of using the negative of the motion is done to keep the stiffness matrix symmetric.

Modification of the matrix equation of motion for a near-field analysis is similar to the process outlined above. Additional degrees of freedom are

added to the system of equations for the nodes along the bottom of the near-field domain. The base motion is prescribed to be the displacement of these nodes by the same approach as for the free-field domain.

#### 4.4 Consistent Nodal Forces

Imposing a displacement boundary condition is sufficient for a one-dimensional analysis. In the case of a two-dimensional analysis, additional boundary conditions must be imposed on the sides of the near-field domain. As previously discussed in Section 2.3, the near-field domain consists of quadrilateral elements surrounding the foundation and the embedded structure.

The effects that the far field imposes on the near-field are represented by the hyperelement and the nodal forces that it transfers to the near-field domain. The nodal force consists of an equivalent nodal force due to the displacement of the hyperelement, and a consistent nodal force which represents the internal traction between the hyperelement and the near-field. An illustration of the process is shown in Figure 4.5.

The nodal force represents the ground motion that occurs below the hyperelement, which is transferred through the hyperelement and manifests itself as force applied at the side interfaces of the near-field. The equivalent nodal force is the amount of force that must be applied on the hyperelement interface, in the absence of ground motion, to produce the same amount of displacement as produced by the ground motion under the hyperelement.



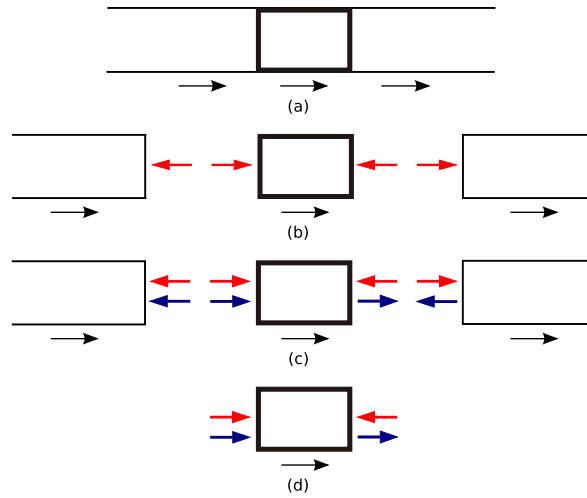


Figure 4.5: Equivalent Nodal Forces

Consider a regular layered medium under horizontal base excitation as shown in Figure 4.6.

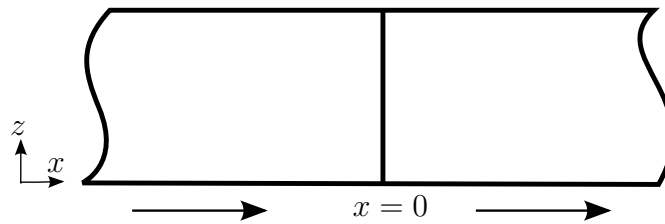


Figure 4.6: Cross-Section of Regular Layered Medium

The free-field solution applies to the domain everywhere, including at the  $x = 0$  cross section. We assume that the free-field motion is

$$\mathbf{U}_f = \begin{Bmatrix} U_{1x} \\ 0 \\ \cdot \\ \cdot \\ U_{nx} \\ 0 \\ U_{base} \\ 0 \end{Bmatrix} \quad (4.12)$$

The opposite displacement vector  $\mathbf{U}_c$  is considered such that when superimposed to the free-field displacement above, produces zero displacement everywhere except the base. The base displacement is still the prescribed ground motion.

$$\mathbf{U}_c = \begin{Bmatrix} -U_{1x} \\ 0 \\ \cdot \\ \cdot \\ -U_{nx} \\ 0 \\ 0 \\ 0 \end{Bmatrix} \quad \mathbf{U}_f + \mathbf{U}_c = \begin{Bmatrix} 0 \\ 0 \\ 0 \\ 0 \\ 0 \\ U_{base} \\ 0 \end{Bmatrix} \quad (4.13)$$

The force that is required to enforce the zero displacement on the hyper-element interface is found by multiplying the stiffness matrix of the hyper-element with the negating displacement  $\mathbf{U}_c$ . The equivalent nodal force that must be applied on the near-field to produce the free-field displacement on the interface will be the negative of this force, which is expressed as:

$$\mathbf{F}_c = -\mathbf{S}\mathbf{U}_c \quad (4.14)$$

where  $\mathbf{S}$  is the hyper-element stiffness matrix as defined in Equation 2.97.

The layered medium in Figure 4.6 can then be cut at  $x = 0$  to reveal the tractions acting on both hyperelements. Opposite tractions will be exerted by the hyperelement on the near-field domain, and these tractions can be represented by consistent nodal forces, as shown in Figure 4.7.

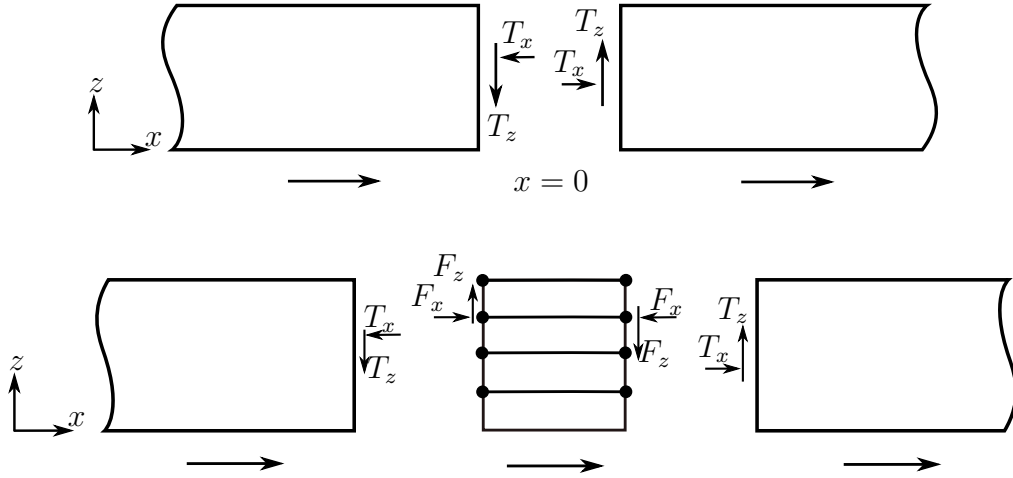


Figure 4.7: Consistent Nodal Forces

The consistent nodal forces for the hyperelement have been previously derived in Section 2.3, and the expression for the consistent nodal force is given in Equation 2.90. For a one-dimensional free-field analysis, the displacement vector does not vary with  $x$ . Therefore, the first term in Equation 2.90 vanishes. Consistent nodal forces applied on the near-field are opposite of the forces acting on the hyperelement. Therefore, for a free-field displacement  $\mathbf{U}_f$ , the consistent nodal force applied is given by:

$$\mathbf{F}_d = -\mathbf{D}\mathbf{U}_f \quad (4.15)$$

where

$$\mathbf{D}_i = \frac{1}{2} \begin{bmatrix} 0 & -\lambda_i & 0 & \lambda_i \\ -G_i & 0 & G_i & 0 \\ 0 & -\lambda_i & 0 & \lambda \\ -G_i & 0 & G_i & 0 \end{bmatrix} \quad (4.16)$$

The forces calculated in Equation 4.15 are for the interface of the right hyperelement. For the left hyperelement interface, the forces would act in the opposite direction. Therefore, the total nodal force to be applied on the left interface is:

$$\mathbf{F}_{nodal} = -\mathbf{S}_l \mathbf{U}_c + \mathbf{D} \mathbf{U}_f \quad (4.17)$$

and on the right interface:

$$\mathbf{F}_{nodal} = -\mathbf{S}_r \mathbf{U}_c - \mathbf{D} \mathbf{U}_f \quad (4.18)$$

## 4.5 Solution Process for System of Equations

A regular assembly of the matrix equation of motion consists of simply mapping the local degrees of freedom to the global degrees of freedom for each element stiffness matrix. However, a finite element based global stiffness matrix is mostly a band matrix. Expressing the stiffness matrix as a sparse matrix is beneficial in reducing memory requirements as well as computational effort in solving the system of equations.

An efficient way to represent the sparse matrix is through the compressed column storage. The elements of a two-dimensional matrix are stored by recording the pairing of row indices and the nonzero values of the elements

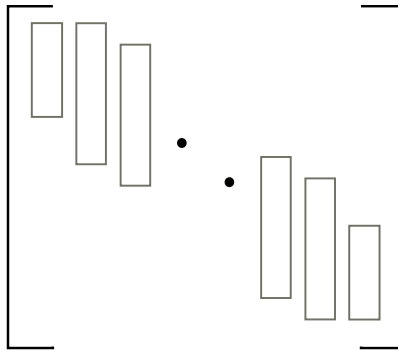


Figure 4.8: Banded Stiffness Matrix

of successive columns. Indices of the first nonzero elements of the matrix columns are also recorded as column pointers. The stiffness matrix in Figure 4.8 is reorganized as below:

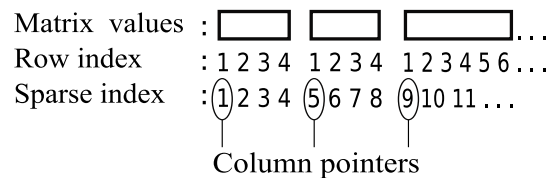


Figure 4.9: Reorganized Stiffness Matrix

In order to take advantage of the sparse-matrix format, the element stiffness matrices are assembled directly into the compressed column storage of the global stiffness matrix. Contribution matrices that map the location of the dense matrix elements to its sparse counterpart, shown in Figure 4.10, facilitate the assembly process. Each column of the first contribution matrix in Figure 4.10 logs the dependence between a global degree of freedom and all other global degrees of freedom. The relationship is determined by examining

the relationship in the element stiffness matrices. By using this approach, the size of the matrix is reduced to approximately the number of degrees of freedom multiplied by the width of the band. The mapping is done for the width of the band.

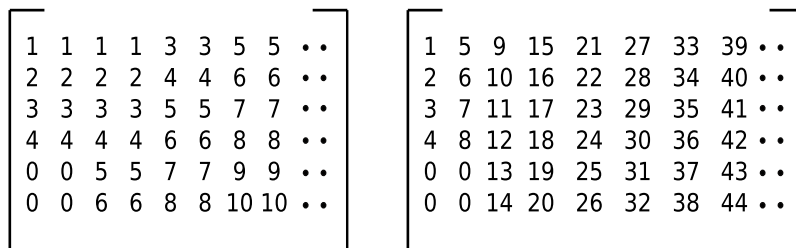


Figure 4.10: Row Indices for Global Matrix Elements and Corresponding Sparse Matrix Indices

The elements of the first contribution matrix are numbered sequentially in a second contribution matrix as shown in Figure 4.10. The sequential numbering represents the indices of the column compressed sparse matrix. For a given column and row index pair in the first contribution matrix, the corresponding location of the element in the sparse matrix is indicated by the value of the second contribution matrix. Rearranging the first contribution matrix as a vector in column major will produce the row index sparse vector. The first row of the second contribution matrix represents the column pointer of the sparse vector.

The global stiffness matrix can be assembled in sparse format once the relationship between the global matrix row indices and the sparse matrix value

indices are determined. Element stiffness matrices are assembled to the sparse format one column at a time by following the mapping shown in Figure 4.10. Assembly is done for the load vector using a similar approach. The procedure described above is designed for banded matrices, but it is also applicable to non-banded matrices as well.

## 4.6 Application of LU Decomposition

A linear system of equations with a triangular matrix can be solved much more easily through either back substitution or forward substitution. A proper square non-singular matrix  $\mathbf{A}$  can be written as an upper triangular matrix  $\mathbf{U}$  through Gaussian elimination. Factors of the row operations are recorded into a lower triangular matrix  $\mathbf{L}$  with unit diagonal entries. The matrix  $\mathbf{A}$  is then written as:

$$\mathbf{A} = \mathbf{LU} \tag{4.19}$$

where

$$\mathbf{L} = \begin{bmatrix} 1 & 0 & 0 & \cdots & 0 \\ L_{21} & 1 & 0 & & 0 \\ L_{31} & L_{32} & 1 & & \vdots \\ \vdots & & & \ddots & 0 \\ L_{n1} & L_{n2} & L_{n3} & \cdots & 1 \end{bmatrix} \quad \mathbf{U} = \begin{bmatrix} U_{11} & U_{12} & U_{13} & \cdots & U_{1n} \\ 0 & U_{22} & U_{23} & & U_{2n} \\ 0 & 0 & U_{33} & & U_{3n} \\ \vdots & & & \ddots & \vdots \\ 0 & 0 & 0 & \cdots & U_{nn} \end{bmatrix} \tag{4.20}$$

In practical applications, pivoting is included in the decomposition process to ensure efficiency. Both sides of the linear system of equations are multi-

plied by a permutation matrix  $\mathbf{P}$  prior to matrix decomposition. The pivoted system of equations becomes:

$$\mathbf{PAx} = \mathbf{d} \quad (4.21)$$

where  $\mathbf{d} = \mathbf{Pb}$ . By decomposing the matrix product  $\mathbf{PA}$  into a product of  $\mathbf{L}$  and  $\mathbf{U}$ , the equation becomes:

$$\mathbf{L(Ux)} = \mathbf{d} \quad (4.22)$$

which can then be written as two separate equations made up of triangular matrices:

$$\mathbf{Ly} = \mathbf{d} \quad (4.23)$$

$$\mathbf{Ux} = \mathbf{y} \quad (4.24)$$

The solution of the original system of equations is found by first solving Equation 4.23 using forward substitution. The result is substituted into Equation 4.24 which is then solved by back substitution.

Application of the sparse format allows for even further improvements of the process of solving linear systems. A process of LU decomposition for sparse matrices is discussed by Li et al. (2011) in the manual for the SuperLU code. SuperLU is a code developed by Li et al. (2011) to efficiently solve linear systems with sparse matrices through the use of LU decomposition.

The procedure of the SuperLU code consists of adjustments to the LU decomposition process previously described. Instead of using one permutation



matrix, the  $\mathbf{A}$  matrix is premultiplied by a row permutation matrix  $\mathbf{P}_r$  and a column permutation matrix  $\mathbf{P}_c$ . This process maximizes the sparsity of the triangular matrices as well as increases the stability of the numerical process. Additionally,  $\mathbf{A}$  is premultiplied by two diagonal matrices to reduce sensitivity of the result to perturbations of the  $\mathbf{A}$  matrix. Further details are described by Li et al. (2011).

The matrix  $\mathbf{A}$  is thus written as:

$$\mathbf{A} = (\mathbf{D}_r^{-1} \mathbf{P}_r^{-1} \mathbf{L} \mathbf{U} \mathbf{P}_c^{-1} \mathbf{D}_c^{-1}) \quad (4.25)$$

where

$\mathbf{P}_r$  : Row permutation matrix

$\mathbf{P}_c$  : Column permutation matrix

$\mathbf{D}_r$  : Row equilibration diagonal matrix

$\mathbf{D}_c$  : Column equilibration diagonal matrix

The SuperLU solution process consists of expressing the linear system as:

$$\begin{aligned} \mathbf{x} &= \mathbf{A}^{-1} \mathbf{b} \\ &= (\mathbf{D}_r^{-1} \mathbf{P}_r^{-1} \mathbf{L} \mathbf{U} \mathbf{P}_c^{-1} \mathbf{D}_c^{-1})^{-1} \mathbf{b} \\ &= \mathbf{D}_c (\mathbf{P}_c (\mathbf{U}^{-1} (\mathbf{L}^{-1} (\mathbf{P}_r (\mathbf{D}_r \mathbf{b})))) \end{aligned} \quad (4.26)$$

where the process of evaluating  $(\mathbf{L}^{-1} (\mathbf{P}_r (\mathbf{D}_r \mathbf{b})))$  and  $(\mathbf{U}^{-1} (\mathbf{L}^{-1} (\mathbf{P}_r (\mathbf{D}_r \mathbf{b}))))$  is done through forward and back substitutions instead of calculating the inverse. SuperLU stores the matrices in the compressed column format as well.

SuperLU allows for efficient solution of multiple linear systems with identical left-hand side. The solution process is divided into three steps: initialization, LU factorization, and computation of solution. The processes can be independently executed and the results of each step stored for repeated use. Once a linear system is solved, all intermediary variables including the triangular matrices can be reapplied. Calculating the solution of a linear system with different right-hand sides only requires adjustment in the third process.

The above solution process is implemented by SuperLU and is used in this research to solve the equivalent linear system of equations.

#### **4.7 Soil-Property Adjustments using Perturbation Method**

A soil-structure system can be analyzed for a constant set of soil properties. The nonlinear behavior of soil necessitates repeated iterations to account for change in soil properties due to deformation. Updating soil properties leads to a new stiffness matrix in each iteration, and thus the process of factorization must be repeated for a changing left-hand side. The factorization process is one of the most computationally consuming part of the process.

The approach proposed herein to avoid repeated factorization is to form an equivalent linear soil-structure system with a constant left-hand side. This can be achieved by using the small-strain soil properties to construct the stiffness matrix, and then keeping the stiffness matrix constant throughout the entire analysis. Change in soil properties due to deformation will eventually be reflected in the right-hand side of the linear system instead of the left-hand

side, which allows for a one-time LU factorization. The SuperLU solution process is compartmented to allow the results of a previous factorization to be used in further analysis, which allows it to efficiently solve multiple linear systems with the same left-hand side.

Changes in the soil properties can be accounted for without changing the left-hand side by using the perturbation method. A perturbation method was previously described by Ikeda (2008) and has been extended in this work. The equation of motion is expressed using perturbation analysis, and the perturbation terms are moved to the right-hand side. In this manner, the equation of motion retains the small-strain stiffness matrix, and only the loading of the system is changed.

With an equation of motion

$$\mathbf{K}\mathbf{U} = \mathbf{P} \quad (4.27)$$

the quantities of the analysis can be written in terms of a constant baseline and small perturbations of increasing order:

$$\mathbf{K} = \mathbf{K}^{(0)} + \varepsilon\mathbf{K}^{(1)} + \varepsilon^2\mathbf{K}^{(2)} + \dots \quad (4.28)$$

$$\mathbf{U} = \mathbf{U}^{(0)} + \varepsilon\mathbf{U}^{(1)} + \varepsilon^2\mathbf{U}^{(2)} + \dots \quad (4.29)$$

$$\mathbf{P} = \mathbf{P}^{(0)} + \varepsilon\mathbf{P}^{(1)} + \varepsilon^2\mathbf{P}^{(2)} + \dots \quad (4.30)$$

where  $\varepsilon$  represents the extent of perturbation. These quantities are substituted

into the equation of motion (Equation 4.27) to obtain:

$$\begin{aligned} & (\mathbf{K}^{(0)} + \mathbf{K}^{(1)} + \varepsilon^2 \mathbf{K}^{(2)} + \varepsilon^3 \mathbf{K}^{(3)} + \dots) (\mathbf{U}^{(0)} + \varepsilon \mathbf{U}^{(1)} + \varepsilon^2 \mathbf{U}^{(2)} + \varepsilon^3 \mathbf{U}^{(3)} + \dots) \\ & = \mathbf{P}^{(0)} + \varepsilon \mathbf{P}^{(1)} + \varepsilon^2 \mathbf{P}^{(2)} + \varepsilon^3 \mathbf{P}^{(3)} + \dots \end{aligned} \quad (4.31)$$

when expanded and rewritten the latter equation becomes:

$$\begin{aligned} & \mathbf{K}^{(0)} \mathbf{U}^{(0)} + \varepsilon \mathbf{K}^{(0)} \mathbf{U}^{(1)} + \varepsilon^2 \mathbf{K}^{(0)} \mathbf{U}^{(2)} + \varepsilon^3 \mathbf{K}^{(0)} \mathbf{U}^{(3)} \\ & = \mathbf{P}^{(0)} + \varepsilon [\mathbf{P}^{(1)} - \mathbf{K}^{(1)} \mathbf{U}^{(0)}] + \varepsilon^2 [\mathbf{P}^{(2)} - \mathbf{K}^{(1)} \mathbf{U}^{(1)} - \mathbf{K}^{(2)} \mathbf{U}^{(0)}] \\ & \quad + \varepsilon^3 [\mathbf{P}^{(3)} - \mathbf{K}^{(1)} \mathbf{U}^{(2)} - \mathbf{K}^{(2)} \mathbf{U}^{(1)} - \mathbf{K}^{(3)} \mathbf{U}^{(0)}] + \dots \end{aligned} \quad (4.32)$$

The above expression is expected to be true for any value of  $\varepsilon$ , including  $\varepsilon$  equal to zero. It is then possible to continuously take the derivatives of the above expression with respect to  $\varepsilon$ , to come up with the equations appropriate for the orders of the perturbation. The zeroth order of the perturbation is expressed as:

$$\mathbf{K}^{(0)} \mathbf{U}^{(0)} = \mathbf{P}^{(0)} \quad (4.33)$$

which corresponds to the soil-structure system with small-strain soil properties.

The zeroth order serves as a starting point of the analysis to provide a first approximation towards the solution of  $\mathbf{U}$ . Additional orders of the perturbation provides refinement to the solution. Further derivation of Equation 4.32 gives the next orders of perturbation as follows:

First Order:

$$\mathbf{K}^{(0)}\mathbf{U}^{(1)} = \mathbf{P}^{(1)} - \mathbf{K}^{(1)}\mathbf{U}^{(0)} \quad (4.34)$$

Second Order:

$$\mathbf{K}^{(0)}\mathbf{U}^{(2)} = \mathbf{P}^{(2)} - \mathbf{K}^{(1)}\mathbf{U}^{(1)} - \mathbf{K}^{(2)}\mathbf{U}^{(0)} \quad (4.35)$$

Third Order:

$$\mathbf{K}^{(0)}\mathbf{U}^{(3)} = \mathbf{P}^{(3)} - \mathbf{K}^{(1)}\mathbf{U}^{(2)} - \mathbf{K}^{(2)}\mathbf{U}^{(1)} - \mathbf{K}^{(3)}\mathbf{U}^{(0)} \quad (4.36)$$

Analysis of the equivalent linear system can be simplified by limiting the change of  $\mathbf{K}$  as a first-order perturbation. Representing the iterative changes of  $\mathbf{K}$  as higher order requires keeping track of every sequential change to the stiffness matrix, which will become memory intensive for many iterations. First-order representation only requires the storage of one perturbation of the stiffness matrix.

Additionally, for the soil-structure system of interest, the analysis is conducted for a given earthquake motion and unchanging consistent nodal forces. Therefore, perturbations of  $\mathbf{P}$  do not need to be considered in the analysis.

The simplification produces a set of equations which represents the iterative first-order procedure to be used in the equivalent linear analysis of soil structure systems. The procedure is illustrated in the flowchart in Figure 4.11

yielding a system of equations with a constant left-hand side, and a changing right-hand side. Using the perturbation method is very beneficial in the sense that when using LU decomposition to solve the system, only one LU factorization needs to be carried out. This implementation aligns well with SuperLU's ability to reuse the initial factorization to solve multiple linear equations efficiently. Even in the right-hand side, only the  $\mathbf{U}$  changes, and the matrix that multiples  $\mathbf{U}$  stays constant.

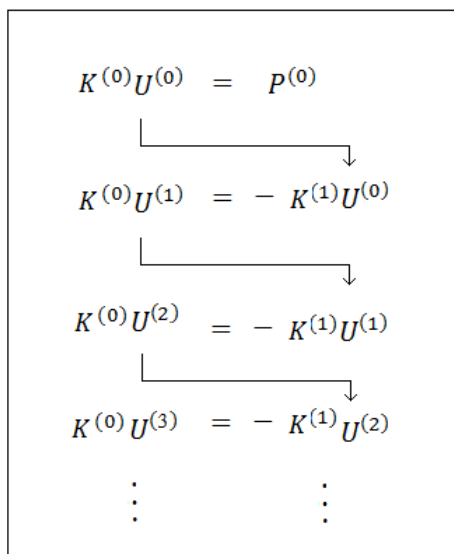


Figure 4.11: Iterative Process of First Order Perturbation Method

Limiting  $\mathbf{K}$  to a first-order perturbation has the advantage of keeping the right-hand side computationally simple, with an unchanging matrix multiplier, and only  $\mathbf{U}$  changes. The matrix multiplication of the right-hand side is also efficient because the sparse mapping and all the other BLAS preparations for matrix-vector multiplications must be done only once.

The computational effort involved in the evaluation of further iterations in Figure 4.11 for higher-order solutions is minimal compared to the effort involved in LU factorization for the initial calculation.

The procedure shown in the flowchart can be extended to continuously find higher orders of the displacement, making the approximation of  $\mathbf{U}$  even more accurate. The final approximation of  $\mathbf{U}$  is obtained from summing up all the perturbation orders of  $\mathbf{U}$  found through the process outlined in Figure 4.11. A convergence criterion can be applied to end the iterative process once higher-order displacements fall under a certain defined threshold.

The traditional approach to conducting equivalent linear analysis is to solve the linear system of equations for every iteration of the process. Every time the soil properties are updated, a new stiffness matrix is developed, the solution process of solving the equation of motion involves solving the new stiffness matrix and factorizing it again.

The perturbation approach provides an efficient process for recalculating the site response for successive updated soil properties due to deformation level changes. The perturbation analysis efficiently determines the site response of the new equivalent linear system without the need to factorize the new stiffness matrix.

By examining Equation 2.75, for an equivalent linear analysis of the soil structure system, we have

$$\mathbf{K} = \mathbf{G} - \omega^2\mathbf{M} \quad (4.37)$$

We expand  $\mathbf{G}$  out as a perturbation series, in terms of perturbation

$$\mathbf{G} = \mathbf{G}^{(0)} + \varepsilon \mathbf{G}^{(1)} + \varepsilon^2 \mathbf{G}^{(2)} + \dots \quad (4.38)$$

Site-response analysis due to adjustment of soil properties is done one frequency at a time, and the change in stiffness matrix is also done one frequency at a time. Therefore, only  $\mathbf{G}$  changes. For each frequency,  $\omega^2\mathbf{M}$  does not change from one set of soil properties to the next, because the density  $\rho$  is assumed to not be strain-dependent, and also volume change is assumed to be negligible.

The zeroth order of the perturbation is therefore expressed as:

$$\left(\mathbf{G}^{(0)} - \omega^2\mathbf{M}\right)\mathbf{U}^{(0)} = \mathbf{P}^{(0)} \quad (4.39)$$

Equation 4.39 corresponds to the soil structure system with initial soil properties, and  $\mathbf{G}^{(0)} - \omega^2\mathbf{M}$  is the small strain dynamic stiffness matrix.

$\mathbf{P}^{(0)}$  is the loading of the soil structure system, which includes enforced displacement input ground motion boundary condition and consistent nodal forces.

Equation 4.39 provides the initial site-response analysis for small strain soil properties for each excitation frequency of the analysis. Calculation of site property adjustment appropriate with the level of deformation from the site response produced from Equation 4.39 produces a new stiffness matrix.



Knowing the new stiffness matrix, the first order of the stiffness matrix can be expressed as:

$$\mathbf{K}^{(1)} = \mathbf{G}^{(1)} \quad (4.40)$$

where  $\mathbf{G}^{(1)}$  is the difference between the shear modulus stiffness matrix with updated soil properties and small strain stiffness matrix. Therefore, the first order of perturbation which includes the updated soil property in the analysis is expressed as:

$$\left(\mathbf{G}^{(0)} - \omega^2\mathbf{M}\right)\mathbf{U}^{(1)} = -\mathbf{G}^{(1)}\mathbf{U}^{(0)} \quad (4.41)$$

We assume  $\mathbf{K}$  is only expressed up to the first order. Therefore, the changes in  $\mathbf{G}$  are assumed to be expressed up to the first order only as well. Therefore,  $\mathbf{G}^{(2)}$ , etc. vanish. The second order of perturbation is then:

$$\left(\mathbf{G}^{(0)} - \omega^2\mathbf{M}\right)\mathbf{U}^{(2)} = -\mathbf{G}^{(1)}\mathbf{U}^{(1)} \quad (4.42)$$

The expression of higher order follows the same pattern. These equations can be solved similarly to the zeroth order equation with just a change in the right-hand side. Therefore, the same iterative process shown in the flowchart of Figure 4.11 can be used to solve for the site response  $\mathbf{U}$  due to updating of soil properties.

Equivalent linear analysis in the frequency domain requires site response calculation for each incremental frequency. The analysis above consists of the evaluation of site response with the perturbation applied for one frequency at a time. The excitation frequency  $\omega$ , and thus the stiffness matrix of

the system, is constant throughout the perturbation process for that excitation frequency.

However, a new stiffness matrix will need to be assembled for each additional frequency step in the analysis. Factorization of the stiffness matrix will need to be done for all frequencies analyzed. With the number of frequencies analyzed ranging in the thousands, the process quickly becomes computationally expensive.

A proposed solution to the issue is to apply the perturbation approach to also analyze the site response due to different excitation frequencies, in terms of perturbations from the site-response analysis of a reference excitation frequency. The equation of motion for different frequencies have the same loading and similar stiffness matrices. We take the difference between the stiffness matrix for a certain frequency and a reference frequency, and we apply the perturbation method to evaluate the site response for that frequency using the factorization of the original stiffness for the reference frequency.

The perturbation method is first applied to the site-response analysis for the initial soil properties. The site-response analysis is done for each frequency in the analysis, and the soil properties are the same for all frequencies for the initial analysis. The change in the stiffness matrix from one frequency to another will only be reflected in the  $\omega^2\mathbf{M}$  term.

A site-response analysis using the initial soil properties is done for a

reference frequency  $\omega_{ref}$ . The equation of motion that corresponds to  $\omega_{ref}$  is

$$(\mathbf{G}_{\gamma=0} - \omega_{ref}^2 \mathbf{M}) \mathbf{U} = \mathbf{P} \quad (4.43)$$

$\mathbf{G}_{\gamma=0}$  refers to the part of the stiffness matrix composed of the small-strain properties. The solution for the reference frequency serves as the zeroth order solution for the perturbation analysis of other frequencies, that is:

$$\mathbf{K}^{(0)} = (\mathbf{G}_{\gamma=0} - \omega_{ref}^2 \mathbf{M}) \quad (4.44)$$

Because the analysis is done for the initial set of properties, the difference in the stiffness matrix between an equivalent linear system with frequency  $\omega$  and the reference frequency, is

$$\mathbf{K}^{(1)} = -(\omega^2 - \omega_{ref}^2) \mathbf{M} \quad (4.45)$$

and the first order perturbation displacement is found by solving

$$(\mathbf{G}_{\gamma=0} - \omega_{ref}^2 \mathbf{M}) \mathbf{U}^{(1)} = (\omega^2 - \omega_{ref}^2) \mathbf{M} \mathbf{U}^{(0)} \quad (4.46)$$

As previously, we assume  $\mathbf{K}$  is only expressed up to the first order, and the changes in  $\omega^2 \mathbf{M}$  are assumed to be expressed up to the first order only as well. The second order of perturbation is then:

$$(\mathbf{G}_{\gamma=0} - \omega_{ref}^2 \mathbf{M}) \mathbf{U}^{(2)} = (\omega^2 - \omega_{ref}^2) \mathbf{M} \mathbf{U}^{(1)} \quad (4.47)$$

The expression of higher-order follows the same pattern. Therefore, the same iterative process shown in the flowchart of Figure 4.11 can be used to solve for the initial site response  $\mathbf{U}$  for the different frequencies of the analysis.

The process of using the perturbation method for different frequencies can be extended to solve for the site response for different frequencies of the updated soil properties analysis. A reference analysis is needed to serve as the zeroth order solution for the updated soil properties case. Choosing a reference case that consists of the updated soil properties requires factorization of a new stiffness matrix. A more efficient method is to reuse the reference case from the initial analysis which has already been factorized.

The reference case has the same form as in Equation 4.36. The difference in the stiffness matrix between the updated soil properties system case with frequency  $\omega$  and the reference case is

$$\mathbf{K}^{(1)} = \mathbf{G}^{(1)} - (\omega^2 - \omega_{ref}^2) \mathbf{M} \quad (4.48)$$

where  $\mathbf{G}^{(1)}$  is as previously defined. The first order perturbation displacement is found by solving

$$\left( \mathbf{G}_{\gamma=0} - \omega_{ref}^2 \mathbf{M} \right) \mathbf{U}^{(1)} = - \left[ \mathbf{G}^{(1)} - (\omega^2 - \omega_{ref}^2) \mathbf{M} \right] \mathbf{U}^{(0)} \quad (4.49)$$

Similarly to the previous cases, the stiffness matrix perturbation is only expressed to the first order. The expression for the higher order displacements follow the same pattern. Therefore, the iterative process in the flowchart of Figure 4.11 can be applied to solve for the site response accounting for the updated soil properties at all frequencies.

# Chapter 5

## Case Studies

The analysis of soil-structure systems can be carried out using the methods and models developed in the previous chapters. To calculate the response of the soil-structure system, the equivalent linear analysis approach is applied and the soil-structure system is approximated using the finite element models developed in Chapter 2. Calculation of the soil-structure system response is carried out to determine the effects of updating soil properties. The application of these methods is carried out for both the free-field case and the near-field case. In both cases, the soil-structure system response is first determined using an initial set of soil properties. Adjustments of soil properties are applied according to the level of deformation calculated in the initial analysis. Further analyses are carried out using the updated soil properties, and iterative calculations of the updated soil-structure system response are carried out until convergence.

The initial properties used in the free-field analysis correspond to the small-strain properties of the soil. Iterations of the free-field analysis will yield a converged value for the soil properties, which are considered to be the soil properties consistent with the free-field response. The strain-consistent values

obtained for the free-field case are then used as the initial soil properties for the near-field analysis. The near-field response is then calculated for both the free-field converged properties and for the near-field converged properties obtained through further iterations.

It is of interest to study the effects of updating soil properties on the overall soil-structure system response, and to determine the cases where these effects are most significant. The effects of using strain-consistent soil properties are determined by calculating the additional response of the soil-structure system attributable to the change in soil properties. The calculation of this additional response is done by applying the perturbation approach to the analysis method.

The significance of updating soil properties is examined for two case studies. The first case study represents a hypothetical typical massive structure on top of an embedded foundation. The second case study represents a real-life scenario of structures vulnerable to resonant motions propagated through soft soils. Various configurations of the foundation will be examined in both case studies.

## **5.1 Theoretical Case Study**

The theoretical case study entails the analysis of a massive structure on an embedded foundation. The foundation is embedded in a deep soil layer of 240 meters depth. The hypothetical massive structure is formulated on the basis of parameters typical of nuclear power plants:

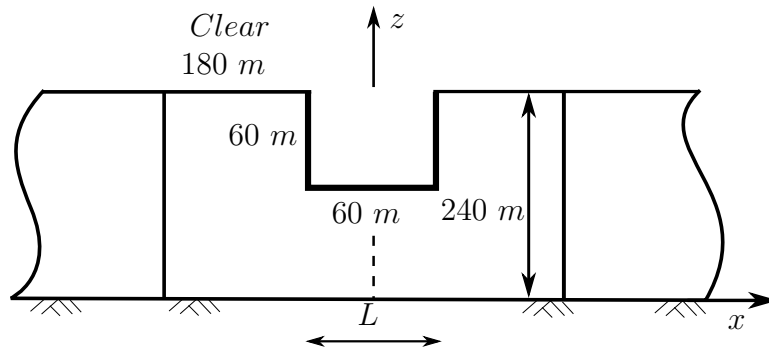


Figure 5.1: Embedded Foundation Supporting Massive Structure

Width of foundation :  $L = 60 \text{ m}$

Depth of embedment :  $D = 60 \text{ m}$

Sidewall height :  $E = 60 \text{ m}$

The soil properties for the theoretical study are chosen to be:

$$G = 80000000 \frac{N}{m^2} \quad (5.1)$$

$$\rho = 2000 \frac{kg}{m^3} \quad (5.2)$$

$$\nu = 0.4 \quad (5.3)$$

$$\beta_{soil} = 0.05 \quad (5.4)$$

The representation of the nuclear reactor structural mass is simplified by assuming a point mass connected to the foundation as described in the soil-structure model in Chapter 2.

The structural parameters are chosen as follows:

$$K_{str} = 1.42 \cdot 10^{11} \frac{kg}{s^2} \quad (5.5)$$

$$M_{str} = 1 \cdot 10^8 \text{ kg} \quad (5.6)$$

$$H_{str} = 15 \text{ m} \quad (5.7)$$

$$\beta_{str} = 0.8 \% \quad (5.8)$$

The soil-structure model used assumes a rigid foundation, i.e. no rotation of the structural beam in relation to the foundation. The choice of ground motion is the 1940 El Centro earthquake motion as described in Chapter 3.

The properties defined above for the theoretical case study are used along with the input ground motion to determine both the free-field and the near-field response of the soil domain and the structure. Comparison of the free-field and near-field structural response is shown in Figure 5.2.

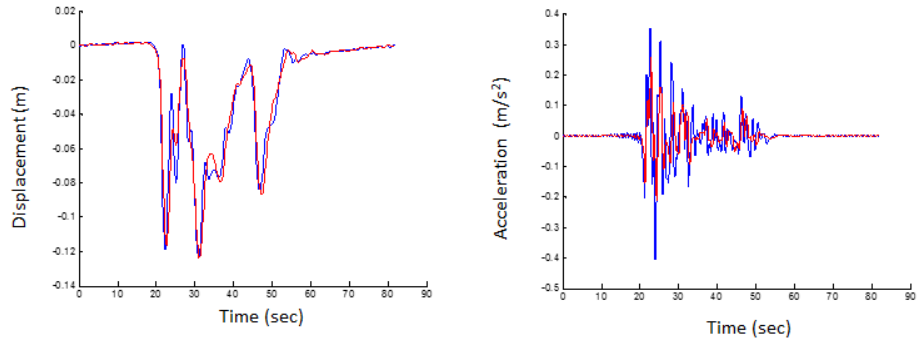


Figure 5.2: Structural Response from One-Dimensional and Two-Dimensional Analyses



The difference of the soil response can be seen by comparing the difference of the horizontal displacement for the free-field and the near-field analysis. One of the contributing factors to the difference of response is the difference in converged values of soil properties between the two analysis. The converged soil properties for the free-field and the near-field analysis are illustrated in Figure 5.3.

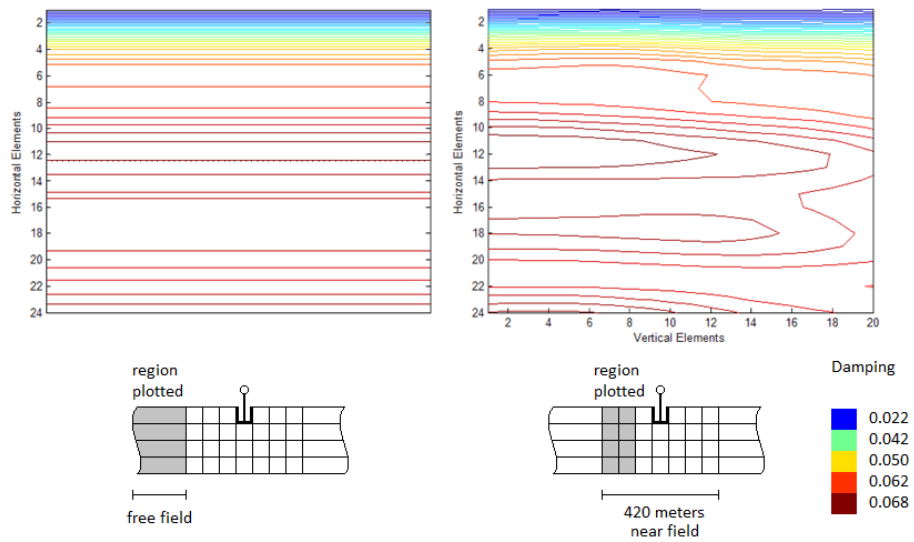


Figure 5.3: Converged Soil Properties in the Free Field and Near Field

In the free-field case, the iteration of properties is conducted with respect to one direction: the vertical. This represents a simplification of the strain-consistent adjustment near the foundation. The near-field analysis further adjusts the soil properties as seen in the above figure, with more significant adjustments closer to the embedded foundation.

In Figure 5.3, it is also noted that the near-field solution far away from the inclusion converges to the free-field solution as expected. This observation serves as a verification of the near-field analysis procedure. The observation can further be corroborated by conducting a near-field analysis of a non-embedded foundation. For various clearance distances for the near-field analysis, the adjustment of soil properties is seen in Figure 5.4 to be identical to the free-field adjustments.

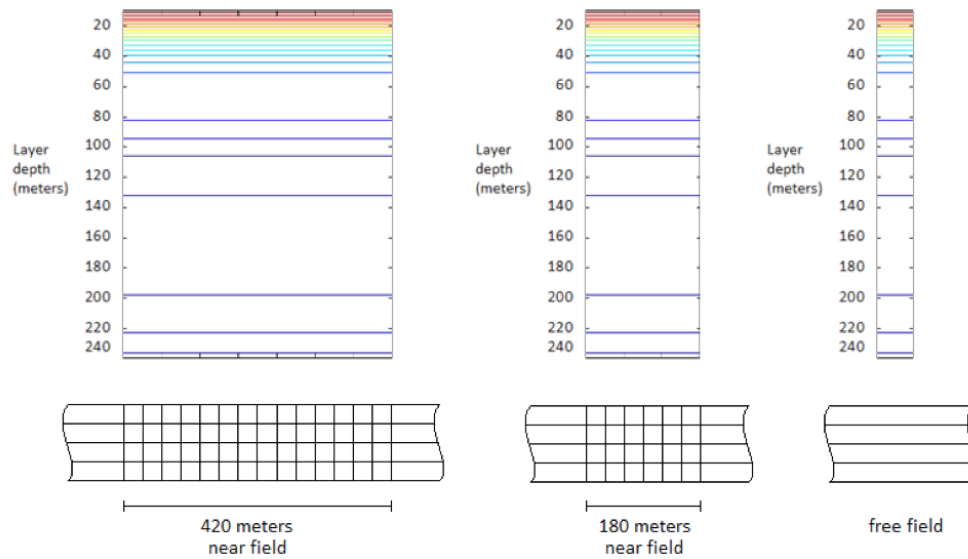


Figure 5.4: Near-Field Adjustments for Various Clearances

The strain levels achieved as well as the soil-property adjustments for the free-field case are shown in Figure 5.5. The results match the level of adjustments observed in the near-field analysis for a surface foundation (with no structural mass).

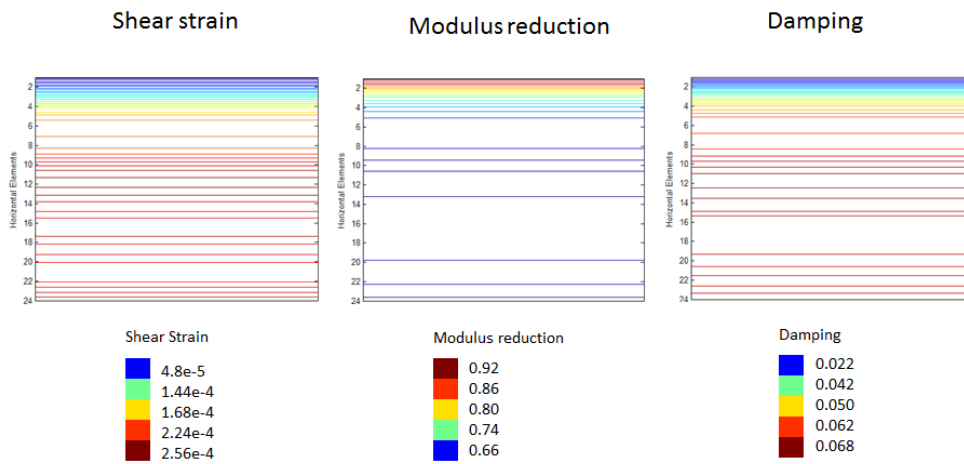


Figure 5.5: Converged Strain-Consistent Free-Field Properties

For the near-field analysis, the response for different configurations of the near-field region is calculated to show the progression of the adjustments of soil properties due to configurational changes. The near-field adjustments are first calculated for a case where the soil is excavated without the presence of an overlying foundation. The next progression is to adjust the properties taking into account the embedded foundation. Lastly, a complete near-field analysis is conducted including the structural mass in the analysis.

The levels of deformation experienced in each of these three cases are shown in Figure 5.6:

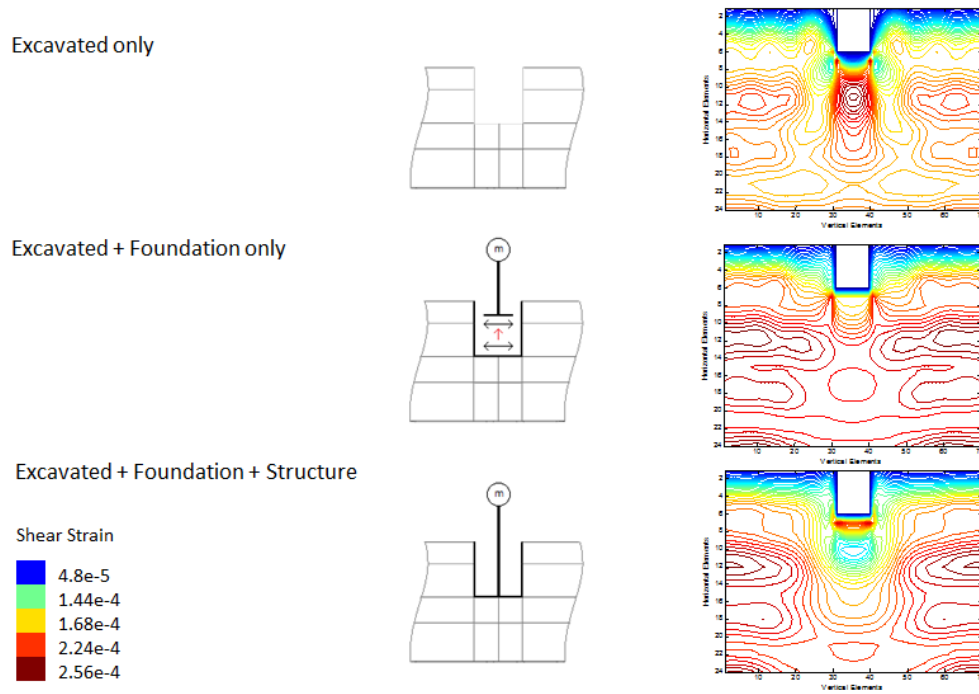


Figure 5.6: Converged Shear Strain Level from Near-Field Analysis

The strain consistent adjustment of properties for the three cases are as follows:

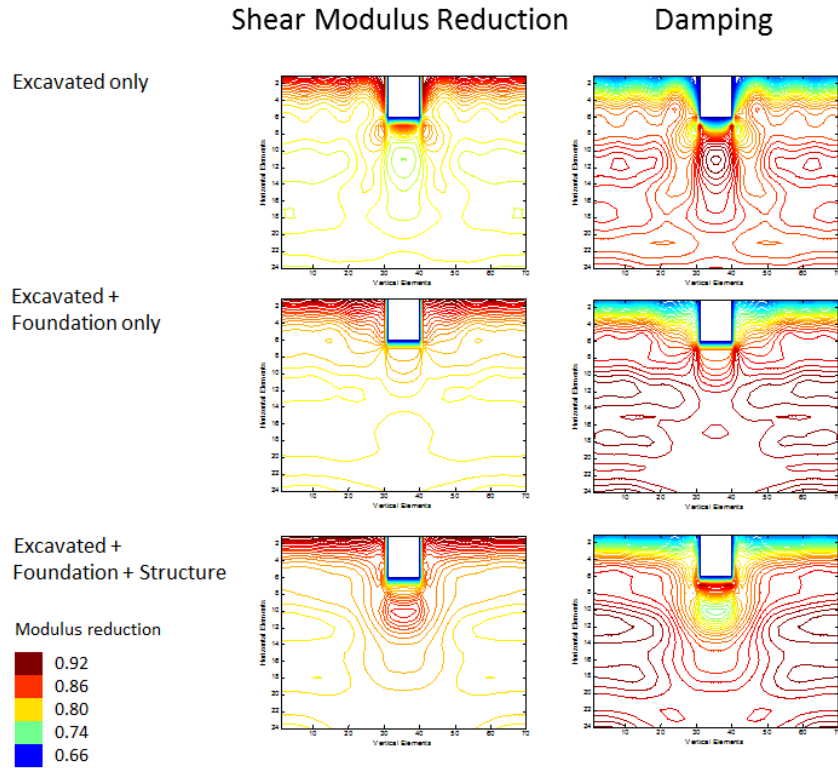


Figure 5.7: Converged Strain-Consistent Near-Field Properties

The results show that the rigid foundation provides an overall effect of reducing the strain levels in the soil elements near the foundation, especially underneath the foundation. The reduction of the strain level contributes lower adjustments of the soil properties underneath the foundation, but the adjustments are still significant when compared to the free-field adjustments.

The difference between the response of the excavation-only case compared to the case with foundation represents the kinematic interaction due to the presence of the foundation. The difference between the response without and with the structure represents the inertial interaction due to the response of the structure providing feedback to the foundation. These effects can be seen by comparing the foundation responses for the three cases as shown in Figure 5.8.

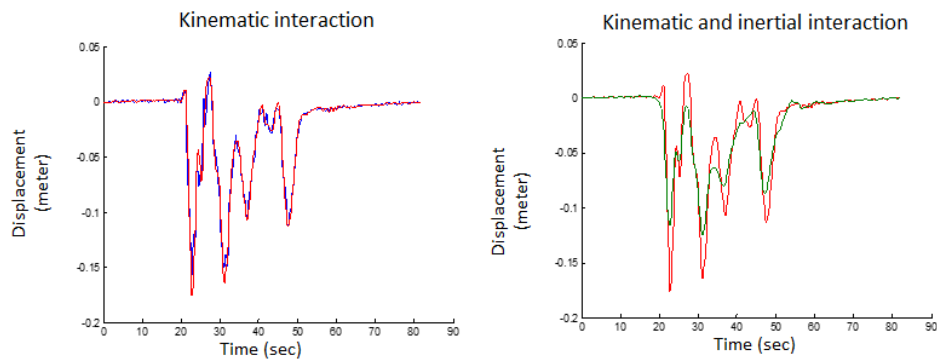


Figure 5.8: Kinematic and Inertial Interaction Effects on Structural Response

The kinematic interaction provides insight to the level of soil-structure interaction that occurred. The soil-structure system responses are provided in Figures 5.9 and 5.10 for both the uncoupled and coupled response of the foundation and the structure. Comparison of the structural acceleration and the foundation rotation highlights the effects of considering the kinematic interaction in the analysis by coupling the foundation and structure response.

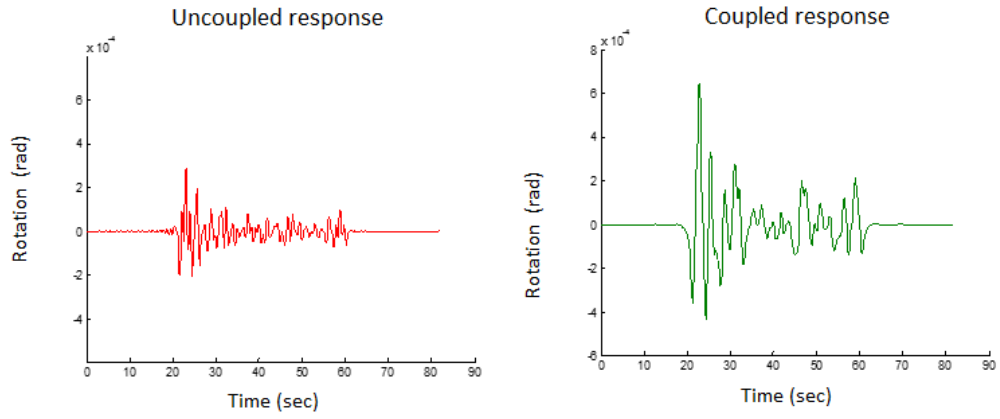


Figure 5.9: Foundation Rotation

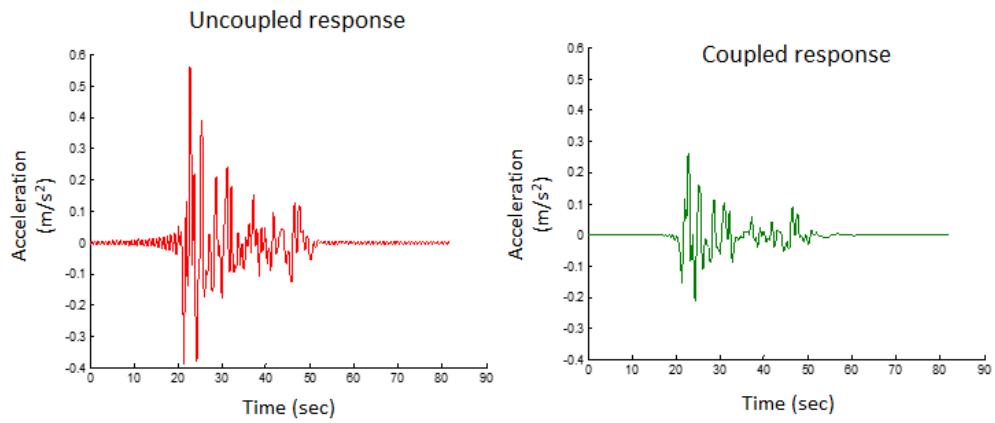


Figure 5.10: Structural Acceleration

## 5.2 Mexico City Case Study

In order to expand on the insights obtained from the hypothetical analysis above, analysis of soil-structure system response is also conducted for multistory buildings heavily damaged during earthquakes. As discussed in Chapter 3, the actual conditions are those for the Mexico City earthquake of 1985, specifically due to the amplification of motion at the SCT site. The structures analyzed have natural periods within the range of periods of the highly amplified motions of the site, between 0.5 to 3 seconds. An illustration of the computational domain is shown in the Figure 5.11.

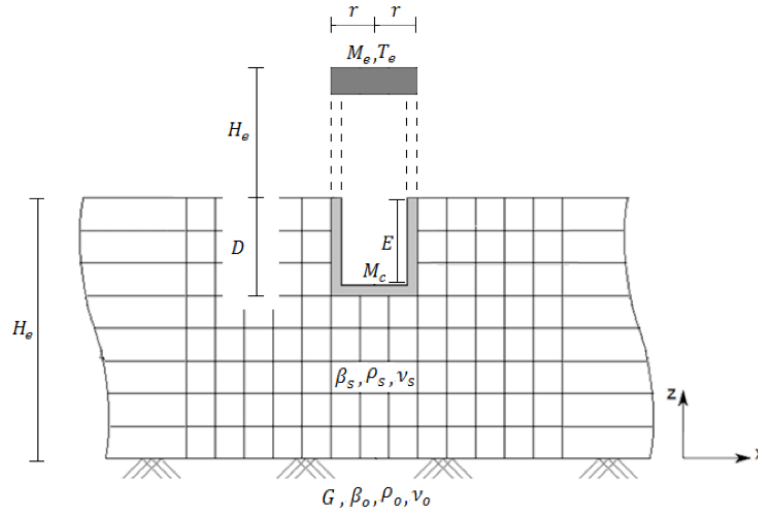


Figure 5.11: Modeling of Mexico City Structure Supported by Embedded Foundation



### 5.2.1 Analysis Parameters

From discussions in Chapter 3, the soil parameters chosen to represent the SCT conditions have been determined to be:

$$T_s = 2 \text{ s} \quad (5.9)$$

$$H_s = 37.5 \text{ m} \quad (5.10)$$

$$\nu_s = 0.45 \quad (5.11)$$

$$\beta_s = 0.02 \quad (5.12)$$

$$C_s = 75 \frac{\text{m}}{\text{s}} \quad (5.13)$$

$$\rho_s = 1386.6 \frac{\text{kg}}{\text{m}^3} \quad (5.14)$$

$$G = 7.8 \cdot 10^6 \frac{\text{N}}{\text{m}^2} \quad (5.15)$$

with the properties of the hard layer taken to be:

$$\nu_o = 0.33 \quad (5.16)$$

$$\beta_o = 0.02 \quad (5.17)$$

$$C_o = 375 \frac{\text{m}}{\text{s}} \quad (5.18)$$

$$\rho_o = 1733.3 \frac{\text{kg}}{\text{m}^3} \quad (5.19)$$

$$G_o = 243.75 \frac{\text{N}}{\text{m}^2} \quad (5.20)$$

$$\rho_o = 1733.3 \frac{\text{kg}}{\text{m}^3} \quad (5.21)$$

The foundation dimensions chosen for the Mexico City case study are based on empirical relationships by Avilés and Pérez-Rocha (1996). Using the soil layer height of 37.5 meters, the foundation dimensions are determined as follows:

$$\text{Width of foundation : } L = 25 \text{ m}$$

$$\text{Depth of embedment : } D = 5 \text{ m}$$

$$\text{Sidewall height : } E = 5 \text{ m}$$

Similarly to the previous case study, the representation of the structural mass is simplified by assuming point masses connected to the foundation. For the Mexico City case, the mass of the structure is represented by two point masses instead of one. Avilés and Pérez-Rocha (1996) mentioned that 20% of the structural mass can be represented as concentrated at the base of the foundation. The remaining 80% of the mass is applied at the effective height of the structure, which is usually about 70% of the actual structural height.

Avilés and Pérez-Rocha (1996) provides the relationship between effective height and natural period for Mexico City structures. Additionally, the mass of the structure is a function of the effective height. The relationships as follows:

$$\frac{H_e}{T_e} = 25 \frac{m}{s} \quad (5.22)$$

$$M_e = 0.15\rho_s\pi r^2 H_e \quad (5.23)$$

Therefore for a natural period of 1 second, the corresponding structural parameters are:

$$H_e = 25 \text{ m} \quad (5.24)$$

$$M_e = 2.55 \cdot 10^6 \text{ kg} \quad (5.25)$$

$$M_c = 6.4 \cdot 10^5 \text{ kg} \quad (5.26)$$

$$K_e = 1.0067 \cdot 10^8 \frac{N}{m} \quad (5.27)$$

The choice of ground motion is the UNAM earthquake motion measured at the CUMV station. The free-field analysis of the SCT site consists of applying the adjusted CUMV ground motion at the bottom of the SCT soil layer profile, and calculating the response at the top of the soil media. The advantage of studying the Mexico City case is that the motion at the top was recorded as well by the SCT station.

### 5.2.2 Analysis of Surface and Embedded Foundations

The response of the soil layer can be better characterized by the response spectra obtained from the analysis. The response spectrum provides illustration of the structural response for a broader range of structural periods. The Mexico City earthquake inflicted on damage on structures with a wide range of periods, especially in the SCT region. The response spectra for the free-field surface response determined by the analysis are shown in Figure

5.12, together with the recorded response spectra at the SCT station.

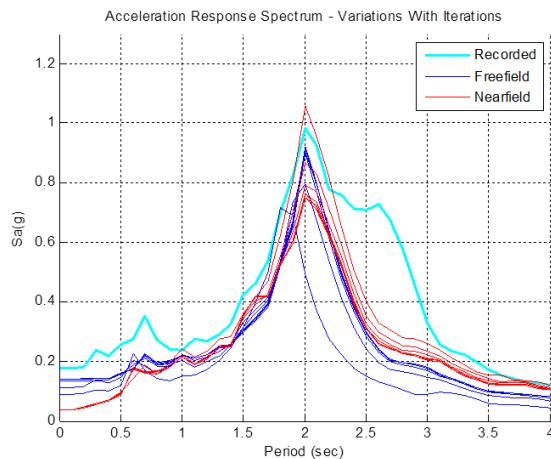


Figure 5.12: Acceleration Response Spectra from Free-Field and Near-Field Iterations

The response spectra determined from the free-field analysis are shown for each iteration of soil properties adjustment. It can be seen that using the initial soil properties based on the SCT profile does not yield a response spectrum close to that recorded at the site. However, further adjustments consistent with the strain levels produces response spectra that approach the recorded motion. The converged soil properties yield surface response very similar to that recorded during the actual earthquake.

With the confidence that the modeled soil profile accurately represents the SCT site conditions, near-field analyses are conducted to analyze the significance of updating soil properties in the near field. The converged soil

properties from the free-field analysis are used as a starting point for the SCT near-field analysis.

An initial near-field analysis is conducted using the converged soil properties from the free-field analysis. The response obtained from this first analysis represents the results that would have been obtained, if further adjustment of the soil properties is not done for the near-field region. In order to study the effects of further adjustment, the near-field analysis is iterated until convergence of the near-field properties has been achieved.

The responses of the soil-structure system are obtained for each iteration of the near-field properties. Response spectra are generated for each iteration and are shown in Figure 5.13.

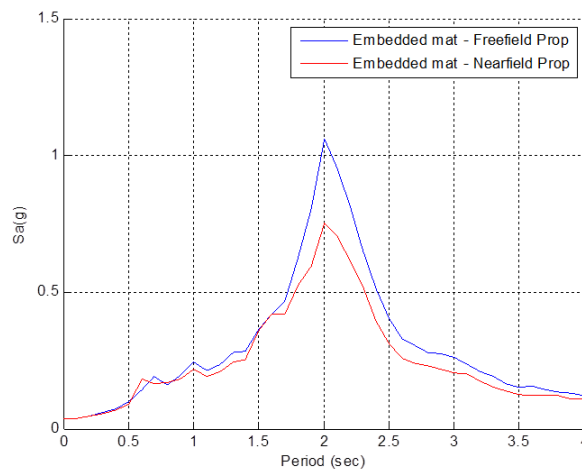


Figure 5.13: Comparison of Embedded Foundation Response using Free-Field and Near-Field Iterated Properties

A progression is evident in the response spectra for the iterations with a general decrease of peak values with further adjustments. Significant differences are observed between the unadjusted response spectra and the response spectra corresponding to the near-field converged properties. Adjusting the soil properties specifically for the near-field region provides a much more accurate representation of the soil-structure response with minimal additional computation.

Various configurations of the foundation are also studied to explore the effects of updating soil properties for the different configurations. For a surface foundation, the additional near-field iterations affects the response spectra as shown in Figure 5.14.

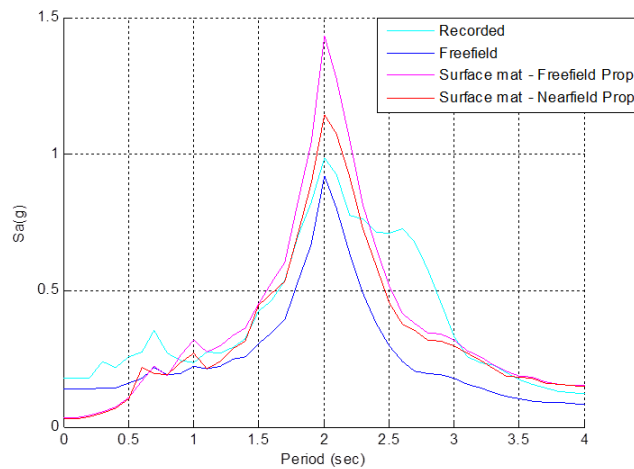


Figure 5.14: Comparison of Surface Foundation Response using Free-Field and Near-Field Iterated Properties

It can be seen from the results, that although there is no embedment of the foundation into the soil, an analysis using the free-field converged properties only yields inaccurate results. Apparently, this is due to the inertial interaction exerted by the motion of the structure on the surface foundation. The structural motion affects the level of damping around the foundation, which affect the foundation response. Conversely, the foundation response affects the structural response by coupling of the system components.

The near-field analysis is also conducted to compare the response of an embedded foundation to the surface foundation. The comparison is provided below for a surface foundation, a mat-only embedded foundation, and an embedded foundation with sidewalls. The response spectra are calculated using the free-field converged soil properties only as well as the near-field converged soil properties.

The responses for all three configurations are significantly reduced when the soil properties are iterated in the near-field region. However, the response for the mat-only foundation is very close to the response of the fully walled foundation. This suggests that the mat of the foundation is more significant in determining the kinematic interaction of the foundation with the soil compared to the effects of the side walls. This will be further explored by varying the wall height (see Figures 5.27 and 5.28).

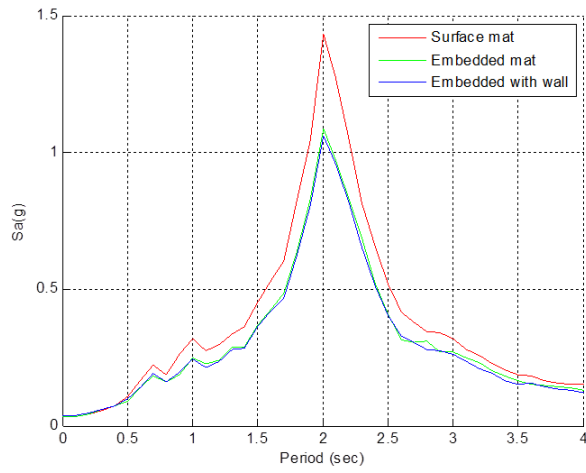


Figure 5.15: Surface vs Embedded Foundation - Free-Field Properties

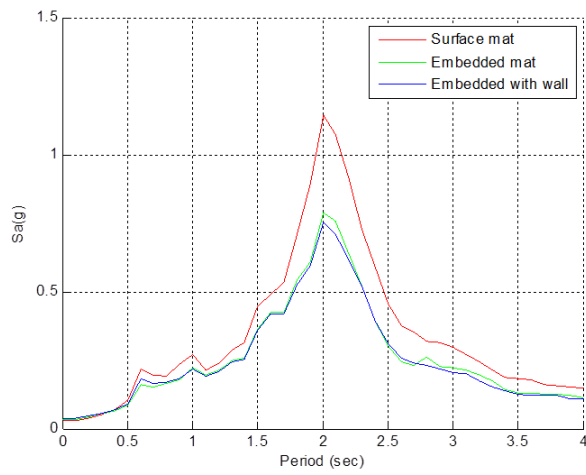


Figure 5.16: Surface vs Embedded Foundation - Near-Field Properties



### **5.2.3 Analysis of Structures of Various Heights**

In addition to varying the configurations of the foundation, analysis of the soil-structure system response is also done for various structural configurations. The height of the structure is varied to represent the range of building heights damaged in the Mexico City earthquake. The response of the foundation is calculated using free-field converged properties only, and compared to the response found using near-field iterated properties.

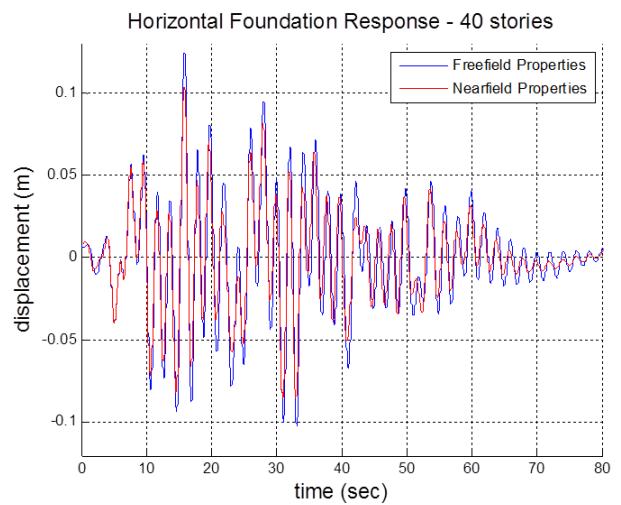
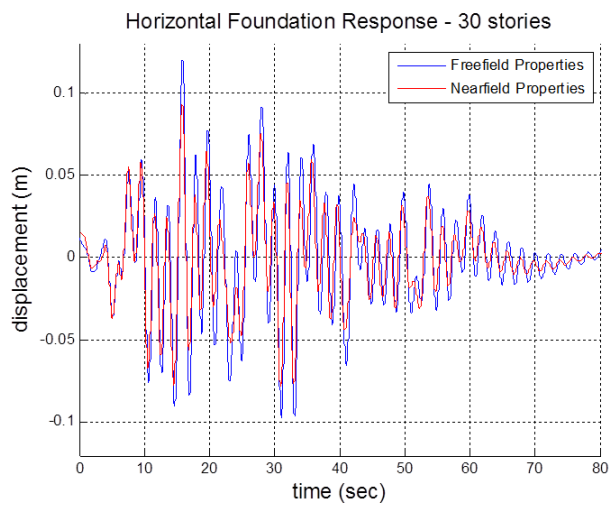
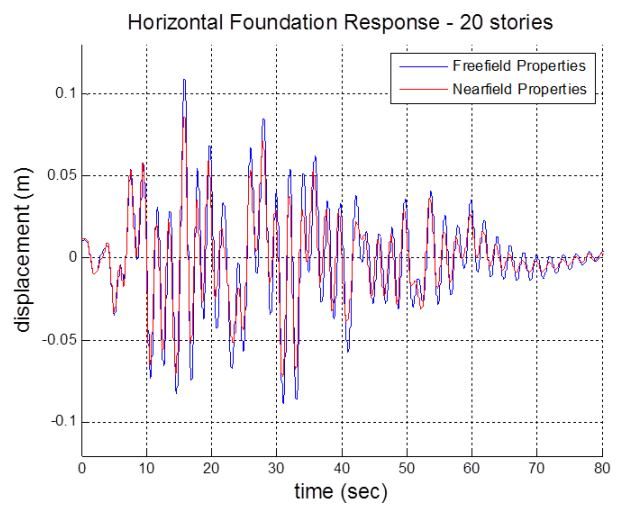
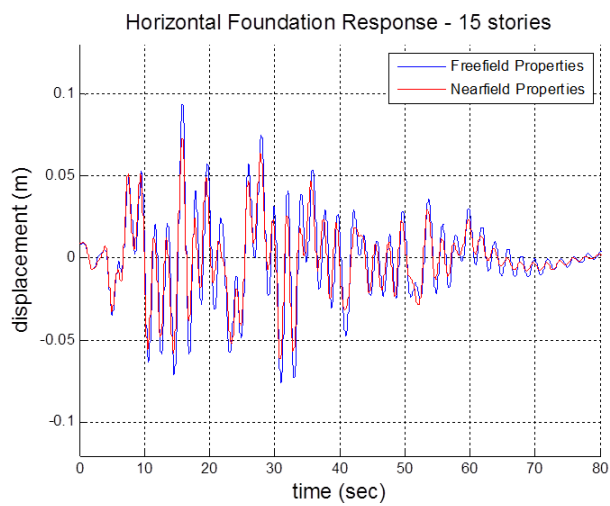
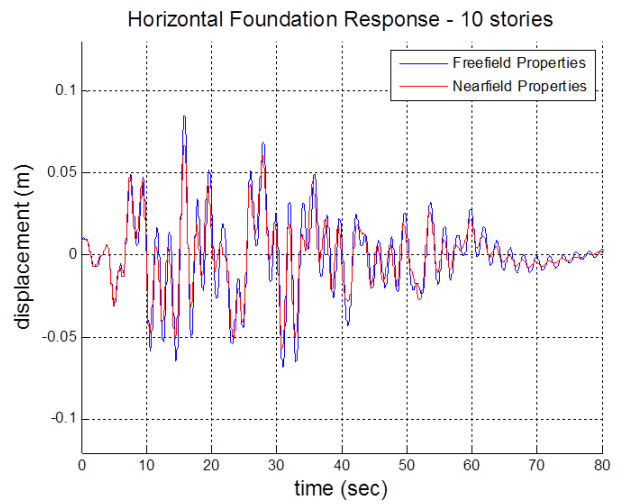
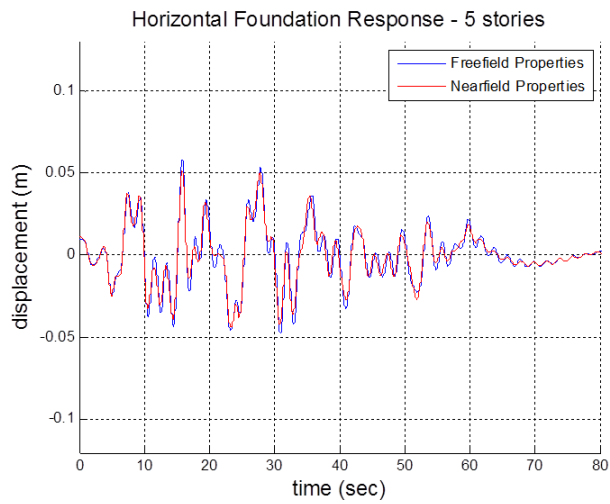


Figure 5.17: Horizontal Response of Foundation for Structures of Varying Heights

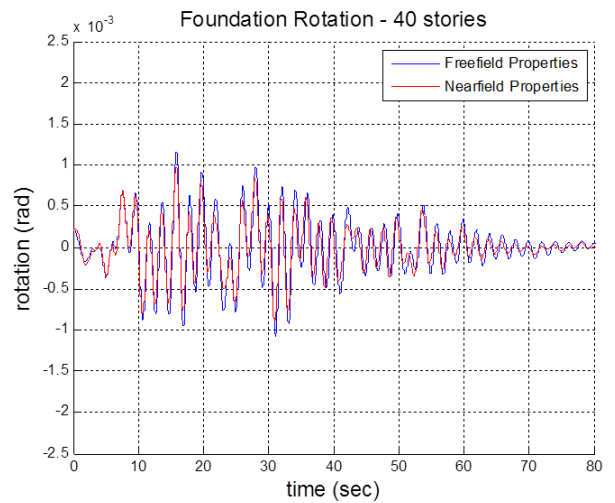
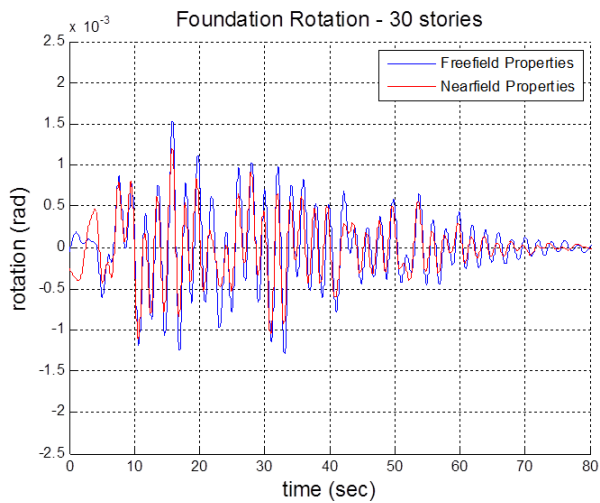
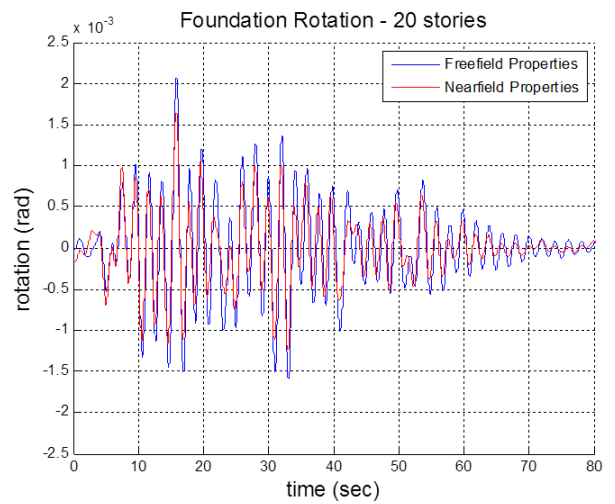
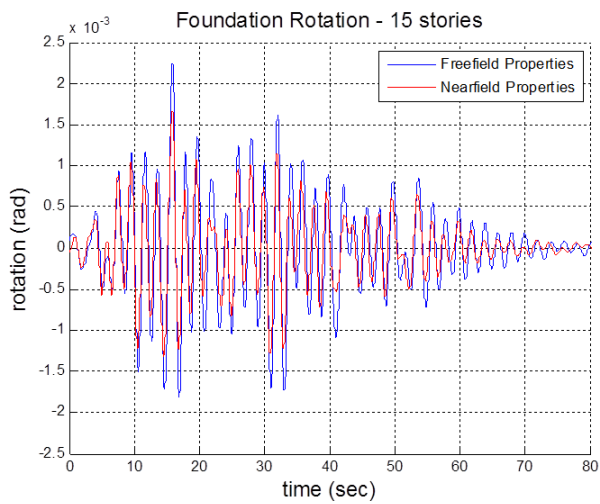
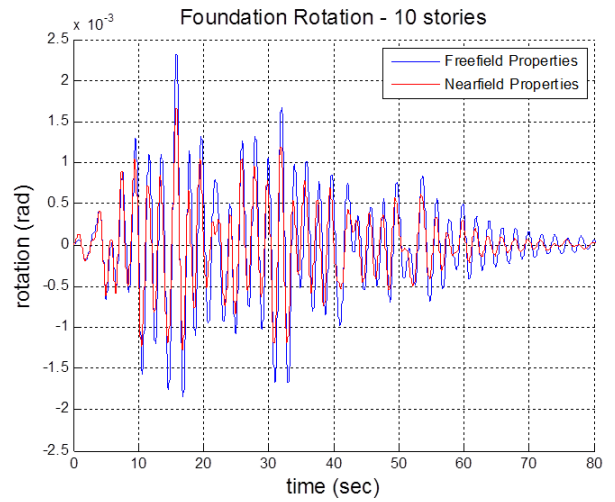
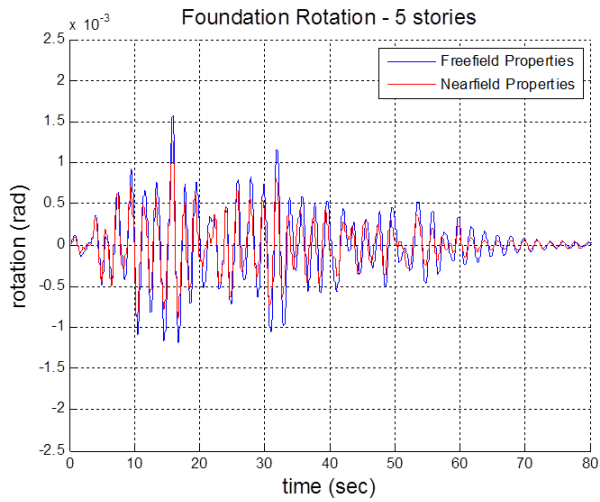


Figure 5.18: Rotational Response of Foundation for Structures of Varying Heights

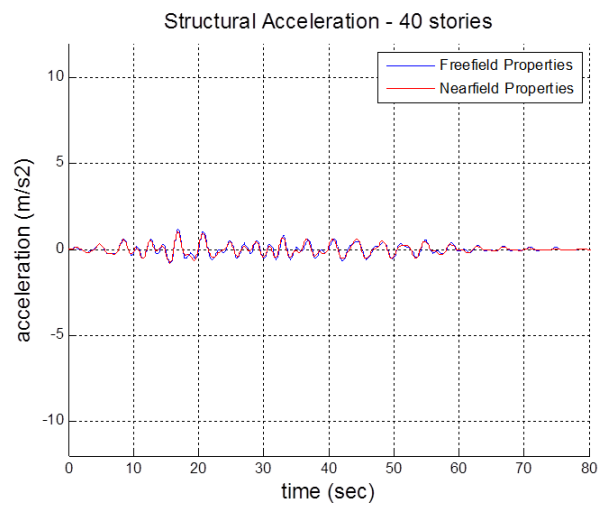
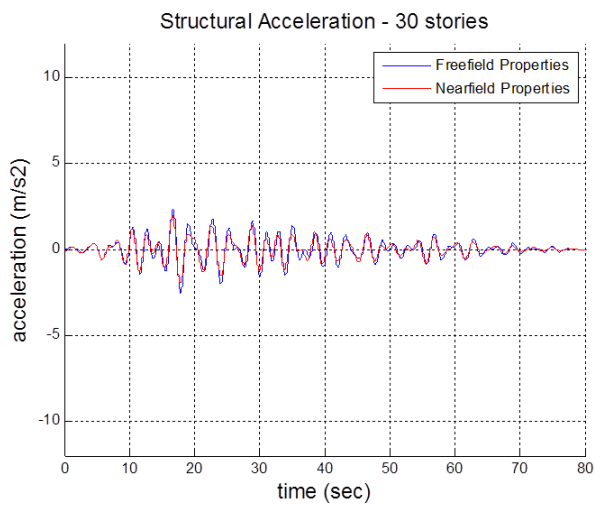
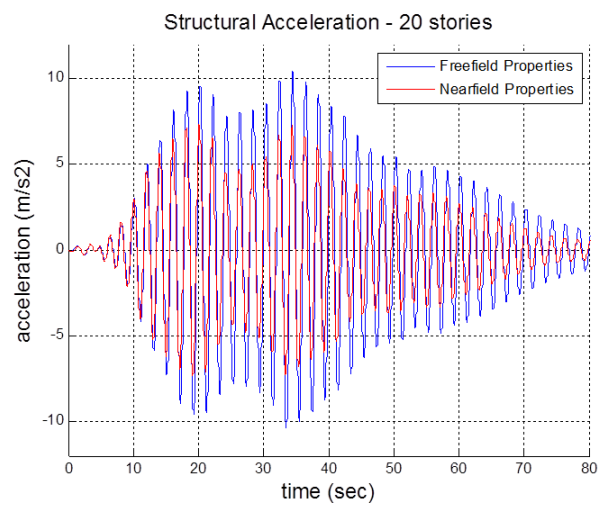
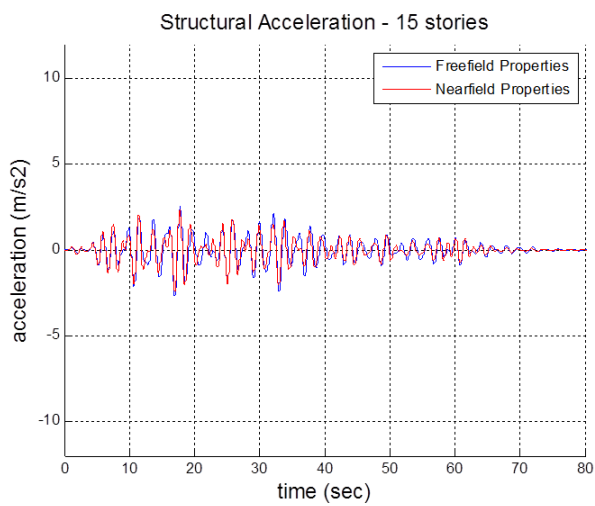
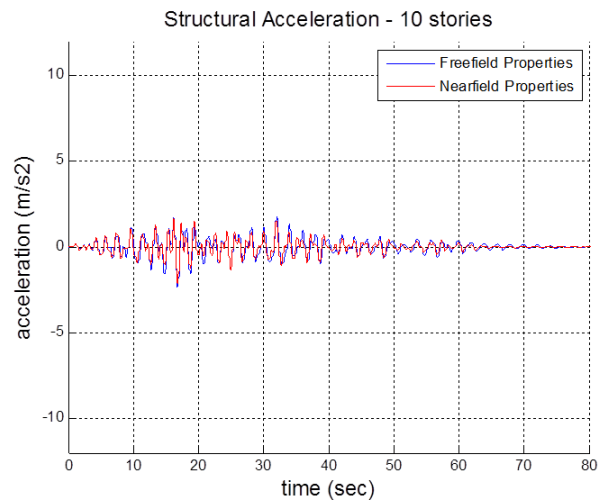
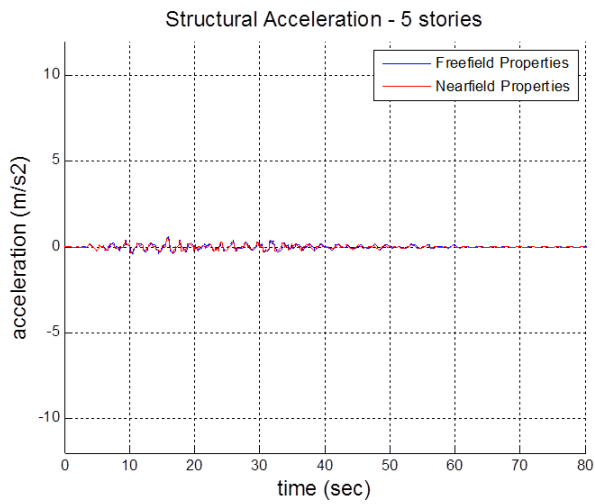


Figure 5.19: Acceleration Response for Structures of Varying Heights

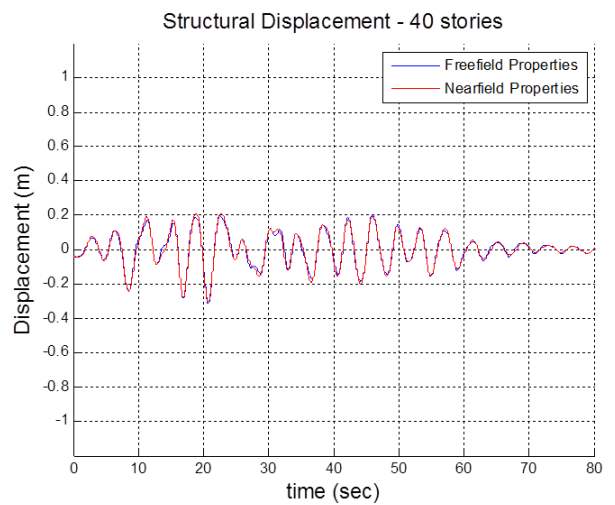
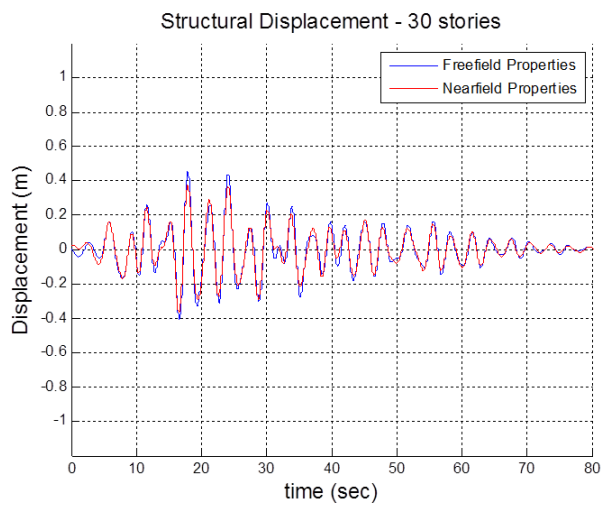
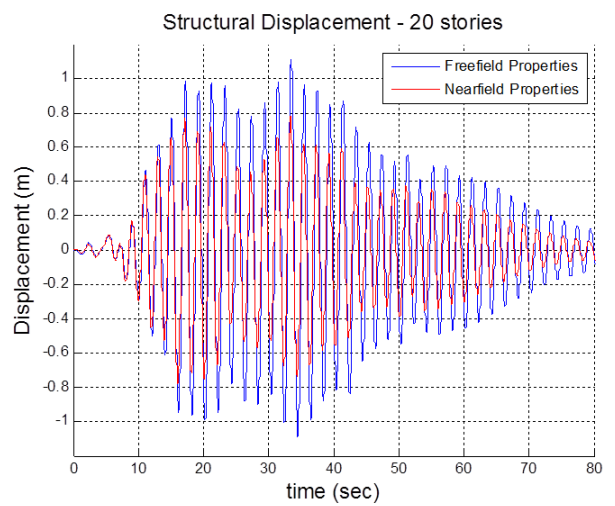
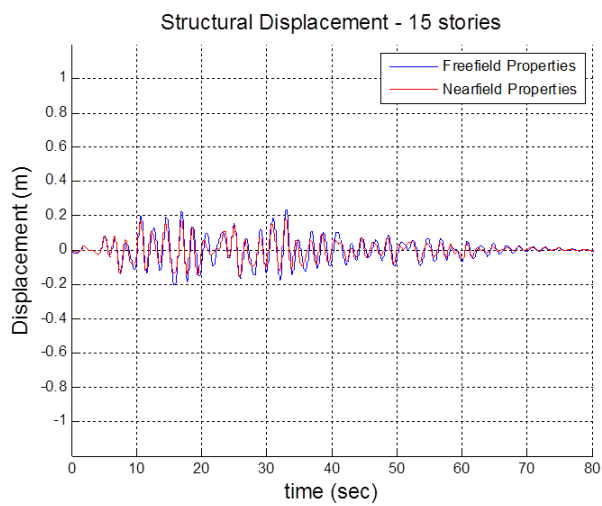
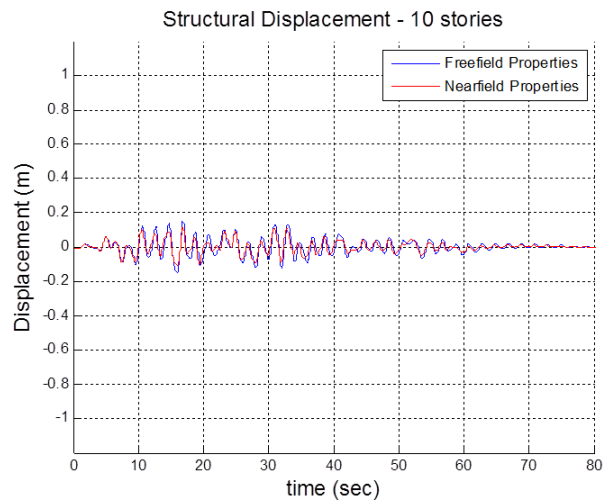
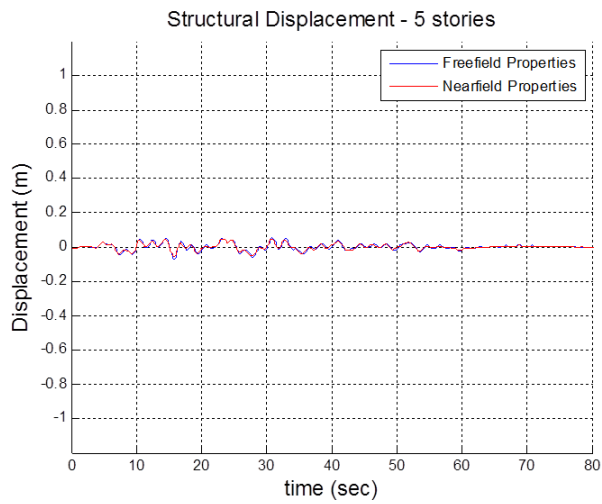


Figure 5.20: Displacement Response for Structures of Varying Heights

From the results above, it is evident that the highest level of response is observed for the 20-story building. This structure has a natural period of approximately 2 seconds. This natural period matches the dominant period amplified by the soft soils at the SCT site, and thus near-resonance is expected.

The calculated responses show reduction in every response parameter when adjustment of soil properties is carried out for the near-field region. The reduction is more significant for structural response compared to foundation response. Also, the reduction is greater for structures with natural period close to the natural period of the soil deposit.

Foundation translation and rotational response do not vary much for different structural heights. The fact that the structural response varied greatly indicates that inertial effects are more significant in determining the soil-structure response. The motion of the structure exerts loading on the foundation which affects the deformation level of nearby soil. The level of inertial effects can be inferred by examining the change in modulus and damping near the foundation.

The strain levels for the analysis of different building heights are given below. The corresponding reduced modulus and soil damping are also presented to show the localized effects by the structure, which near-field iterations account for.

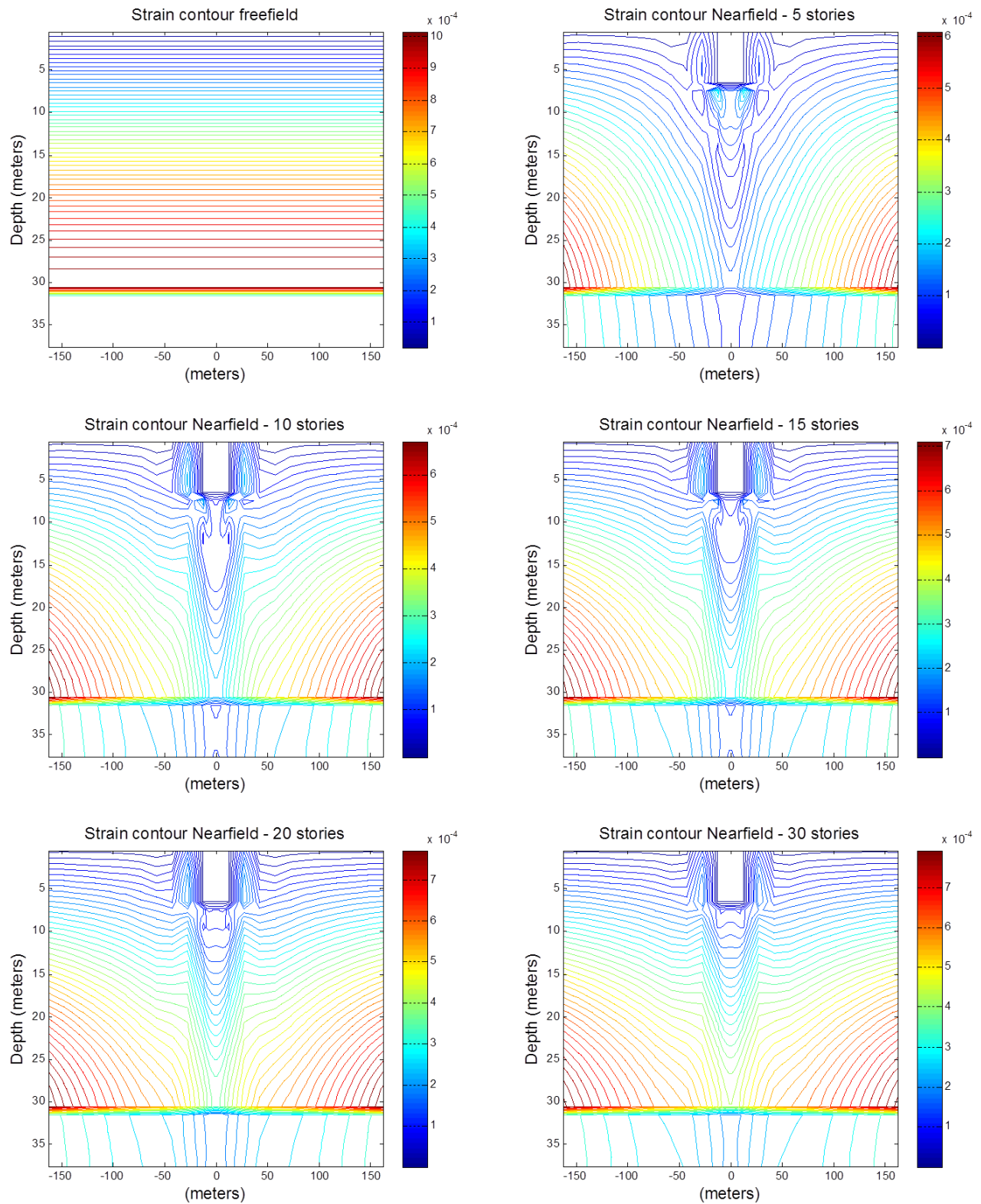


Figure 5.21: Converged Strain Levels for Structures of Varying Heights

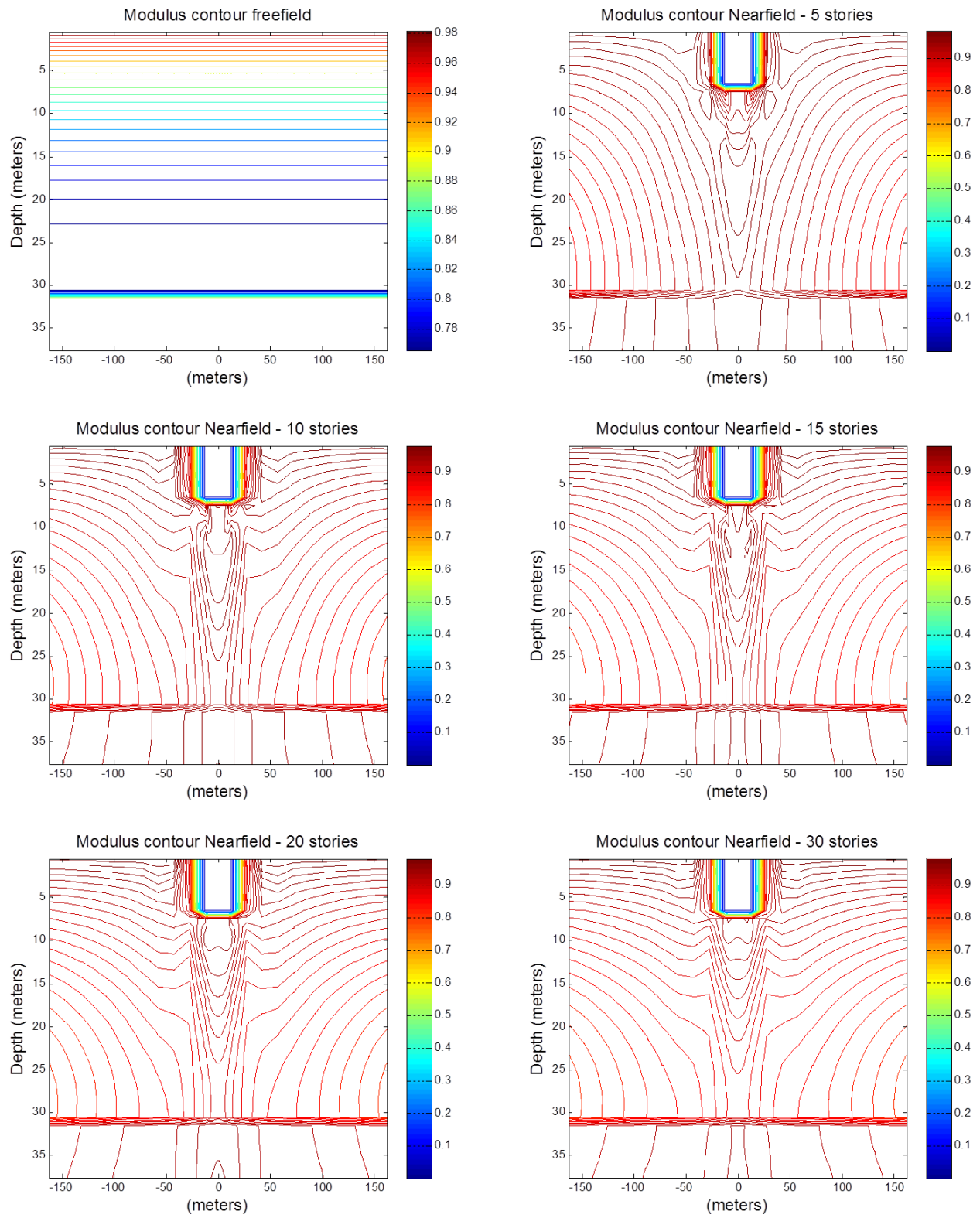


Figure 5.22: Converged Shear Modulus Levels for Structures of Varying Heights



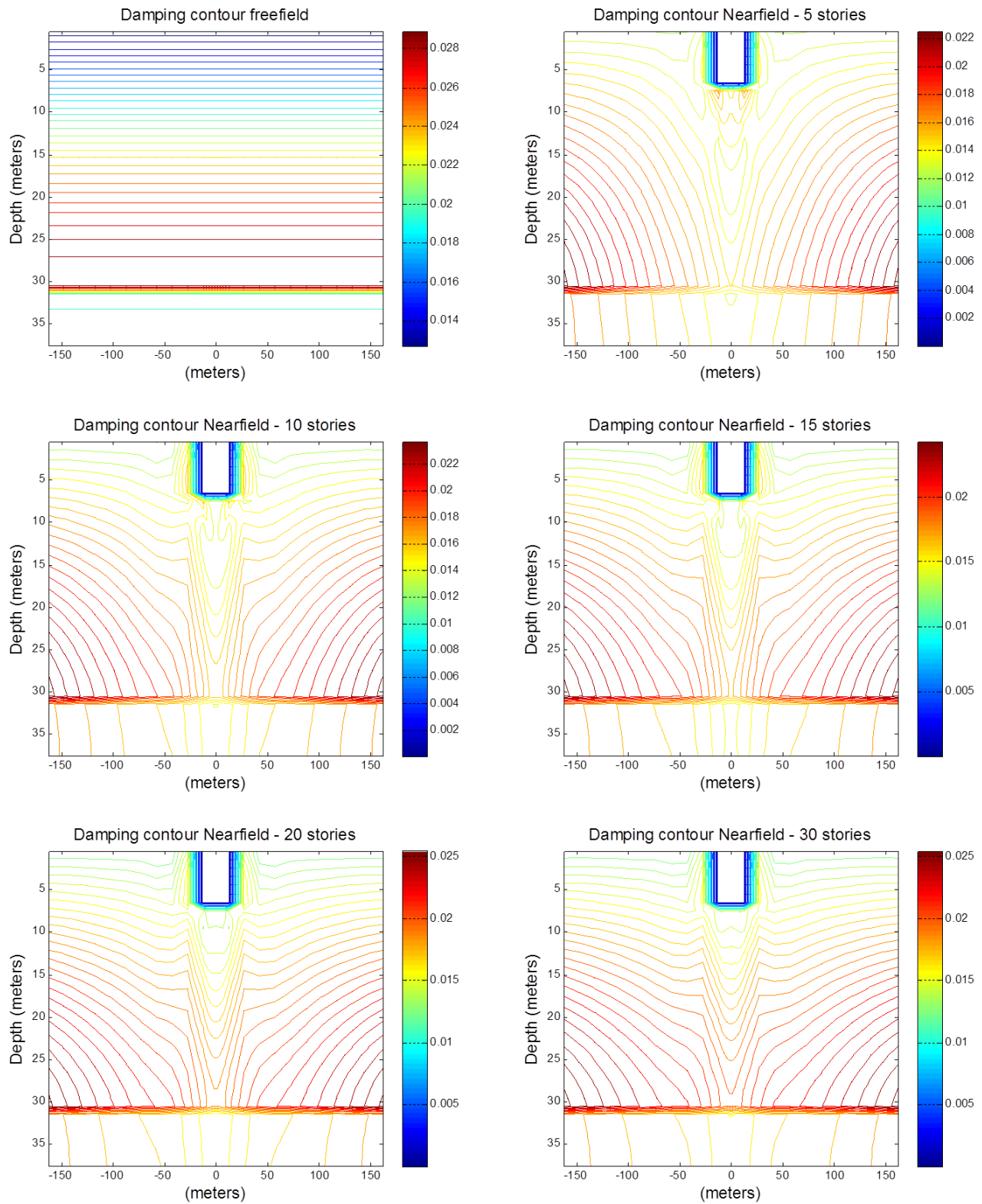


Figure 5.23: Converged Damping Levels for Structures of Varying Heights

### 5.2.4 System Response for Various Foundation Depths

The effects of foundation depth on the soil-structure response is also examined. The initial foundation depth of 5 meter is considered shallow, and deeper embedment of 7 meters and 10 meters are considered. Calculation of the soil-structure response is done using both free-field converged properties as well as near-field converged properties. The results are provided below.

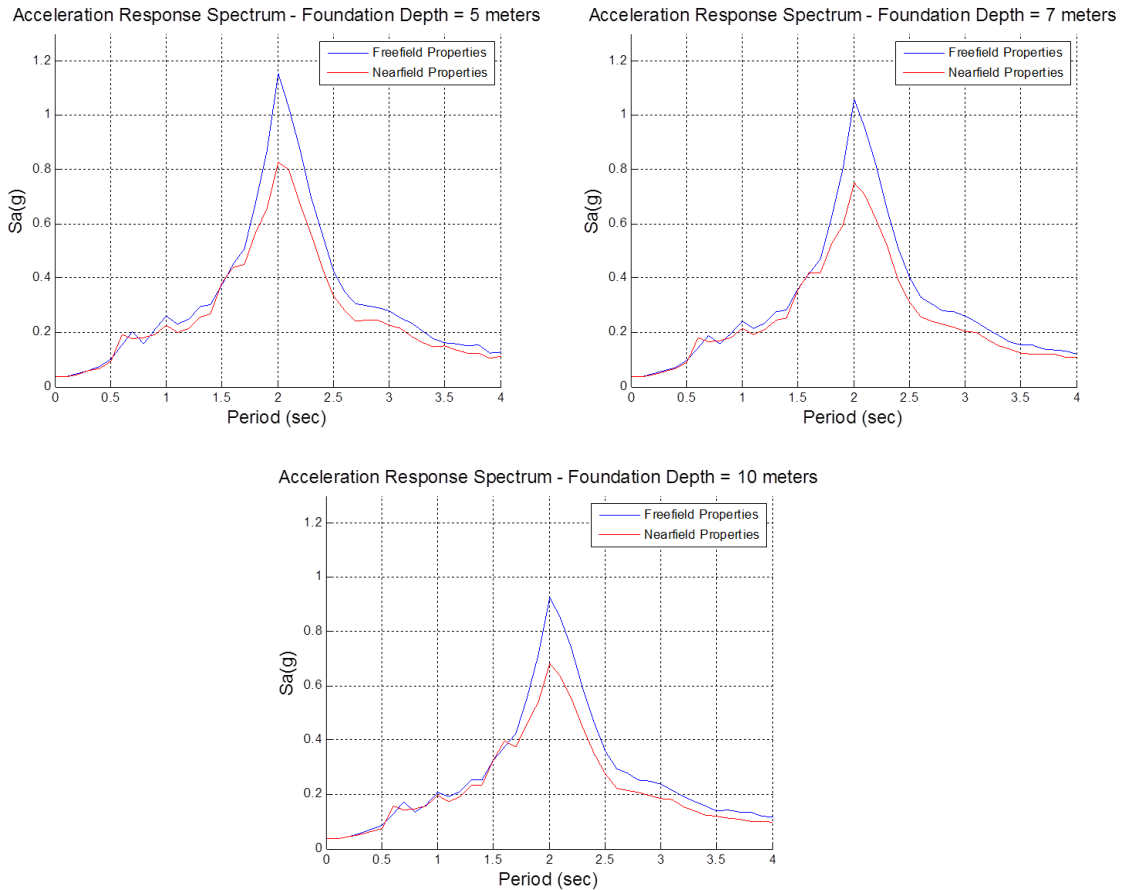
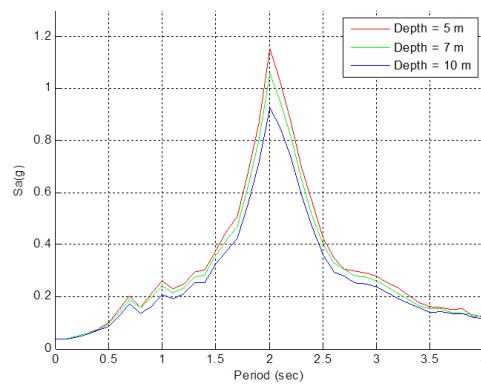
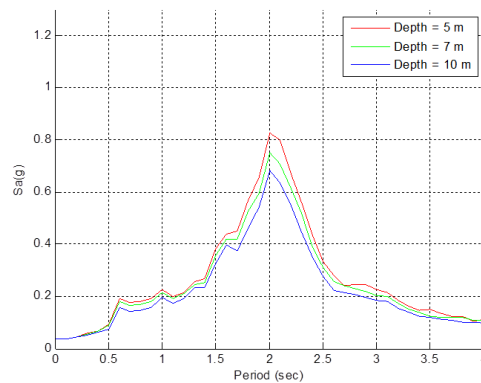


Figure 5.24: Acceleration Response Spectra for Various Foundation Depths obtained using Free-Field and Near-Field Converged Properties

For all foundation depths it can be concluded that adjusting the soil properties consistently with the level of deformation results in significant reduction of the acceleration response spectra. Additionally, comparison of the response spectra for the different embedment depths shows that shallower foundations experience higher levels of acceleration.



(a) Various Foundation Depth - Free-Field Properties



(b) Various Foundation Depth - Near-Field Properties

Figure 5.25: Comparison of Acceleration Response Spectra for Various Foundation Depths

The reduction in the level of response for deeper foundations is justified because deeper foundations encounter greater resistance from the surrounding soil and thus the motions of the foundation and structure are reduced. The level of deformation experienced in each scenario along with the soil properties adjustments are shown in the following figures.

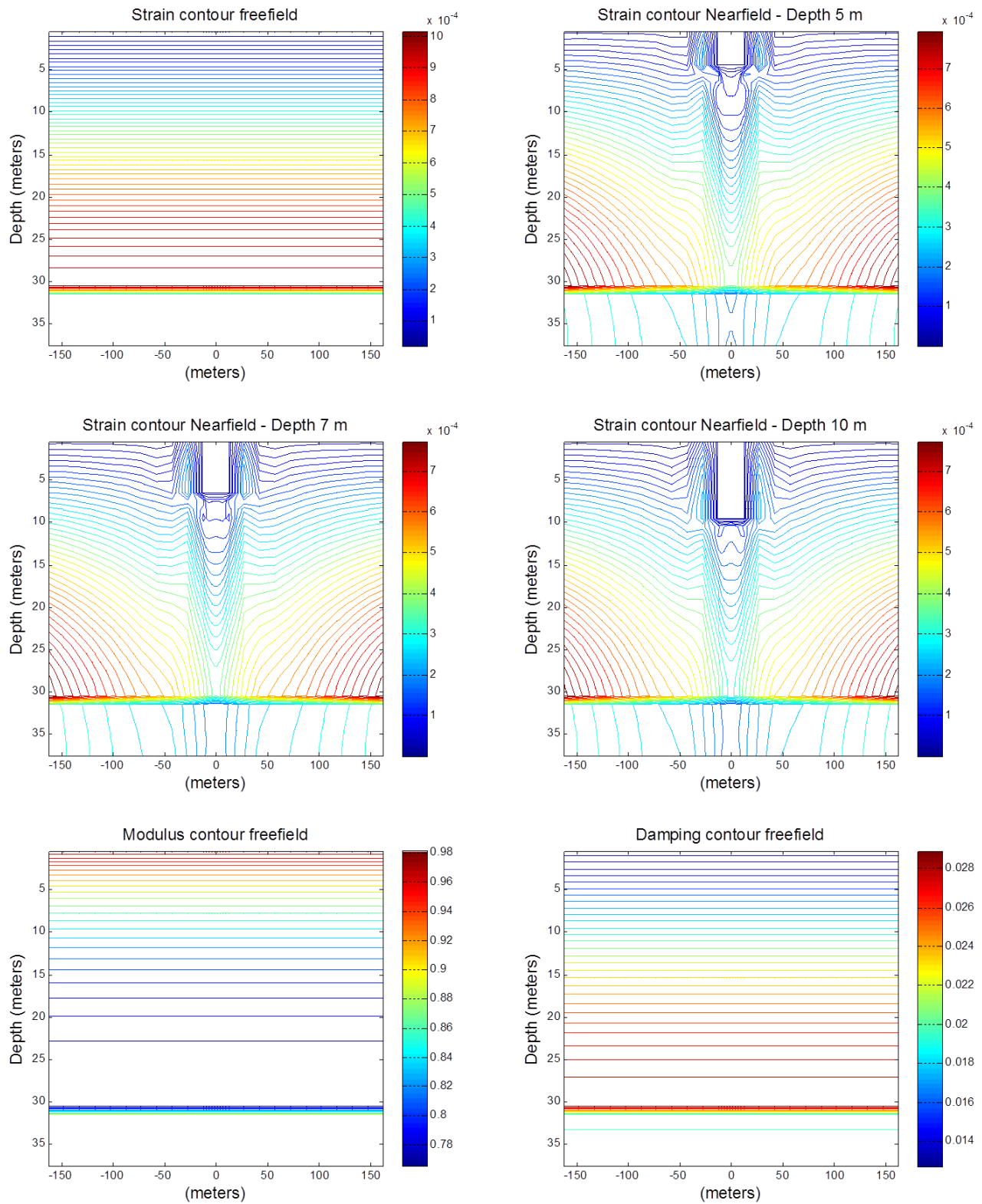
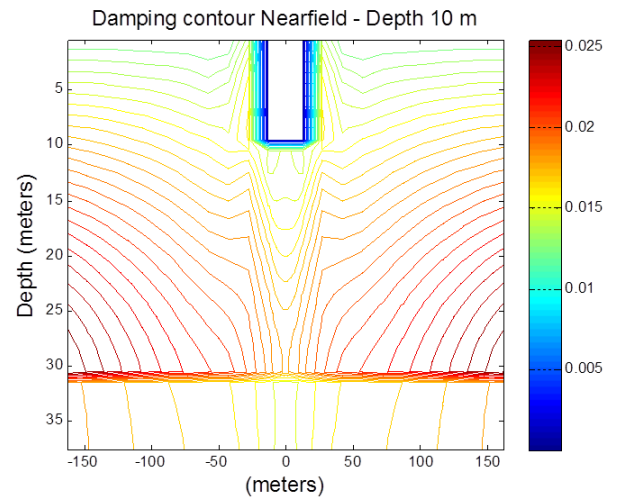
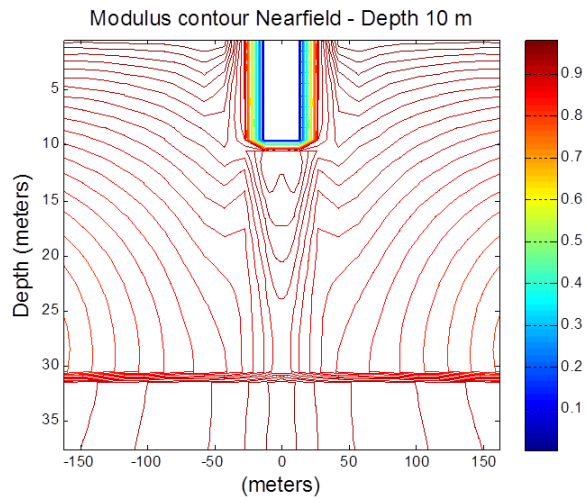
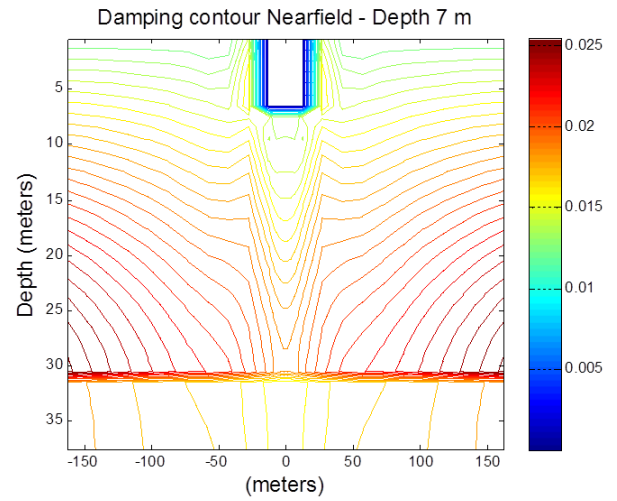
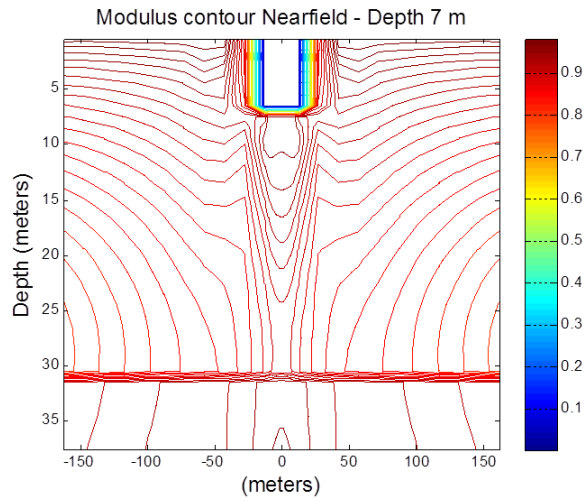
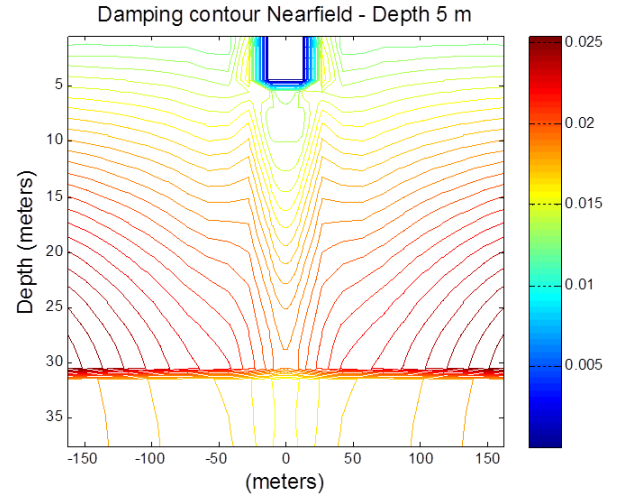
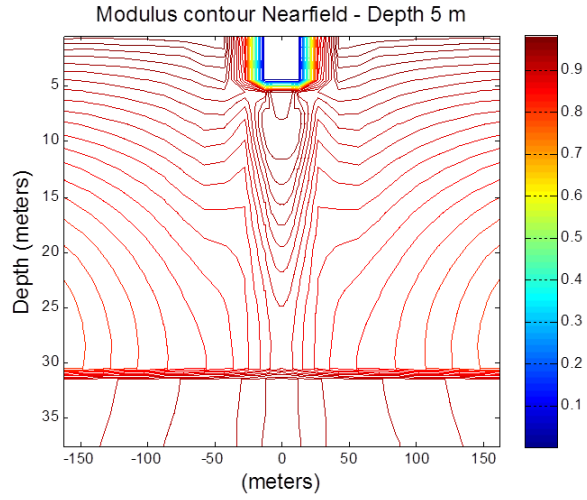
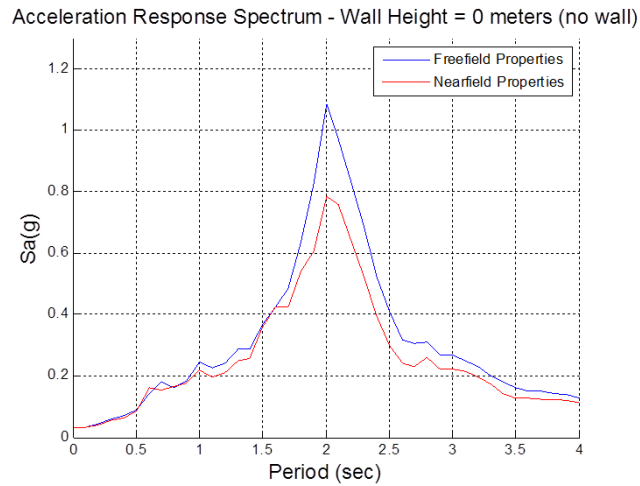


Figure 5.26: Converged Soil Properties for Various Foundation Depths

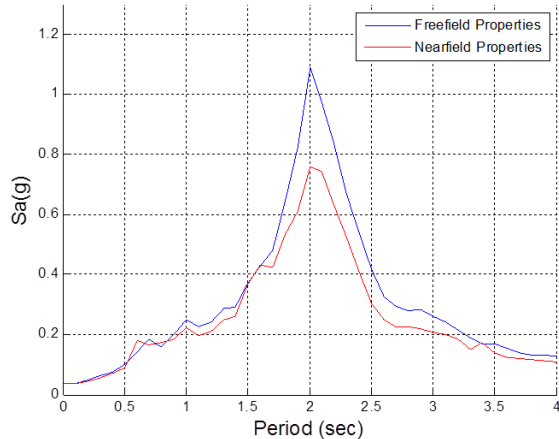


### 5.2.5 System Response for Various Foundation Sidewall Heights

The sidewalls of the foundation were suspected to be a less significant factor affecting the soil-structure system response. The effects of the sidewalls are studied by varying the wall height of both side walls for a foundation embedded 7 m deep. The wall heights are set to be 0 m corresponding to a mat foundation, 3 m, and 7 m which corresponds to a fully walled foundation. The response is calculated using both the free-field converged properties and the near-field iterated properties.



Acceleration Response Spectrum - Wall Height = 3 meters (partial wall)



Acceleration Response Spectrum - Wall Height = 7 meters (full wall)

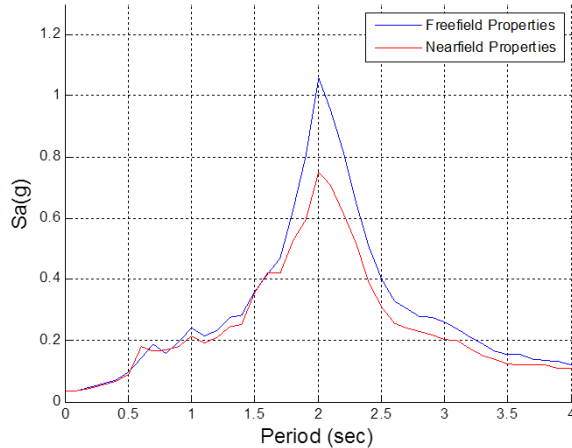


Figure 5.27: Acceleration Response Spectra for Various Foundation Wall Heights obtained using Free-Field and Near-Field Converged Properties

The general trend of response reduction due to adjustment of the near-field soil properties is observed. However, the effects on the soil-structure system response can be seen to be small. Foundation depth seems to be more



of a significant factor compared to height of sidewalls. This can be seen by comparing the response spectra for different wall heights in Figures 5.28.

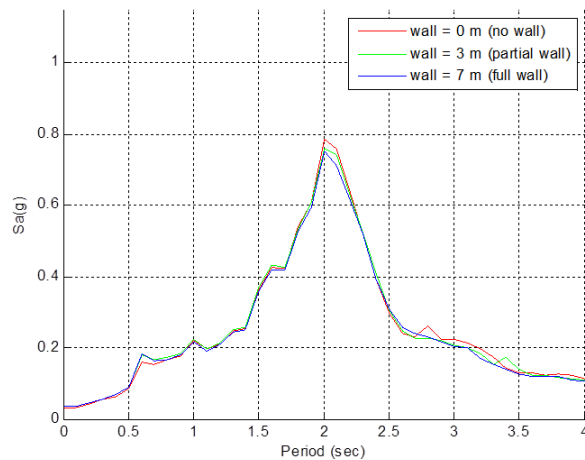


Figure 5.28: Comparison of Acceleration Response Spectra for Various Foundation Wall Heights

This observation can be explained by looking at the effects the sidewall height has on the foundation. Higher sidewalls produce an overall stiffer foundation. However, at the same time these higher sidewalls capture more loading from the soil due to the larger area of contact with the sidewall. These effects tend to negate each other, and thus the overall effect on the system response is less pronounced. Although the response spectra are not significantly affected by the wall height, examination of the strain level demonstrates changes near the foundation walls. The modulus reduction is also somewhat affected in this region, although damping does not vary as much.

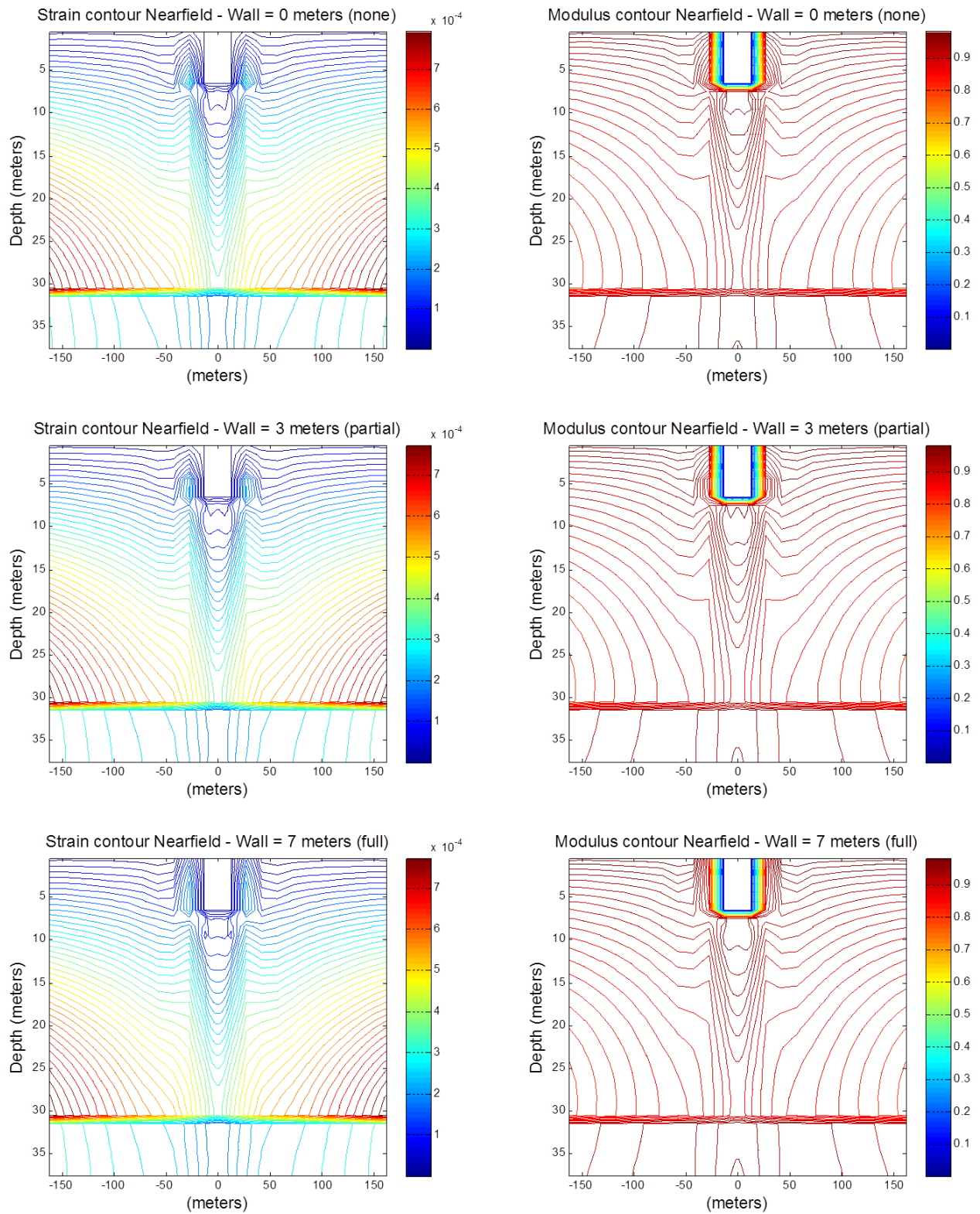


Figure 5.29: Converged Soil Properties for Various Foundation Wall Heights

The analyses of soil-structure system response for various foundation and structural configurations have demonstrated that it is indeed important to continue iterations of soil properties in the near-field region. Even in terms of the time-domain response of the soil, adjustments of the properties provide an adequate prediction of the actual time-history motion at the surface. A comparison shown in Figure 5.30 demonstrates the agreement of the predicted free-field response with respect to the recorded SCT motion.

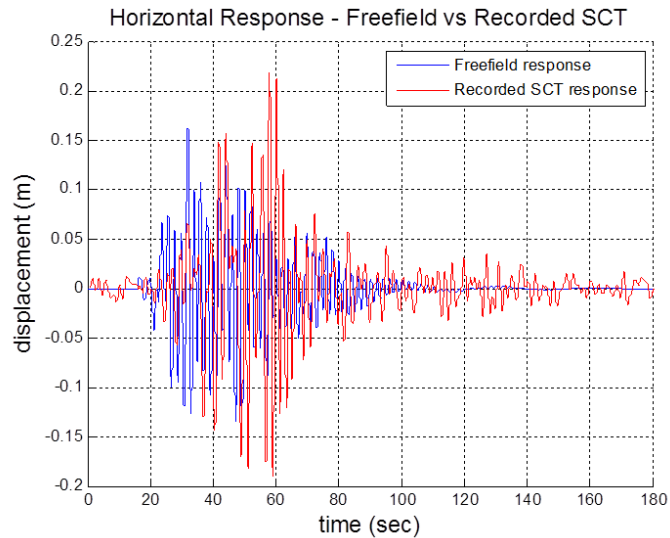


Figure 5.30: Horizontal Response Equivalent Linear Analysis vs Recorded SCT Motion

Apart from demonstrating this significance, the various analyses conducted also provide additional insights into the soil domain towards the soil property adjustments. Figure 5.31 summarizes the level of deformation expe-

rienced due to an input ground motion at the bottom, for the various analysis studied in this chapter. The progression of the level of deformation with changes in the configuration shows that the most significant change occurs when the structure is accounted for. The interaction of the structure with the soil provides additional loading to the soil region around the foundation, which affects the strain levels and consequently the soil property adjustments in the near-field region.

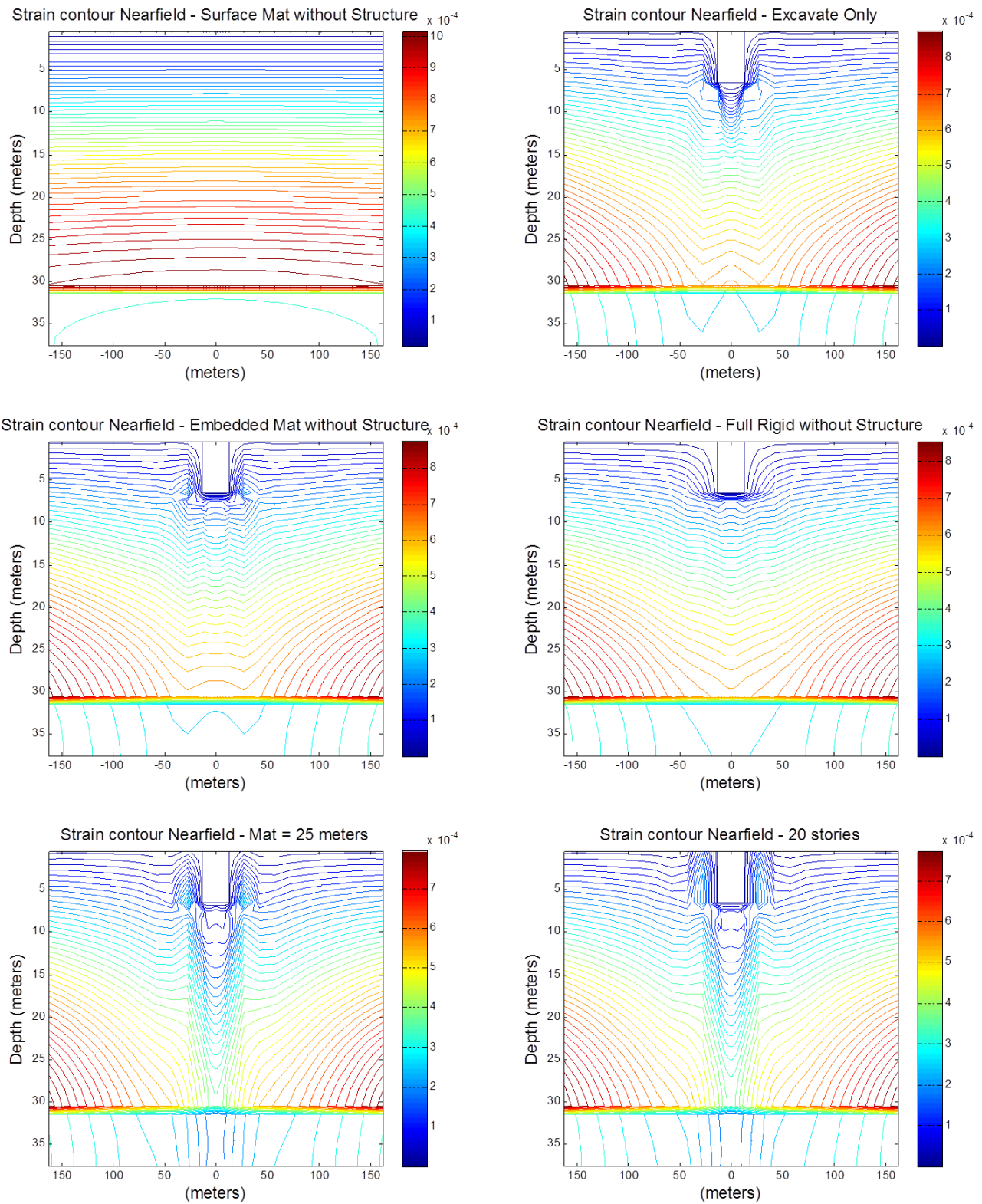


Figure 5.31: Converged Deformation Level for Various Configurations

## Chapter 6

### Conclusion

This dissertation has explored the methods of analysis and determination of the response of soil-structure systems using soil properties adjusted for the level of deformation. Finite-element modes have been implemented for the soil and the rigid foundation. A simple model for the soil-structure system has been adopted to represent the effects of structural mass on the soil and vice versa.

Procedures were developed in this study to efficiently calculate the soil-structure system response both in the free field and the near field. Additionally, a procedure involving the use of a perturbation method has been developed to efficiently account for the numerous incremental changes in soil properties. The use of sparse matrices and the LU decomposition were incorporated into the numerical procedures to further optimize the solution process.

The numerical procedures developed in this study were applied to a theoretical case representing massive structures such as nuclear plants. Furthermore, an analysis was undertaken to apply the procedures on actual events such as of the 1985 Mexico City earthquake to determine the importance of updating soil properties in the near-field region. For all the different founda-

tion and structural configurations analyzed, the response of the soil-structure system was significantly reduced when the near-field soil properties were adjusted.

It is the conclusion of this study that soil-property adjustments in the analysis of soil-structure systems must be applied in the near-field in addition to the free-field adjustments. Using free-field only adjustments may be convenient for analysis using traditional methods, but the analysis results are likely to yield an overly conservative design. Conducting near-field iterations, by the efficient process demonstrated herein, will permit greater design efficiency.

Further research is possible and desired to extend the findings of present study. One possibility for improvement in further research is the use of a continued-fraction absorbing boundary condition as the bottom boundary of the soil domain. Representing the bottom of the domain with a halfspace instead of rigid bedrock allows for a more accurate representation of wave motion in the soil.

## Bibliography

- J. Avilés and L. E. Pérez-Rocha. Evaluation of interaction effects on the system period and the system damping due to foundation embedment and layer depth. *Soil Dynamics and Earthquake Engineering*, 15(1):11–27, 1996.
- J. Avilés and L. E. Pérez-Rocha. Design concepts for yielding structures on flexible foundation. *Engineering Structures*, 27(3):443–454, 2005.
- M. Celebi, J. Prince, C. Dietel, M. Onate, and G. Chavez. The culprit in Mexico City-amplification of motions. *Earthquake spectra*, 3(2):315–328, 1987.
- M. B. Darendeli. Dynamic properties of soils subjected to 1994 Northridge earthquake. Master’s Thesis, University of Texas at Austin, 1997.
- M. B. Darendeli. *Development of a new family of normalized modulus reduction and material damping curves*. Ph.D. Dissertation, University of Texas at Austin, 2001.
- R. Dobry and M. Vucetic. Dynamic properties and seismic response of soft clay deposits. *Proc. Int. Symp. on Geotechnical Engineering of Soft Soils, Mexico City, Mexico*, 2:51–87, 1987.
- B. Hardin and V. Drnevich. Shear modulus and damping in soils: Design



- equations and curves. *Journal of Soil Mechanics & Foundations Div*, 98 (sm7):667–692, 1972.
- M. Hudson, I. Idriss, and M. Beikae. *QUAD4M: a computer program to evaluate the seismic response of soil structures using finite element procedures and incorporating a compliant base*. Center for Geotechnical Modeling, Department of Civil and Environmental Engineering, University of California, Davis, 1994.
- I. Ikeda. *Analysis of wave motion in irregular layered media using a finite-element perturbation method*. Ph.D. Dissertation, University of Texas at Austin, 2008.
- A. Jaime. *Características dinámicas de la arcilla del valle de México*. Ph.D. Dissertation, Ciudad Universitaria, 1987.
- A. Jaime and M. Romo. The Mexico earthquake of September 19, 1985—correlations between dynamic and static properties of Mexico City clay. *Earthquake spectra*, 4(4):787–804, 1988.
- E. Kausel. An explicit solution for the Green functions for dynamic loads in layered media. *NASA STI/Recon Technical Report N*, 82:29505, 1981.
- A. R. Kottke. *A comparison of seismic site response methods*. Ph.D. Dissertation, University of Texas at Austin, 2010.
- A. R. Kottke and E. M. Rathje. Technical manual for strata. *University of California, Berkeley*, 2008.

- S. L. Kramer. *Geotechnical earthquake engineering*. Pearson Education, 1996.
- J. Leon, A. Jaime, and A. Rabago. Dynamic properties of soils-preliminary study. *Institute of Engineering, UNAM*, 1974.
- X. S. Li, J. W. Demmel, J. R. Gilbert, L. Grigori, M. Shao, and I. Yamazaki. SuperLU users' guide. *Internet Address: [http://crd. lbl. gov/~xiaoye/SuperLU/superlu\\_ug. pdf](http://crd.lbl.gov/~xiaoye/SuperLU/superlu_ug.pdf)*, 2011.
- J. Lysmer et al. SASSI—a computer system for dynamic soil-structure interaction analysis. *Report No. UCB IGT/81-02, University of California, Berkeley*, 1981.
- G. Masing. Eigenspannungen und verfestigung beim messing. In *Proceedings of the second international congress of applied mechanics*, pages 332–335, 1926.
- E. Ovando-Shelley, A. Ossa, and M. P. Romo. The sinking of Mexico City: Its effects on soil properties and seismic response. *Soil Dynamics and Earthquake Engineering*, 27(4):333–343, 2007.
- M. Romo and A. Jaime. Dynamic characteristics of some clays of Mexico Valley and seismic response of the ground. *Mexico City: Instituto de Ingenieria*, 1986.
- M. Romo, A. Jaime, and D. Reséndiz. The Mexico earthquake of September 19, 1985-general soil conditions and clay properties in the Valley of Mexico. *Earthquake spectra*, 4(4):731–752, 1988.

- P. Schnabel, J. Lysmer, and H. Seed. SHAKE—A computer program for response analysis of horizontally layered sites. *Earthquake Engineering Research Centre, University of California, Berkeley, CA*, Report No. EERC 72-12, 1972.
- H. Seed, M. Romo, J. Sun, A. Jaime, and J. Lysmer. The Mexico earthquake of September 19, 1985—relationships between soil conditions and earthquake ground motions. *Earthquake Spectra*, 4(4):687–729, 1988.
- H. B. Seed and I. Idriss. Soil moduli and damping factors for dynamic response analyses. *College of Engineering, University of California, Los Angeles, CA*, Report EERC 70-10, 1970.
- J. P. Stewart, A. O.-L. Kwok, Y. M. Hashash, N. Matasovic, R. Pyke, Z. Wang, and Z. Yang. Benchmarking of nonlinear geotechnical ground response analysis procedures. *Pacific Earthquake Engineering Research Center, Berkeley, California*, PEER Report 2008/04, 2008.
- A. Tena-Colunga, E. A. Godínez-Domínguez, and L. E. Pérez-Rocha. Vulnerability maps for reinforced concrete structures for Mexico City’s metropolitan area under a design earthquake scenario. *Earthquake Spectra*, 23(4):809–840, 2007.
- M. Vucetic and R. Dobry. Effect of soil plasticity on cyclic response. *Journal of Geotechnical Engineering*, 117(1):89–107, 1991.

G. Waas. *Linear two-dimensional analysis of soil dynamics problems in semi-infinite layered media*. Ph.D. Dissertation, University of California, Berkeley, 1972.

L. Zeevaert. Foundation engineering for difficult subsoil conditions. *Van Nostrand Reinhold Company*, 1971.

# Vita

Pasca R. Patta was born in Bandung, Indonesia. In July 2006, he received his Bachelor of Engineering degree from Institut Teknologi Bandung. Then, he directly went to The University of Texas at Austin to pursue his doctorate degree in civil engineering.

Permanent address: Bandung, West Java, Indonesia

This dissertation was typeset with L<sup>A</sup>T<sub>E</sub>X<sup>†</sup> by the author.

---

<sup>†</sup>L<sup>A</sup>T<sub>E</sub>X is a document preparation system developed by Leslie Lamport as a special version of Donald Knuth's T<sub>E</sub>X Program.